UC San Diego

UC San Diego Electronic Theses and Dissertations

Title

Model error estimation in composite impact response prediction using hierarchical Bayes networks

Permalink

https://escholarship.org/uc/item/77q0c7vb

Author

Salas Mendez, Pablo Antonio

Publication Date

2010

Peer reviewed|Thesis/dissertation

eScholarship.org Powered by the California Digital Library
University of California

UNIVERSITY OF CALIFORNIA, SAN DIEGO

SAN DIEGO STATE UNIVERSITY

Model Error Estimation in Composite Impact Response Prediction using Hierarchical Bayes Networks

A dissertation submitted in partial satisfaction of the

requirements for the degree Doctor of Philosophy in

Engineering Sciences (Applied Mechanics)

by

Pablo Antonio Salas Mendez

Committee in charge:

University of California, San Diego

Professor David J. Benson, Chair
Professor Frank E. Talke
Professor Marc A. Meyers

San Diego State University

Professor Satchi Venkataraman, Co-Chair
Professor Eugene Olevsky

2010

Copyright

Pablo Antonio Salas Mendez, 2010

All rights reserved.

The dissertation of Pablo Antonio Salas Mendez is approved, and it is acceptable in quality and form for publication on microfilm and electronically:

_____

_____

_____

_____

Co-Chair

_____

Chair

University of California, San Diego

San Diego State University

2010

TABLE OF CONTENTS

Signature Page . . . iii

Table of Contents . . . iv

List of Figures . . . vi

List of Tables . . . ix

Acknowledgments . . . x

Vita . . . xi

Abstract of the Dissertation . . . xiii

Chapter 1 Introduction . . . 1

Chapter 2 Predicting Ballistic Impact Response of Laminated Composites . . . 7
2.1 Observed Impact Response of Composite Materials . . . 9
2.2 Analytical Models for Impact Applications . . . 11
2.3 Predicting Failure in Composites . . . 14
2.3.1 Failure Criteria . . . 14
2.3.2 Damage and Fracture Mechanics . . . 16

Chapter 3 Methodologies for Uncertainty Propagation and Quantification . . . 19
3.1 Uncertainty Quantification Approaches . . . 21
3.1.1 Non-probabilistic methods . . . 22
3.1.2 Probabilistic Methods . . . 23
3.1.3 Alternative Approaches for Uncertainty Quantification . . . 25
3.2 Model Validation Approaches . . . 27
3.3 Modeling the Response of Composites in the Presence of Uncertainties . . . 31

Chapter 4 Analysis and Model Parameter Uncertainty Investigation in Composite Laminates . . . 34
4.0.1 Sources of Model Uncertainty in Progressive Failure Analysis . . . 38
4.0.2 Modeling Uncertainty Included in Progressive Failure Robustness and Predictability Investigations . . . 42
4.1 Laminate Designs Optimized for Predictable Failure in the Presence of Design Variability . . . 43
4.1.1 Laminate Design Problem Chosen for Investigation . . . 44
4.1.2 Optimum Designs of Laminates for Predictable Failure Under Ply Angle Variability . . . 45
4.2 Reliability Analysis of Laminates with Ply Angle Variations and Model Uncertainty . . . 47
4.2.1 Quasi-Isotropic Laminate . . . 48
4.2.2 Laminate Obtained from Deterministic Optimization for Maximum Energy Absorption . . . 50

4.2.3 Laminate Obtained from Optimization for Maximum Energy Absorption at 95% Reliability . . . 55
4.2.4 Laminate Obtained from Optimization for Maximum Energy with Constraints for Failure Mode Separation . . . 58
4.3 Reliability Optimization of Laminates with Ply Angle Variations and Model Uncertainty . . . 61

Chapter 5 Composite Model Implementation . . . 66
5.1 Numerical Implementation of Polymer Model . . . 67
5.1.1 Goldberg's Model . . . 67
5.1.2 Implementation Background - Backward Euler Integration . . . 69
5.1.3 Model Discretization Scheme . . . 70
5.1.4 Ridder's Method . . . 72
5.1.5 Rate Dependence of Elastic Modulus . . . 74
5.1.6 Damage Model . . . 75
5.1.7 Verification of Polymer Model Implementation . . . 75
5.2 Fiber Orthotropic Model . . . 76
5.3 Composite Material Model . . . 80
5.4 Composite Model Results . . . 84

Chapter 6 Bayesian Network Implementation . . . 88
6.1 Bayesian Networks . . . 89
6.1.1 Bayes Network Theory and Gibbs Sampling . . . 89
6.2 Single Level Algebraic Example . . . 92
6.3 Multilevel Example Problem . . . 101

Chapter 7 Composite Multilevel & Hierarchical System Problem . . . 110
7.1 Sources of Modeling and Physical Uncertainties on Composite-Impact Problems . . . 112
7.2 Composite Impact Problem Test . . . 115
7.2.1 Polymer level . . . 116
7.2.2 Fiber level . . . 116
7.2.3 Composite Unidirectional Lamina level . . . 117
7.2.4 Composite Lamina with Fiber Angle Orientation level . . . 118
7.2.5 Ballistic Impact level . . . 118
7.3 Bayesian Network Implementation using Response Surface Models . . . 120
7.4 Composite System Implementation within the Bayesian Framework . . . 122
7.5 Introducing Modeling, Numerical and Experimental Errors into the Bayesian Network . . . 126
7.6 Composite Multilevel Example . . . 129

Chapter 8 Summary and Conclusions . . . 139

Bibliography . . . 141

LIST OF FIGURES

Figure 2.1: Ballistic impact simulation. The predicted response exhibits prominent shear plugging 10

Figure 4.1: Summary of the energy absorption characteristic of different laminate design when subjected to ply angle variations of different magnitude 46

Figure 4.2: Effect of model uncertainties on the progressive failure energy absorption characteristic of a $\pi/6$-quasi-isotropic laminate 49

Figure 4.3: Effect of model uncertainties and design variations on energy absorption statistics for the laminate deterministically optimized for maximum energy absorption 51

Figure 4.4: Progressive failure history for laminate optimized for maximum energy absorption with model uncertainties (varied from laminate to laminate). The progressive failure response of 100 MCS samples is shown for the design analyzed with (a) ply stress uncertainties (b) Failure criterion interaction term F12 uncertainties (c) stiffness degradation factor Em uncertainties (d) all model uncertainties combined. The line with asterisk marks represents the progressive failure of the design without any model uncertainty. The solid lines represent the progressive failure of 100 laminates analyzed with model uncertainties 52

Figure 4.5: Strain energy absorption history for laminate optimized for maximum energy absorption with all model uncertainties included varied from (a) laminate to laminate (b) ply to ply. The line with asterisk marks represents the strain energy absorption of the design without any model uncertainty. The solid lines represent the strain energy absorption of 100 laminates analyzed with model uncertainties 54

Figure 4.6: Effect of model uncertainties on energy absorption statistic for reliability optimization laminate optimized for maximum energy absorption and analyzed with model imperfections 57

Figure 4.7: Effect of model uncertainties on energy absorption statistic for laminate deterministically optimized for maximum energy absorption with constraints for strain separation between consecutive failures in different modes analyzed with model imperfections 59

Figure 4.8: Effect of model uncertainties on energy absorption statistics for reliability optimization laminate optimized for maximum 95% reliability value of energy absorption in the presence of ply angle variations and model uncertainties 62

Figure 5.1: Experimental and computed shear response for PR520 resin at medium (1.76/sec) and high (420/sec) strain rates 76

Figure 5.2: Experimental and computed tensile response for PR520 resin at medium (1.4/sec) and high (510/sec) strain rates 77

Figure 5.3: Experimental and computed shear response for 977-2 resin at medium (1.91/sec) and high (518/sec) strain rates 78

Figure 5.4: Experimental and computed tensile response for 977-2 resin at medium (1.31/sec) and high (365/sec) strain rates 79
Figure 5.5: Elastic response of the fiber followed by softening 80
Figure 5.6: Schematic representation of composite lamina micromechanical unitcell. (a) Quarter of the micromechanical unitcell. (b) Discretized representation of the micromechanical unitcell 82
Figure 5.7: Experimental and computed response for IM7/977-2 [10 degree] composite lamina at medium (0.56/sec) and high (320/sec) strain rates 85
Figure 5.8: Experimental and computed response for IM7/977-2 [45 degree] composite lamina at medium (1.2/sec) and high (405/sec) strain rates 86
Figure 5.9: Experimental and computed response for IM7/977-2 [90 degree] composite lamina at medium (1.09/sec) and high (405/sec) strain rates 87

Figure 6.1: Bayes network schematic representation 90
Figure 6.2: Analytical example predicted response y_{mod} (solid line) and true response y_{true} (dash line) 94
Figure 6.3: Analytical example true and predicted responses. The predicted response y_{mod} (solid lines), mean of the true response y_{true} (dash line) and measured response y_{meas} (circle marks) once variability in a and error ϵ_{exp} were incorporated are shown 96
Figure 6.4: Model prediction y_{mod} (solid line), mean of true response y_{true} (dash line) and updated prediction (diamond marks). The dotted lines represent the 95% confidence intervals for y_{true}. The shaded area represents the 95% confidence intervals for the update prediction (diamond marks) 102
Figure 6.5: Schematic representation of hierarchical algebraic system example 103
Figure 6.6: Bayes network representation of hierarchical algebraic system example 105
Figure 6.7: Estimated posterior distributions for model error coefficient $\hat{\beta}_1$ . . 108
Figure 6.8: Estimated posterior distributions for model error coefficient $\hat{\beta}_2$ . . 109

Figure 7.1: Schematic representation of sub-system and system main sources of physical, modeling and numerical uncertainty 113
Figure 7.2: Schematic representation of the composite multilevel and hierarchical system 119
Figure 7.3: Schematic representation of Polymer Model FEM Implementation 123
Figure 7.4: Schematic representation of Polymer Model OpenBugs Implementation 124
Figure 7.5: Time evolution of inelastic strain tensor component using response surface models 125
Figure 7.6: Schematic representation of the composite system with response surface models incorporated 127
Figure 7.7: Schematic representation of Bayes network with all errors incorporated 130

Figure 7.8: Inelastic strain true and predicted responses. The model prediction ϵ_x^I (solid line), true response $\epsilon_{x_{true}}^I$ (dash line) and updated prediction (diamond marks) were plotted. The shaded area represents the 99% confidence intervals for the updated prediction (diamond marks) 135

Figure 7.9: Composite lamina ($\theta = 0^\circ$) true and predicted responses. The model prediction $\sigma_x^{\theta=0^\circ}$ (solid line), true response $\sigma_{x_{true}}^{\theta=0^\circ}$ (dash line), true prediction excluding $\epsilon_{mod}^{\theta=0^\circ}$ (dotted line), updated prediction excluding $\epsilon_{mod}^{\theta=0^\circ}$ (square marks) and updated prediction including $\epsilon_{mod}^{\theta=0^\circ}$ (diamond marks) were plotted. The shaded area represents the 99% confidence intervals for the updated prediction (diamond marks) 136

Figure 7.10: Composite lamina ($\theta = 10^\circ$) true and predicted responses. The model prediction $\sigma_x^{\theta=10^\circ}$ (solid line), true response $\sigma_{x_{true}}^{\theta=10^\circ}$ (dash line), true prediction excluding $\epsilon_{mod}^{\theta=10^\circ}$ (dotted line), updated prediction excluding $\epsilon_{mod}^{\theta=10^\circ}$ (square marks) and updated prediction including $\epsilon_{mod}^{\theta=10^\circ}$ (diamond marks) were plotted. The shaded area represents the 99% confidence intervals for the updated prediction (diamond marks) 137

Figure 7.11: Ballistic impact test true and predicted responses. The model prediction V_p (solid line), true response $V_{p_{true}}$ (dash line), true prediction excluding ϵ_{mod}^{bal} (dotted line), updated prediction excluding ϵ_{mod}^{bal} (square marks) and updated prediction including ϵ_{mod}^{bal} (diamond marks) were plotted. The shaded area represents the 99% confidence intervals for the updated prediction (diamond marks) . 138

LIST OF TABLES

Table 4.1: Elastic Properties of AS4/3501-S Graphite-Epoxy Material 44
Table 4.2: Maximum Strengths of AS4/3501-S Graphite-Epoxy Material . . 44
Table 4.3: Probability of failure events following the deterministic failure sequence when subjected to model uncertainties and ply angle variations (1° standard deviation) for the reliability optimization design 58
Table 4.4: Probability of failure events following the deterministic failure sequence when subjected to model uncertainties and ply angle variations (1° standard deviation) for the laminate deterministically optimized for maximum energy absorption with failure mode separation constraints 60
Table 4.5: Probability of failure events following the deterministic failure sequence when subjected to model uncertainties and ply angle variations (1° standard deviation) for the laminate obtained from reliability optimization in the presence of model uncertainties and ply angle variations 63

Table 6.1: Estimated mean values for $\hat{\mu_a}$ and $\hat{\sigma_a}$ μ_a 99
Table 6.2: Estimated mean values for the mean and standard deviation of y_{meas} (y_{true}, $\sigma_{\epsilon_{exp}}$) and y_{mod} ($\mu_{y_{mod}}$, $\sigma_{y_{mod}}$) 99
Table 6.3: Prior distributions for model error coefficients β_i 101
Table 6.4: Mean μ and standard deviation σ of posterior distributions for model error coefficient β_i 101
Table 6.5: Sampled values of $y_{1_{true}}$, $y_{2_{true}}$, $z_{1_{true}}$, $z_{2_{true}}$ and w_{true} over the design space 104
Table 6.6: Prior distributions for model error coefficient $\hat{\beta}_1$ 106
Table 6.7: Prior distributions for model error coefficient $\hat{\beta}_2$ 107
Table 6.8: Mean μ and standard deviation σ of posterior distributions for model error coefficient $\hat{\beta}_1$. The true values of $\hat{\beta}_1$ (assumed to be unknown) are also presented 107
Table 6.9: Mean μ and standard deviation σ of posterior distributions for model error coefficient $\hat{\beta}_2$. The true values of $\hat{\beta}_2$ (assumed to be unknown) are also presented 108

Table 7.1: Polymer material model input parameters X_{pol} 117
Table 7.2: Fiber material model input parameters X_{fib} 117
Table 7.3: Projectile input parameters 119
Table 7.4: Available data for V_p (mt/sec) 132
Table 7.5: Prior Distributions for Model Error Coefficient β_1 134
Table 7.6: Prior Distributions for Model Error Coefficient β_2 134

ACKNOWLEDGMENTS

I would like to thank my advisors, Dr. Satchi Venkataraman and Dr. David Benson for all their support and guidance throughout my PhD; my committee members, Dr. Frank Talke, Dr. Eugene Olevsky and Dr. Marc Meyers for their time and consideration; Dr. Efrem Vitali for all his help and valuable suggestions; The JDP program and the Boeing Company for supporting this work and last but not least, all my family and friends that have supported me during all these years. Thank you all.

Chapter 4, in full, is a reprint of the material as it appears in Laminate Optimization Incorporating Analysis and Model Parameter Uncertainties for Predictable Failure. Pablo Salas and Satchi Venkataraman. Structural & Multidisciplinary Optimization, Vol. 37, No. 6, February 2009, p. 541-555. The dissertation author was the primary investigator and author of this paper.

Chapter 5, in full, is a reprint of the material as it appears in Numerical Implementation of Polymer Visco-plastic Equations for High Strain Rate Composite Models. Pablo Salas, David J. Benson, Satchi Venkataraman, Matti Loikkanen. ASCE Journal of Aerospace Engineering, Vol. 22, No. 3, p. 304-310, July 2009. The dissertation author was the primary investigator and author of this paper.

VITA

2001	B. S., Mechanical Engineering, University of Los Andes, Venezuela
2003-2005	Research Assistant, Department of Aerospace Engineering, San Diego State University
2005	M. S., Engineering (Aerospace Engineering), San Diego State University
2005-2007	Graduate Teaching Associate, Department of Aerospace Engineering, San Diego State University
2007-2009	Research Assistant, Department of Mechanical and Aerospace Engineering, University of California, San Diego
2009-2010	Graduate Teaching Associate, Department of Aerospace Engineering, San Diego State University
2010	Ph. D., Engineering Sciences (Applied Mechanics), Joint Doctoral Program, University of California, San Diego and San Diego State University

PUBLICATIONS

S. Venkataraman and P. Salas. Optimization of Performance and Failure Predictability in Composite Laminates Undergoing Progressive Failure. *AIAA-2005-2225, Proceedings of the 46th AIAA/ ASME/ ASCE/ AHS/ ASC Structures, Structural Dynamics and Materials Conference*, Austin, Texas, April 2005.

S. Venkataraman and P. Salas. Improving Predictability in Progressive Failure Response by Eliminating Competing Failure Modes. *Proceedings of the 2005 ASME International Mechanical Engineering Congress and Exposition (IMECE2005-81994)*, Austin, Texas, April 2005.

S. Venkataraman and P. Salas. Optimum Design of Structural Fuses for Tailoring Robust and Predictable Progressive Failure. *Proceedings of the 47th AIAA/ASME/ASCE/AHS/ ASC Structures, Structural Dynamics, and Materials Conference*, Newport, Rhode Island, April 2006.

P. Salas and S. Venkataraman. Incorporating Model Uncertainties and Variability in Optimization of Laminates for Predictable Failure. *AIAA-2006-7040, Proceedings of the 11th AIAA/ ISSMO Multidisciplinary Analysis and Optimization Conference*, Portsmouth, Virginia, September 2006.

S. Venkataraman and P. Salas. Optimization of Composite Laminates for Robust and Predictable Progressive Failure Response. *American Institute of Aeronautics and Astronautics Journal*, 45(5):1113-1125, May 2007.

P. Salas & S. Venkataraman. Controlling Failure Using Optimum Structural Fuses for Robust and Predictable Progressive Failure. *Structural & Multidisciplinary Optimization*, Vol. 34, No. 6, December 2007, p. 473-489.

P. Salas, D. J. Benson, S. Venkataraman, M. Loikkanen, K. Housen. A Composite Material Model for High Strain Rates. *Proceedings of the ASCE Earth & Space Conference* 2008, March 3-5, Long Beach, CA, USA.

P. Salas & S. Venkataraman. Laminate Optimization Incorporating Analysis and Model Parameter Uncertainties for Predictable Failure. *Structural & Multidisciplinary Optimization*, Vol. 37, No. 6, February 2009, p. 541-555.

P. Salas, D. J. Benson, S. Venkataraman, M. Loikkanen. Numerical Implementation of Polymer Visco-plastic Equations for High Strain Rate Composite Models. *ASCE Journal of Aerospace Engineering*, Vol. 22, No. 3, p. 304-310, July 2009.

P. Salas, S. Venkataraman, D. J. Benson. Modeling Error Estimation in Response Prediction of Multilevel Composite Systems using Bayesian Networks. *Work in Progress*

ABSTRACT OF THE DISSERTATION

Model Error Estimation in Composite Impact Response Prediction using Hierarchical Bayes Networks

by

Pablo Antonio Salas Mendez

Doctor of Philosophy in Engineering Sciences (Applied Mechanics)

University of California, San Diego, 2010

San Diego State University, 2010

Professor David J. Benson, Chair

Professor Satchi Venkataraman, Co-Chair

Predicting the failure response of complex systems often requires computational models that can capture the nonlinear response of the material and structure across multiple scales. Typically, the output response is a direct result of the complex interactions of different phenomena at different scales of the hierarchical system. Therefore, computed model errors correspond to accumulated model errors that have been propagated across several levels of the system. The objective of the current work is to identify and quantify the errors introduced by computer analytical models at different scales in the ballistic impact response simulation of a composite laminate. To that end, a Bayesian network based framework was implemented to systematically estimate the model contribution of uncertainty to the response prediction at each sub-scale of the composite problem. The developed method can be used for optimal allocation of validation resources by determin-

ing the type and number of experimental tests needed to reduce uncertainty at different subsystems levels of large engineering systems.

Chapter 1

Introduction

The use of composite materials has increased in recent years for a wide range of engineering applications. Composite materials offer the advantage of light weight, high stiffness, high strength properties and the increased design freedom to tailor properties. In crash applications, composite materials can increase energy absorption and dissipate a significant amount of the impact energy through material failure. Composites can carry substantial loads after first ply failure. When designed appropriately, the residual strength and stiffness of composite laminates loaded above the initial failure limit can be significant. All of these advantages are often offset by limitations introduced by the complexity of the material analysis, design, testing, and manufacturing.

Predicting the failure response of composite structures is difficult due to the large number of material failure modes they introduce, in addition to structural failure modes. Likewise, determining the load-carrying capacity of composite laminates after initial failure is challenging. The failure process in composite laminates (from onset of material failure to ultimate collapse) is typically referred to as progressive failure. In the

progressive failure of a laminate, multiple plies fail progressively and each ply has several different modes of failure. For example, the ply can experience fiber failure, matrix failure, or fiber-matrix shear failure. As plies fail, the stiffness properties of each ply experienced degradation depending on the failure mode, until the laminate reaches ultimate failure. Remarkable advances have been made in recent years in the development of progressive failure analysis procedures and material degradation models for composite structures. However, development of analysis models for response prediction of composite structures still constitutes an active area of research.

Validating the response of large composite systems is challenging. Composite structures resemble complex systems in that they have many failing components with multiple failure modes at different sub-system levels. The hierarchical nature of complex problems makes it difficult to validate analytical models. Validating the response at the system level requires quantifying various sources of uncertainty and error at various sub-system levels. General theoretical frameworks for model validation and uncertainty quantification of complex systems have been developed over the years. The use of Bayesian updating methods and Bayesian network models to update prediction response for composite systems as more tests from different levels become available can help identify various sources of uncertainty. Such approaches have been developed for simple structural problems and their implementation for model validation of response prediction of composite structures will be investigated.

Ballistic impact response of composite laminates exhibit the complex failure behavior at different problem sub-scales that makes it difficult to validate the predicted response. It constitutes a good test problem for the model validation effort. The first step in the current effort was the implementation of a numerical analysis model to pre-

dict the response of composite materials upon ballistic impact. The analytical model will be used together with Bayesian uncertainty quantification approaches. Validating the response of composites under ballistic-impact requires quantifying the uncertainty at different sub-system levels (e.g polymer level, fiber level, composite lamina level, etc). Each subsystem can be represented by a node in the Bayes network. Once experimental evidence becomes available for response at any level (one or more nodes in the Bayes network), the posterior statistics for responses at all levels can be updated and the system global response validated. In this work, methodologies to quantify uncertainty at different sub-scales of composite laminates subjected to impact loading will be investigated. As the problem complexity increases, often times the available test data for validation of all component levels decreases. The goal is to develop a general framework for complex systems uncertainty quantification in the presence of limited experimental data.

The reminder of the section provides a brief description of each chapter. A general overview of the existent literature on ballistic impact of composite materials was presented in Chapter 2. Experimental tests showed that composite materials exhibit a wide range of failure mechanisms under different projectile shapes and impact velocities. Several constitutive models for response prediction of composites under high strain rates have been developed over the years. Macromechanical and micromechanical approaches have been predominately used to predict the composite response. The failure and damage progression of the material has been modeled through different approaches, such as failure criteria, energy methods, fracture mechanics and damage mechanics. Failure criteria in particular remains one of the most common and practical approaches used in the failure prediction of composites under a wide variety of loading conditions.

Uncertainty quantification has been already integrated on design optimization

and progressive failure analysis of composite structures. However, much work remains to be done on uncertainty quantification of hierarchical composite systems. A general review of the existent approaches that could be used to quantify uncertainty on ballistic impact simulations of composite structures was presented in Chapter 3. Probabilist statistical methods constitute the most traditional approach for uncertainty propagation. Monte Carlo simulation, latyn hypercube sampling and response surface methods are some of the most widely used statistical methods. Non-statistical methods such as moment and stochastic differential equation methods constitute less computational expensive alternatives. Non-probabilistic approaches include sensitivity analysis and fuzzy theory. Model validation and verification approaches have been developed for a wide range of engineering applications. Those well suited for uncertainty quantification of multilevel and hierarchical systems (e.g. Bayes theory) were investigated.

Before moving on to the multilevel uncertainty quantification exercise, the effect of modeling errors on a computationally inexpensive problem was investigated. In Chapter 4, the progressive failure of optimized composites was used as an example problem to investigate how modeling uncertainties affect the predicted response of composite laminates. The effects of different modeling deficiencies such as uncertainties in the homogenization models used for stiffness calculations, micromechanics models used for calculating the ply or constituent level stresses, the failure criteria used for predicting failure, and the models used to degrade ply properties after initial failure were investigated. Different optimized composite laminate designs were analyzed and compared to illustrate the interaction among model uncertainties and physical variability and their effect on failure predictability of the composite laminates.

A computational model to simulate the ballistic impact response of composite

structures was implemented in order to carry out the modeling uncertainty investigation of multilevel hierarchical systems. The numerical implementation of the constitutive material model for composite materials subjected to large deformations was described in Chapter 5. Viscoplastic constitutive material models have been developed to account for the effects of hydrostatic effects and inelastic strains in polymer materials. The numerical implementation of Goldberg's polymer model into LS-DYNA finite-element commercial code was described in detail. Special attention was given to the use of effective algorithms for solving the model nonlinear rate dependent viscoplastic equations. Existent experimental data was used to verify the accuracy and robustness of the computational polymer model. A phenomenological fiber model and a michromecanical unitcell model were used to obtain the resultant stresses in the composite. The composite model was validated with existent data from experimental composite coupon tests.

The theoretical framework of the uncertainty quantification methodology used for error estimation of the composite system problem was described on Chapter 6. A brief introduction to Bayesian networks theory was presented. The free Markov Chain Monte Carlo method software OpenBugs was used to conveniently implement the network. The basic procedure to implement a Bayesian network, incorporate different sources of uncertainty (e.g. experimental errors) in the network and estimate modeling errors was illustrated with simple algebraic examples. A simple methodology to estimate modeling errors at different levels of a multilevel system was presented.

The general methodology for modeling error quantification was used to implement the Bayesian network for the composite system problem, as described in Chapter 7. A general overview of the different sources of uncertainty that ballistic impact problems exhibit was first presented. The different levels that comprise the composite system

problem were described in detail. In order to implement the Bayesian network, response surface models were used to reproduce the composite model predictions (described in Chapter 5) within OpenBugs and propagate the corresponding uncertainty among different levels of the composite system. Once the Bayesian network for the composite problem was implemented, the model error estimation methodology was used to investigate if, given limited experimental data, it is possible to quantify the modeling error at different subsystem levels of the composite system. Finally, the conclusions and future work were discussed on Chapter 8.

Chapter 2

Predicting Ballistic Impact Response of Laminated Composites

Predicting the response of composite materials is difficult due to the complex failure mechanisms that composites exhibit along with the highly nonlinear nature of their response. In recent years, a great deal of effort has been invested in developing failure criteria, modeling, and analysis procedures for accurately predicting the failure of composite structures under nonlinear transient progressive failure conditions [1]. Although remarkable advances have been made in the development of progressive failure analysis procedures and material degradation models for composite structures, predicting the response of composites even under quasi-static loading has proved to be difficult [2].

Various failure criteria and progressive failure material degradation models were compared in the recently concluded three-part World Wide Failure Exercise (WWFE).

Part-A [1] of the study asked proponents of the various models to predict initial failure and progressive failure response of a set of problems that had different geometries subjected to different loading regimes. Part-B [3] of the study compared the predictions with tests and asked proponents to explain reasons for large differences between predictions and experiments. The proponents of models were also allowed to make modifications of their models based on the tests to improve their predictions. In Part-C [4] of the study, five additional failure models were investigated and compared to the existing models. These models were more mechanistic as compared to the traditional phenomenological models.

The studies showed that no single theory could predict exact initial failure and progressive failure in all loading regimes [5]. The mechanistic models worked better than phenomenological models. However, they required expert intervention to decide what mechanisms to include and when to include them. The models were assigned points and ranked based on their performance. It was surprising to see that phenomenological models (e.g Tsai-Wu failure criterion) were included in the higher ranks. In their recommendations, the organizers of the study indicate that the models available at present are quite satisfactory for predicting initial failure, but that more work is needed to develop mechanistic material degradation models for progressive failure analyses [2]. It was shown that the models that were highly ranked and provided good predictions for many cases could provide poor predictions for other cases. The recommendation was to characterize the conditions under which the model predictions are poor and use that information in the design [2].

In order to predict the impact response of composite structures, additional features not considered in progressive failure analysis of composite structures under quasi-static loading conditions need to be incorporated into the model analysis. Simulating the

response upon ballistic impact requires characterizing the strain rate sensitivity of the material, additional failure mechanisms and failure events at very small spatial and temporal scales. The current chapter provides a brief overview of the failure characteristics experimentally observed in ballistic impact tests of composites, different methodologies and approaches available for modeling the impact response and some of the challenges associated with predicting the material behavior under such conditions.

2.1 Observed Impact Response of Composite Materials

Characterizing the multiple failure mechanisms that composites exhibit for impact problems is challenging [6]. Flanagan et al. [7] studied the failure characteristics of several textile composites subjected to low, medium and high velocity impacts. The damage progression analysis was carried out for different types of fabric (Kevlar, Twaron and Spectra), different material processing methodologies (weaving, braiding and needle punching) and different manual consolidation techniques. Some of the observed failure phenomena included fiber breakage, matrix cracking, fiber pullout, delamination and shear plugging. The results showed that the main failure modes at low impact velocities (maximum amount of strain energy dissipated, often the target resists penetration) included intense transverse deflection, matrix cracking and delamination, while at high velocities (where kinetic energy represents the main energy mechanism and target penetration is granted), shear plugging, fiber breakage and delamination constituted the critical failure modes.

At high velocities, shear failure represents the dominant failure mechanism lead-

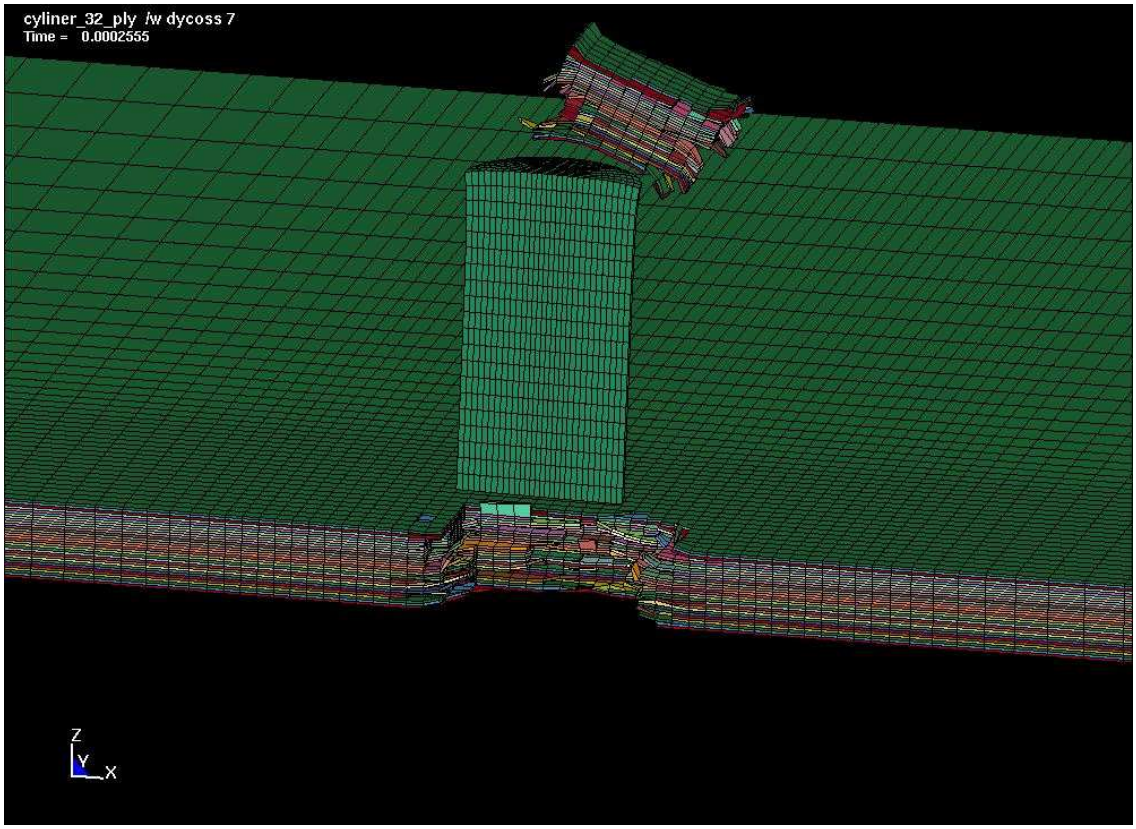

Figure 2.1: Ballistic impact simulation. The predicted response exhibits prominent shear plugging

ing to shear plugging [8, 9]. The studies showed that as the impactor moved into the high velocity regime, there was a reduction in debris mass that corresponded to the onset of shear plugging formation. At the back face of the target, material damage in the form of fiber breakage and fiber pullout was observed and was generally but not always confined to the periphery of the penetration area. Other investigations have found that severe delamination can occur at the back face of the laminate and extend by several times the diameter of the impactor [10]. The critical failure modes in the composite are greatly influenced by the strength properties of the fiber [11]. Shear plugging seemed to be the dominant failure mode for laminates made of low strength fibers, while extreme delamination was observed when high strength fibers were used.

Different failure mechanisms are triggered by a variety of factors such as the velocity of the impact, the strength properties of the composite and the laminate stacking configuration. Furthermore, coalesced failure modes can lead to bifurcations in the energy absorption response and unpredicted failure [12]. Significant effort has been devoted to the development of analytical models that can simulate the complex response of the composite as well as accurately predict the damage progression and failure of the material [13]. Currently, active research in this area involves not only improving the accuracy of the material model predictions, but also improving the computational efficiency of the models with practical applications in mind.

2.2 Analytical Models for Impact Applications

In order to develop more accurate composite material models that are suitable for high ballistic impact applications, it is important to correctly characterize the response of the polymer matrix materials commonly used in composites, which are known for their strain rate sensitivity [14]. It has been demonstrated that the deformation of the matrix constituent has a big effect in the overall response of the composite material. Zhang [15] showed that for high explosive composite materials containing small volume fractions of polymer binder (around 7 %), the strain response of the composite was highly dominated by the strain rate dependent deformation of the polymer.

In the last two decades, efforts have been made to develop constitutive models that capture the nonlinear deformation and strain rate sensitivity of the polymer material. In the earlier efforts, macromechanical approaches were predominantly used, due to their simplicity and computational efficiency. Sun and Chen [16] modeled the polymer

matrix elasto-plastic response using J_2 flow theory. Stress-strain curves for off-axis composites under tension were computed by using a micromechanical approach. However, the obtained curves were then used to develop a simpler macromechanical composite model. Tsai et al. [17] proposed a visco-plastic model that uses a one parameter plastic potential function proposed by Sun and Chen [18] that assumes little plasticity occurs in the composite longitudinal direction to model the nonlinear response of the composite. Espinoza et al. [19] proposed a 3-D anisotropic visco-plastic model for woven composites based on the quadratic yield function adapted by Sun and Chen [18] and incorporates thermal effects into the plastic flow constitutive equation. Ballistic numerical simulations were performed by using a contact model and mesh adaptivity in addition to the visco-plastic model.

A common approach to model the inelastic response of the polymer is to modify constitutive models originally used to represent the plastic and viscoplastic deformation of metals. Weeks and Sun [20] have developed models similar to those typically used to describe plasticity in metals, such as the Johnson-Cook model [21], to account for the strain rate dependency of the composite. Goldberg et al [22, 23] defines the effective inelastic strain of the polymer by employing a modified version of the Bodner-Partom viscoplastic model [24] commonly used for metals. The effects of hydrostatic stresses, which unlike metals can not be neglected, are included in the model by using associative flow rules such as the Druker-Prager yield criterion [25].

Alternative approaches have been investigated for modeling the composite response. Chen et al [26] implemented an anisotropic plasticity model using the smoothed particle hydrodynamics (SPH) methodology [27, 28]. In the model, the elasto-plastic model was coupled with an equation of state and failure criteria. Wang et al [29] investi-

gated the effect of different strain rates in the strength of unidirectional composites. In their approach, the composite was modeled as having multiple parallel fibers that satisfy a visco-elastic model that incorporates an elastic model coupled with a generalized Maxwell model.

In recent years, given the advances in computational technology, there has been a push to develop more complex models that accurately capture the physics of the material response. Micromechanical models are better suited to analyze phenomena such as localized failure of the constituents, strain rate sensitivity and creep [30]. Micromechanical approaches have been used to model the interaction between matrix and fiber and simulate the composite deformation under high loading scenarios. Tsai and Chen [31] implemented a viscoplastic model for composites under high strain rates that uses the generalized method of cells GMC [32] in order to model the individual constituents of the composite. The GMC method is an extension of the representative volume elements (RVE) method [33], intended to analyze more complex geometries than the RVE method, which is limited to relatively simple geometrical configurations. In this methodology, the domain is divided into subsections or cells, which allows for a detailed representation of the individual constituents. Zheng et al [34] implemented a micromechanical model based on the Goldberg et al. polymer model [22] into the commercial finite element software LS-DYNA [35]. Shell elements were used for computational efficiency and analysis of single shell elements were conducted to verify the composite model. Zhu et al [36, 37] implemented a 3-D micromechanical model where unit cell divisions are used to analyze composites subjected to high impact loading. The effects of transverse shear loading in the inelastic response of the composite and the strain rate dependency of the composite under different ply stacking sequences and loading/boundary conditions were investigated.

2.3 Predicting Failure in Composites

Different approaches are available to simulate the damage and failure of composites [38]: failure criteria, energy based damage growth, fracture mechanics, plasticity and damage mechanics. Stress-strain based failure criteria are among the most popular and are usually used in combination with fracture mechanics and damage mechanics approaches. Numerous failure criteria have been develop for composites, particularly under quasi-static conditions. However, they are still widely used for predicting the failure response of composites under a wide range of loading scenarios (including ballistic impact response) given the simplicity of their implementation. On the other hand, fracture and damage mechanic approaches are increasingly being used as analytical models allow for more complex and accurate representations of the material failure response.

2.3.1 Failure Criteria

For isotropic materials, the biaxial stress states in the material are represented by defining the failure envelopes, usually based on the principal stresses and final strengths. However, for composites, failure prediction is more complex, mainly because for orthotropic materials there is a directional dependency on the elastic properties, ultimate strengths and therefore the stresses [39]. Multiple failure criteria have been used for composites. Not all of them can predict the failure mode in the material, only that failure has occurred. Assuming plane stress conditions, the vast majority of the failure models require four independent elastic properties (the elastic moduli in the fiber and transverse directions, the in-plane shear modulus and the major Poisson's ratio) and five independent strengths (the tensile and compressive strengths in the longitudinal and the transverse

direction and the in-plane shear strength). Some of the most popular failure criteria employed in composites include the Maximum Stress and Strain Criteria [40], Hashin Criterion [41], and quadratic failure criteria such as the Maximum Work Theory or Tsai-Hill Criterion [42] and Tsai-Wu Criterion [43].

Among the leading theories of the last World Wide Failure Exercise [2], three well-known failure criteria were used to detect ply failure, namely the Maximum Strain failure criteria (Boggeti et al. [44]), Tsai-Wu quadratic failure criterion (Kuraishi et al. [45]) and Maximum Stress failure criterion (Zinoviev et al. [46], Puck et al. [47] and Cuntze et al. [48]). The Tsai-Wu failure criterion does not differentiate between fiber and matrix failure, so subsequent criteria were implemented in the Tsai model to distinguish between both types of failure [45]. Puck [47] and Cuntze [48] used the Maximum Stress criterion only to determine fiber failure. Both theories referred to matrix related failure as inter-fibre failure. Puck [47] used the Mohr failure criterion for brittle materials [49] to identify three separate inter-fiber modes of failure, namely, failure in transverse tension, moderate transverse compression and large transverse compression. Cuntze [48] uses stress invariants to define the basic failure conditions. Transverse tensile failure, fiber-matrix interface failure (assumed to mark the onset of failure) and wedge failure (failure of the matrix due to compressive transverse normal stresses) are all modeled using stress invariants and curve parameters that need to be determined from experimental test data. At least for first ply failure, the Tsai, Puck and Cuntze theories were found to predict failure envelopes with the most accuracy for several biaxial quasi-state loading scenarios.

All the previously mentioned theories used properties at the lamina level to define the failure envelopes. Even failure criteria that explicitly make a clear distinction between fiber and matrix failure (e.g. the Hashin failure criterion) use lamina average

properties to predict the failure of the respective constituent. Mayes et al. [50] implemented failure criteria that gather stress information at the constituent level. The general form of quadratic stress interaction failure criteria, such as Tsai-Wu and Hashin, was employed to develop individual constituent failure criteria that require constituent properties as opposed to composite properties. Mayes et al [51] compared the analytical predictions of the developed individual constituent failure criteria against predictions from Tsai-Wu and Hashin failure criteria and experimental data, and showed an improvement in the accuracy of the resultant failure envelopes, particularly with respect to the Tsai-Wu failure criterion. However, the model didn't rank among the leading theories in the World Wide Failure Exercise (at least for the studied load cases and composite configurations).

The interaction between the normal and shear stress states and their effect on the material failure strengths and failure envelopes has also been investigated. Quadratic based failure criteria address this issue (e.g. Tsai-Wu [43]). It has been found that for unidirectional composites, compression loads normal to the fiber direction actually increase the ultimate tension, compression and shear strengths of the lamina in the fiber direction. Off-axis loaded composites also show different yield stress behavior for positive and negative shear loading respectively [52]. Theocaris [53] developed an elliptic anisotropic failure criteria that seems to capture such material behavior, particularly for pure shear induced failure.

2.3.2 Damage and Fracture Mechanics

In composites, studies have suggested that stress-based failure criteria have problems associated with the scale of damage and therefore can not accurately predict the length of cracks in the damaged material [54]. Many commercial FEM codes include

damage scale factors to improve the accuracy of the failure criteria predictions. For that reason, damage mechanics constitute an attractive alternative to model damage in the composite, from onset to fully damaged material. The main advantage in this approach is that material properties can be degraded gradually, allowing for more realistic loss of stiffness, permanent deformation in the material and adequate response of the composite under unloading and reloading conditions.

The damage mechanics and fracture mechanics approaches have also been used to capture interlaminate failure modes in composite laminates, such as multiple delamination and single crack propagation respectively. One common problem involved in delamination predictions, is that modelling the inter-ply resin using finite elements can be computationally very expensive. Researchers have investigated delamination models for composites using the contact interface between shell elements to model the interlaminar failure, resulting in less computational cost. Damage mechanics approaches are used to simulate the interlamina failure by degrading stresses based on stress-strain criteria. Fracture mechanics are then used to define the contact interface by relating the energy dissipated during the delamination process with the material fracture energy [55].

Fracture mechanics approaches seem to be more accurate than failure criteria-strength of material based approaches to model delamination [56]. Failure criteria approaches have problems predicting the length of the cracks. However, fracture mechanics approaches also have problems predicting the grow of the cracks if the length of the crack is not known a priory. Many different parameters determine the type of damage on composite materials due to impact: material properties, geometry, laminate stacking sequence and impactor velocity among others. The velocity of the impactor (greater than 1000 m/s for high velocity impact) and the associated kinetic energy constitute the governing pa-

rameters that control the level and type of damage in the composite. More and more, analytical composite models rely on damage and fracture mechanics approaches due to their potential for describing the whole damage evolution in the material, from onset of failure to the fully damaged material.

Chapter 3

Methodologies for Uncertainty Propagation and Quantification

The stochastic nature of complex engineering systems is well documented in the literature. The outcome of problems such as buckling and crash analysis can vary largely due to small variations in initial conditions and model parameters, making it difficult to compared experimental results with computational simulations [57]. Uncertainties can be classified in two major groups [58]: reducible or epistemic (lack of information or knowledge regarding a particular phenomenon) and irreducible or aleatoric (fluctuations or irregularities in the material properties, problem geometry, boundary conditions and loading scenarios). The physical interactions that lead to large nonlinear responses are stochastic in nature (e.g. instabilities such as buckling and on-off contact of components). The variation experienced can be classified as irreducible uncertainty since it is physically driven rather than a product of the numerical simulation. Modeling and numerical errors (e.g. model assumptions, spatial and temporal discretization of the numerical solutions

and computer precision among others) can be classified as reducible uncertainty since it is possible to minimize their effect in the prediction.

Discussions abound in the uncertainty quantification community as to how best represent reducible uncertainties [59]. Some believe that probabilistic distributions are not the best mathematical representation for reducible uncertainties. Likewise, there is also debate on what exactly falls into the category of reducible uncertainty. It has been discussed if numerical errors that result from numerically solving equations constitute reducible uncertainty. Numerical errors arise in the solution of complex systems since partial differential equations (PDEs) need to be solved in an approximate way. Examples of numerical errors include spatial discretization errors introduced by finite element and finite difference methods, temporal discretization errors introduced by time dependent simulations and errors due to discrete representation of highly nonlinear features. Explicit distinctions have been made between reducible uncertainty (deficiencies in the analysis that result from a lack of knowledge) and errors (deficiencies in the analysis not due to a lack of knowledge) [59].

In order to account for the uncertainties present in large and complex engineering systems, three significant areas need to be addressed [58]: correctly characterize the model parameter uncertainties and variability in the external or environmental conditions; quantify the uncertainty of the analytical model itself and its propagation through large computational models; verify and validate the analytical models. A global uncertainty assessment consists of quantifying the individual and combined effects of aleatoric and epistemic uncertainties. In the context of uncertainty quantification as a means to improve analytical models, it is useful to formally introduce the concept of model validation and verification. Logan et al. [60] offers a definition of model validation and verifica-

tion: "In the world of the Finite Element Method (FEM) and computational analysis, it is sometimes said that verification means solving the equations right and validation means solving the right equations". The goal of any verification and validation exercise is to determine the level of adequacy of a given predictive capability while simultaneously defining what constitutes a tolerable or acceptable risk. Once the verification and validation process has been established, it is necessary to perform a reliability and risk analysis that can ultimately lead to better and well informed investment and trade-off decisions. Logan et al. [61] discuss possible formal methodologies that can be used to make an effective transition from verification and validation to quantification of risk reduction and confidence bounds for improved reliability.

3.1 Uncertainty Quantification Approaches

Uncertainty quantification methods have been widely used in engineering structural analysis to study the non-deterministic response of complex systems subjected to stochastic variations of parameters and system properties. Most of the work in the development of new computational probabilistic procedures has been focused on creating more efficient and cost effective techniques. A review of different techniques from computational stochastic mechanics and their application to different engineering problems was presented by Schueller [62]. Beer et al. [63] provided a brief overview of uncertainty quantification methodologies used in structural robustness design. Similarly, several approaches exist to formulate non-deterministic problems using reliability-based design optimization (RBDO) methods [64].

Three distinctive approaches for characterizing uncertainty can be identified [65]:

interval bounds, membership functions and probability density functions. Interval bounds constitute the simplest way of representing uncertainty. They are used to specify upper and lower bounds for the uncertainty (i.e. maximum and minimum values that input parameters can take). Membership functions provide better detail of the uncertain parameter distribution compared to interval bounds. Possibilistic methods [66] such as fuzzy logic use the information embedded on the membership functions to estimate the response of the system based on incomplete and/or uncertain data. Probability density functions constitute the foundation for the probabilistic analysis of uncertainties. It provides the most complete characterization of parameter uncertainties but requires more information about the real data distribution in order to select the appropriate statistical distribution. Uncertainty quantification approaches are generally classified into non-probabilistic methods and probabilistic methods. A brief overview of the most common methodologies is given next.

3.1.1 Non-probabilistic methods

Interval analysis, fuzzy logic and sensitivity analysis are among the main non-probabilistic methods employed to model uncertainty [65]. In interval analysis, uncertain variables are replaced by the variable's maximum and minimum possible values using interval bounds. Given its simplicity, it is used for problems that don't require a detailed description of the uncertain variable distribution. It is limited to simple problems that don't require a detailed description of the parameter distributions. Fuzzy logic is based on Fuzzy set theory [67]. The input uncertainty is defined through fuzzy variables and membership functions while the output response is represented by fuzzy sets using fuzzy algorithms. In possibilistic methods, uncertainty is represented by using a "distribution of

possibilities" instead of the traditional statistical distributions used in probabilistic theory [68]. Fuzzy logic incorporates the basic conception of "true and false" used in boolean algebra and expands it by allowing different degrees of true and false representations. The variable in question can take any real numerical value contained in the interval [0,1], which can be interpreted as being "more or less" true or false [69]. Sensitivity analysis uses sensitivity derivatives to determine critical parameters that may significantly affect the response [70]. Based on the respective sensitivities, the critical sources of uncertainty can be approximately estimated.

3.1.2 Probabilistic Methods

Probabilistic methods can be further subdivided into sampling based methods and non-sampling based methods. Sampling methods are computationally more expensive than non-sampling methods and include statistical measures such as mean and standard deviation to quantify the response of the systems, establish confidence bounds and provide reliability estimates. Non-sampling methods quantify uncertainty by using analytical rather than statistical means and are less expensive than statistical methods from a computational point of view. In stochastic finite elements (SFEM), the uncertain parameters can be characterized by using either sampling (e.g. Monte Carlo simulation) or non-sampling (e.g. perturbation methods) approaches [71].

Sampling Methods

There are several sampling techniques that can be found in the literature (e.g. simple random sampling [72], systematic sampling [73], stratified sampling [74] and cluster sampling [75]). Monte Carlo simulation, stratified sampling and Latin hypercube sam-

pling are among the most common used ones [76]. Monte Carlo simulation (MCS) is probably the most common (and simplest to implement) stochastic method. The optimal number of samples and simulations need to be determined in order to obtain high values of confidence in the simulations. Multiple random sampling approaches have been used in uncertainty analysis to improve results from crude Monte Carlo simulations (e.g. stratified sampling, adaptive sampling schemes and Monte Carlo Markov Chain methods). Instead of randomly sampling from the entire parameter distribution, such approaches systematically sample the space domain to obtain a uniform and representative group of values that truly reflect the variable distribution. In stratified sampling, the sampling space is divided into homogeneous sub-domains or strata that are individually sampled. The idea is to divide the population into groups that exhibit similar characteristics between them. Latin hypercube sampling (LHS) [77] constitutes a type of stratified sampling where parameter distributions are divided into equal intervals and a random sample is taken from each interval, following the parameter statistical distribution. More uniform representations of uncertain parameters can be obtained when compared to crude random sampling.

Non-Sampling Methods

Examples of non-sampling methods include moment methods (also referred to as perturbation methods) and stochastic differential equation methods. Moment methods are among the most widely and commonly used non-sampling probabilistic methods [78]. The first two moments of the parameter distributions are used to describe the input of the system and Taylor series expansions are computed around the moments to obtain the approximate moments of the output response. The first order reliability method (FORM) and the second order reliability method (SORM) are the best well known moment

methods. An advantage of such methods is that they only require the first moments of the input distributions. On the other hand, because higher order moments are typically ignored, nonlinear state functions can not be accurately represented.

Stochastic differential equation methods (SDE) characterize sources of uncertainty as random fields that can be directly model into the standard differential equations. The polynomial chaos method [79] represents an example of such type of methods. Uncertain quantities are explicitly modeled using Hermite polynomials to expand uncertain variables in the differential equation. The expansion terms can be interpreted as moments (e.g. mean and standard deviation) of the variable. For some applications, a significant reduction on computational cost and comparable reliability of the simulation was obtained when using the polynomial chaos approach instead of Monte Carlo simulation.

3.1.3 Alternative Approaches for Uncertainty Quantification

Probabilistic theory has been traditionally used to model uncertainty in many engineering applications. However, the representation of uncertain data by means of probabilistic methods has been criticized since it assumes previous knowledge on the uncertain data when selecting a probabilistic distribution [80, 81]. Typically, irreducible (aleatory) and reducible (epistemic) uncertainties are not treated separately, which has been shown to lead to an underestimation of the uncertainty levels, particularly when using uniform probability distributions to represent the uncertain data [82]. Therefore, one proposed way to improve uncertainty representation is to individually model each type of uncertainty. Several alternative methodologies have been developed in order to provide a theoretical

framework to incorporate uncertainties by addressing the probability theory shortcomings mentioned above. Helton et al. [83] provides a brief compilation of literature regarding the use of less orthodox methods to characterize epistemic uncertainties. Alternative theories include interval analysis, fuzzy set theory, possibility theory, evidence theory, statistical methods for imprecise data, theory of fuzzy random variables and theory of random sets, rough sets and clouds [84, 85, 86, 87, 88]. Although some theories such as evidence theory are still relatively new, they are starting to be used more and more in problems involving uncertainty data characterization.

The use of non-traditional models to address uncertainty has been considered not only to address the shortcomings of traditional probabilistic methods, but as a logical complement to the latter. At present, skepticism about non-traditional methods is still prevalent in the scientific community due to their alleged inability to correctly model uncertainties and the lack of appropriate numerical procedures to deal with large problems [88]. However, there is an increasing awareness about the capabilities of non-probabilistic and probabilistic/non-probabilistic (mixed) methods. Non-traditional methods have also shown potential for sensitivity analysis strategies capable of fully describing output response sensitivity. The addition of non-traditional methods to the pool of traditional methodologies benefits the design engineering process by making available a wider array of modeling options and providing further adaptability to a new set of problems where probabilistic methods may not be entirely suitable.

3.2 Model Validation Approaches

Comprehensive theoretical frameworks have been developed over the years to include uncertainty quantification analysis as an integral part of the engineering design process. Oberkampf et al. [59] proposed a general framework to fully model and simulate the response of complex systems by systematically identifying sources of uncertainty (irreducible and reducible) and numerical errors and coupling the methodology with a risk assessment procedure. Several phases are clearly identified, from the conceptual modeling of the problem to the numerical solution of the mathematical model.

Oden et al. [89] proposed a multi-scale modeling approach for estimating and controlling modeling error. The basic idea was to define a mathematical model capable of describing a physical system as accurately possible, but impossible or impractical to solve (due to complexity, computational cost and lack of input data). Such model was described as the base, or reference, model and it describes the problem at the smallest temporal and spatial scales (hence its inherent complexity). Next, a physical phenomenon or quantity of interest was investigated. Such quantity can be expressed as an optimal control problem, where the objective is to find a maximum or minimum of the quantity at hand, subjected to a constraint (in this case, the governing equation for the base model mentioned before). The base model may very well be intractable, and so is the optimization problem (also referred to as the dual problem). Alternatively, a surrogate model (a much coarser model that can be solved by using numerical approximations) was considered. The goal was to evaluate the error as the difference between two quantities: one obtained by using the base model (one can think of such model as the exact model) and the other obtained by using a surrogate (approximate) model.

Three major sources of error were considered: modeling error (use of simplified models that may not capture the problem physics entirely), discretization errors (use of discrete numerical approaches to numerically solve the phenomenon governing equations, such as finite element methods) and uncertainty errors (such as lack of data to appropriately characterize the model parameters). Modeling and discretization errors were computed by obtaining error estimators using residual functionals, as described in Oden et al. [90, 91]. The uncertainty error was obtained by using first-order perturbation theory. The three computed errors were then added together and the response of the system was bounded by a total error. The proposed methodology for estimating modeling error was demonstrated by different numerical examples, such as computation of error due to finite element approximations, modeling response of random heterogeneous materials and modeling of atoms based on molecular dynamics.

Bayes theory [92] has been used for model validation purposes. Rebba et al. [93] presented two validation metrics based on the Bayes factor. Given any observed data, the Bayes factor provides an estimation of how well the available data fits a particular model (or the likelihood of the data supporting a model better than other model) by taking the ratio of the relative probabilities of the observations with respect to the model(s). The first metric corresponds to validation given pass/fail data (e.g. estimating failure probabilities). For this case, the Bayes factor was found to be equivalent to evaluating the resultant or posterior probability density function (ratio between relative probabilities of data to models) at the predicted failure probability estimated by the model. The second validation metric corresponds to situations where the model predictions were compared against the observed response, such as displacements or strain measurements. In this case, the Bayes factor becomes the ratio of posterior (relative probability of the model prediction agreeing

with the data) to the initial probability density functions of the predicted response. For both cases, a Bayes factor greater than one suggests that the available data strongly agrees with the predictions. However, even for cases where the factor is significantly greater than unity, it is important to measure the modeling error. Different sources of errors may cancel each other, therefore providing a false sense of confidence in the model predictions.

The proposed error estimation methodology defined several sources of errors: Input data errors (due to assumptions and measurement errors in the input parameters) were estimated by using a first-order sensitivity analysis. Traditionally, this error is characterized as a random variable using a Gaussian distribution. Discretization errors are caused by approximations in the spatial and temporal discretization schemes such as finite element methods. The error was represented as a random variable by using the Richardson extrapolation method [94], which defines the error as a function of the difference between the coarse and fine mesh solutions and the mesh refinement ratio. The uncertainty quantification error corresponds to the sampling error introduced by the sampling methodologies such as Monte Carlo simulations or the truncation error inherent of response surface methods. The Richardson extrapolation method was used again for quantification purposes. The error in the measurement of output quantities (output measurement error) is typically assumed to be a random variable that follows a Gaussian distribution. The model form error (error introduced by the model itself) was computed by subtracting all the previously mentioned errors from the observation error (difference between observations and predictions).

Zhang et al. [15] used the Bayesian approach to incorporate parameter and model uncertainties into the fatigue reliability analysis. The Bayesian approach provides a framework that allows the incorporation of all sources of uncertainties (reducible and

irreducible) in the probabilistic analysis. Often in complex problems, model selection becomes an issue, due to the inherent uncertainty in the models and lack of experimental data. The Bayesian approach can be used to account for several possible parameter distributions and for different analytical models (eg. several crack propagation models in fatigue analysis) by a weighted averaging of their response. As new data becomes available, current information can be updated, allowing the reliability analysis to evolve towards the more accurate models and parameter distributions.

For complex engineering systems, it is common practice to make preliminary model validation at the component system level, using experimental tests under well controlled environments. However, for higher system level validation, experimental data is usually scarce or more difficult and expensive to obtain. Therefore, an alternative is to use component level test information to infer some measure of confidence at the system level. Jiang et al. [95] proposed a hierarchical model that integrates the Bayesian approach with structural equation modeling (SEM) to explore the use of component level data for model validation at system level. SEM is used to model the relationship between both computational model and system level data and lower/component and system level data. Latent variables (variables estimated from other measured or observed variables) were used to establish the link between lower level and higher level data. The Bayesian approach was used to estimate the SEM parameters and assess the validity of the computational model at the global system level.

3.3 Modeling the Response of Composites in the Presence of Uncertainties

Mechanical properties of composites are largely governed by the material properties of the fiber and matrix, fabrication process factors such as effective fiber volume and void volume fractions, fiber orientation misalignment and variable ply thickness [96]. Uncertainties exist not only in the material properties of the constituents but also in the manufacturing processes of composites: fiber misalignment may occur during layup; voids, resin excess, porosity, incomplete curing and uneven ply thicknesses are all difficulties encountered during curing of composites. As a result, uncertainties are also present in the resultant mechanical properties of composites.

The effect of model parameter uncertainties on the failure response of composites has also been investigated. Lyle et al. [97] showed that even small material model uncertainties can lead to large variations in the impact response of a carbon-carbon leading edge. It was demonstrated that the energy absorption upon impact can vary significantly due to inherent sensitivities of the structure to material modeling parameters. Analysis model and parameter model uncertainties can lead to large variations of energy absorption during progressive failure and have a substantial effect in the response robustness of laminate composites. Uncertainties in the material properties, fabrication processes and composite mechanical properties and material model parameters can be represented using uncertainty quantification approaches.

Different probabilistic methodologies have been implemented to include the effect of model and parameter uncertainties in the analysis of composites [98]. Such approaches can assist in the design process and risk assessment of composite structures by identifying

sources of uncertainty at the material, ply, laminate and structural levels. Chen et al. [99] validated a non-parametric probabilistic approach to investigate the dynamic structural response of sandwich composites in the presence of model uncertainties in the low and medium frequency ranges. Classical probabilistic methods such as Monte Carlo analysis have been used in conjunction with finite element methods to study uncertainties in composites. Sensitivity analysis was employed to determine critical material and design parameters.

Multilevel approaches can be particularly effective at systematically identifying high sensitivity parameters [100]: first, a hierarchical sensitivity analysis is used to identify critical components at different levels, namely micromechanical, ply, laminate, substructural and structural levels. Parameters which sensitivity can lead to failure initiation can be determined at this stage. The selected parameters were treated as random variables and a probabilistic analysis was employed to establish the variation range in the nonlinear response of the composite. Empirical fits, using methods such as the probability plotting method, were used to determine the statistical distributions of material properties [101].

Cederbram et al. [102] studied the reliability of composite laminates using first order and second order reliability methods. Zhao et al. [103] investigated the effect of multiple failure sequences in failure of composites. The laminate resembles a structural system made of multiple components that can fail as a result of certain failure sequence combinations. Mahadevan et al. [104] extended the latter approach by incorporating into the analysis a more realistic stiffness degradation that results from progressive failure of components in different modes. The first-order reliability method (FORM) was used to determine the component reliability. Critical failure sequences that can lead to laminate failure were identified by means of the branch and bound method. The overall system

failure probability is determined by the union of the critical failure sequence events. Liu et al. [105] extended the approach into a three-dimensional finite element methodology in order to estimate the ultimate strength failure of more complex composite structures.

Due to the large number of material, manufacturing and model variables that composites exhibit (all of them sources of sensitivity), classical deterministic optimization can result in either unsafe or too conservative designs. Different methodologies have been explored in order to include the effect of uncertainties in optimization of composites. Chao et al. [106] presented a design methodology to model the uncertainty introduced by manufacturing parameters such as ply thickness, fiber orientation and fiber volume fractions in the design optimization of laminate composites. The chance constrained programming technique [107] was used to convert the composite probabilistic problem into an equivalent deterministic one. Kim et al. [108] optimized the laminate ply stacking sequence for maximum bending stiffness and buckling load by using a two-level optimization procedure. Material uncertainties were introduced in the failure criterion by using the convex modeling approach [109] which only requires information on the bounds of the uncertain parameters as opposed to the probability distribution functions needed in stochastic approaches.

Anti-optimization has also been used along with traditional optimization via two-level approaches that exploit the effect of uncertainties at the lower level and use such information to optimize for best performance at the upper level. However, such approaches can be computationally very expensive. Techniques to address this issue have been studied. Liao et al. [110] added parameter uncertainty and sensitivities to the constraint formulation, which allows the solutions of the anti-optimization problem from an analytical rather than numerical point of view.

Chapter 4

Analysis and Model Parameter Uncertainty Investigation in Composite Laminates

Predicting progressive failure response in complex structures is challenging. Complex systems develop interactions in the physical response between components and between failure events at different scales that often lead to competing failure paths. The number of these paths increases as design and analysis model complexity increase. As a result, structural response may become highly unpredictable because small changes in geometry, loading, or material properties can completely alter the failure path. Composite structures exhibit such unpredictability. Composite materials increase the complexity of structural systems because they introduce many additional failure modes and exhibit failure responses across various length scales. Interactions among these failure mechanisms make prediction of progressive failure response difficult and challenging. Understanding

the physics and mechanisms that influence progressive failure predictability response of structural systems will enable researchers to develop efficient methods to design structures for robust and predictable failure. Design for predictable failure has applications in fail-safe structural design and design for crashworthiness.

In order to develop such methods, tests are needed to validate models and/or to obtain empirical constants to use in analysis models. It is difficult to extract useful information from tests when the failure response is not robust and predictable. Poor predictability, which is often attributed to lack of adequate modeling and analysis capabilities, has led to focused efforts to develop modeling capabilities that include improved constitutive models for materials, improved structural analysis methods to capture multi-scale failure phenomena, and more efficient numerical tools to increase model fidelity. These developments have enabled researchers to develop more accurate predictions. However, they have not addressed the problem of loss of predictability due to sensitivity. This is because these methods do not address the other major contributors to poor predictability: the structures inherent sensitivities to small variations. Furthermore, increased fidelity modeling of failure mechanisms often increases the number of possible failure modes and mechanisms. This increases failure sequence complexity, leading to multiple bifurcations that ultimately affect the failure response of the system. Validating increased fidelity models can be effective if one can identify test specimens that exhibit robust and predictable failure. Designs that have robust and predictable progressive failure will be insensitive to small design variations, small variations in test conditions, and prediction model uncertainties.

In our previous research we investigated factors that affect robustness and predictability of progressive failure response of optimized composite laminates (Venkatara-

man and Salas [12]). We demonstrated that the presence of competing failure sequences lead to bifurcations in the progressive failure response of optimized composite laminates when they are subjected to small random design variability. Methods to eliminate competing failure modes and improve failure predictability were demonstrated and implemented in the laminates optimization. Various laminate designs that were optimized for high energy absorption and exhibit a robust and predictable progressive failure response were obtained.

The only source of uncertainty considered in the above work was variability in ply orientation angles. Optimized laminates with competing failure modes are sensitive to even very small variability (standard deviation of 0.1 about their mean values). Eliminating competing modes that appeared when small variability was introduced was sufficient to make the designs progressive failure robust and predictable even for large ply angle variations. The optimizations for predictable and robust failure were performed using the Tsai-Wu failure criterion and empirical models for ply stiffness degradation. These phenomenological failure criterion and empirical stiffness degradation models are known to have deficiencies. A natural question that arises is, how valid or useful are designs optimized for performance and predictability when there are uncertainties in the failure model used? We address this question in this section.

The effect of model uncertainties on failure response of composite materials has been investigated. Lyle et al [97] investigated the effect of small model uncertainties in modeling the impact of a carbon-carbon leading edge. They showed that small material modeling uncertainties lead to large variability in the nonlinear and transient displacement responses during impact. For the non-linear impact problem, the transient energy response during impact was shown to exhibit bifurcations that lead to very large differ-

ences in energy absorption during impact. Therefore, it is important to consider model uncertainties when investigating robustness and predictability.

All failure models have weaknesses. Their deficiencies can be characterized as modeling uncertainties. A dilemma exists on how to represent such model uncertainties. It can be argued that because model uncertainties are not inherent, variability can often be reduced. Therefore, they should be treated as errors and not uncertain probabilistic variables. Proponents of this argument have used interval methods to estimate predictable changes that can be expected in the response as a result of the models limitations or uncertainty. An opposing argument to this is that there are various sources that lead to model deficiencies and their cumulative effect can be well represented as a probabilistic uncertainty. We use this latter approach.

A composite laminate example under uniaxial loading is used in our investigation. The energy absorption statistics of several optimized laminate designs subjected to ply angle variability are first presented in order to establish a reference point for laminates analyzed with model uncertainties. The progressive failure response of the laminate examples is analyzed in the presence of model uncertainties and energy absorption measures are computed to help quantify the effect of model uncertainties in the failure predictability of the laminates. Model uncertainties are present in the model parameters (where the parameter exact value is not known) and the model itself (differences when compared to experimental data). We identify the range of differences between model prediction and test results and assume that the response is uniformly distributed in this range. It is demonstrated that although the distribution selection is arbitrary, it is nonetheless quite useful to understand the effects of model uncertainties on failure predictability and robustness. Finally, the composite laminate is optimized using a reliability optimization

procedure where both model uncertainties and variability are included. The progressive failure and energy absorption of the optimized laminate are compared against those that were not optimized taking into account model uncertainty effects.

4.0.1 Sources of Model Uncertainty in Progressive Failure Analysis

Several sources of model uncertainties exist in progressive failure analysis of laminated composite structures. These include uncertainties in models used for calculating the elastic stiffness of a composite material based on its constituents, uncertainties in the recovering ply level stresses from the laminate response, uncertainties in the failure criterion used to detect failure of a ply, uncertainties in the models used to detect ply failure, and uncertainties in the models used for stiffness degradations after partial ply failure. These types of model uncertainties (i.e. models parameter uncertainties and uncertainties of the model itself) are discussed below with respect to classical lamination theory analysis, The Tsai-Wu failure criterion, and a discrete ply discounting method for stiffness degradation. The model uncertainties are characterized using the experimental validations of the composite failure prediction models that were evaluated in the world wide failure exercise comparisons.

Model uncertainty in stress prediction

The WWFE results found that prediction accuracy was poor when the ply is loaded by dominant shear [111]. It was argued that in the presence of dominant shear loading the elastic response of the ply is significantly non-linear and therefore the stresses obtained using linear classical lamination theory analysis lead to uncertainties in ply level

stresses. The stress uncertainty is included only for the failure criterion evaluations. The stress uncertainty in the form of a small random variable is added to the ply level stresses that were calculated from the linear classical lamination theory analysis.

Model parameter uncertainty in failure criterion

In our previous work investigating failure predictability of composite laminates [12, 112] we used a classical lamination theory for calculating stiffness and recovering ply level stresses, the Tsai-Wu phenomenological failure criterion for failure prediction, and a discrete ply degradation scheme to reduce stiffness after failure in matrix, shear and fiber modes. The Tsai-Wu criterion (Equation 4.1) used to predict ply failures is as follows:

$$\begin{aligned} &F_1\sigma_1 + F_2\sigma_2 + F_{11}{\sigma_1}^2 + F_{22}\sigma_2^2 + F_{66}\tau_{12}^2 + 2F_{12}^*\sqrt{F_{11}F_{22}}\sigma_1\sigma_2 = 1 \\ &F_1 = \left(\tfrac{1}{X^T} + \tfrac{1}{X^C}\right), F_2 = \left(\tfrac{1}{Y^T} + \tfrac{1}{Y^C}\right), F_{11} = -\tfrac{1}{X^T X^C} \\ &F_{22} = -\tfrac{1}{Y^T Y^C}, F_{66} = \left(\tfrac{1}{S}\right)^2, F_{12}^* = -\tfrac{1}{2} \end{aligned} \tag{4.1}$$

where $\sigma_1, \sigma_2, \tau_{12}$ are the ply level stresses along fiber direction, transverse to fiber direction and in-plane shear stresses, respectively; X, Y and S are the lamina strengths in the fiber direction, transverse to fiber direction and in shear, respectively, and the superscripts T and C denote tension and compression, respectively. Comparisons of test data for different composite materials reveal that uncertainties exist in the empirical parameters of the Tsai- Wu failure criterion biaxial stress interaction term F_{12}^*. The values of F_{12}^* vary in the range from -1 to 0 (see Table 1, Liu and Tsai [113]) for different materials. Use of this term in the failure criterion accounts for the interaction of the ply-level biaxial stress (stress along fiber and stress transverse to fiber direction). A value

of zero indicates that there is no interaction (leads to Tsai-Hill failure criterion). A value of -0.5 is used by default since this lies in the range of values observed from test data.

Model parameter uncertainty in material elastic stiffness degradation

Composite materials made from fibre-reinforced polymer matrix exhibit different failure modes. When ply failure is detected, a determination of the failure mode is made. The elastic properties of the ply are reduced depending on its failure mode. A ply material can carry loads after it fails in one or more modes until failures completely eliminate the materials elastic stiffness. Modeling uncertainties exist in procedures used to determine failure modes and in the schemes used to degrade the stiffness and strength properties of the laminate after the failure.

The degradation model proposed by Kuraishi et al [111] for use with the Tsai-Wu criterion in progressive failure has only two modes of failure specifiedmatrix failure mode and fiber failure mode. In this scheme, when ply failure is detected, the matrix dominated properties are degraded first. It is assumed that the matrix develops micro-cracks that degrade the stiffness and strength properties. The stiffness and strength properties of the ply detected for failure are reduced as follows: the modulus of the matrix material, the dominant Poissons ratio, and the biaxial interaction term F_{12}^{*} are reduced to 15% of their original values. The modulus of the ply transverse to the fiber direction and the shear modulus are calculated using the reduced matrix modulus. The compressive strength is reduced by a factor defined as a function of the shear modulus reduction $\left(G_{12}/G_{12}^{0}\right)^{n}$, where the value of n is an empirical constant assumed as 0.1. The ply analysis is repeated to re-establish equilibrium and ply level stresses are computed after degradation. If the same ply becomes critical again, its fiber properties are degraded. When fiber failure

mode is detected, all elastic moduli and the Poissons ratio are reduced to 1% of their original values. The 15% reduction of matrix properties is based on empirical validation with test data. In the WWFE exercise, the authors varied the value of ply transverse to fiber direction modulus and the shear modulus between 10 and 20% to correlate their model predictions with test results.

A variation of this degradation scheme has been suggested and tested by Padhi et al [114]. Since the Tsai-Wu failure criterion is not a failure-mode based failure prediction criterion, the terms of the criterion are separated to define failures in matrix, matrix-shear and fiber modes. The mode of failure is determined by identifying the dominant term (one with the largest absolute value) in the failure criterion (Equation 4.2):

$$\begin{aligned} FiberFailure &: F_1\sigma_1 + F_{11}{\sigma_1}^2 \\ MatrixFailure &: F_2\sigma_2 + F_{22}\sigma_2^2 \\ ShearFailure &: F_{66}\tau_{12}^2 \end{aligned} \tag{4.2}$$

Once the failure mode is detected, the ply properties must be degraded. A simple discrete ply discounting method was used to degrade ply properties. In this procedure for ply failure in shear failure mode, G_{12} (Shear Modulus) and ν_{12} (Poisson's ratio) are degraded to 0.1 and zero respectively; for ply matrix failure mode, $E2$ (Elastic Modulus in the matrix direction) and ν_{21} (Transverse Poisson's ratio) are reduced to 0.1 and zero respectively; and for fiber failure mode $E1$ (Elastic Modulus in the fiber direction), $E2$, ν_{12} and $G12$ are all reduced to zero. Such a ply discounting method has been used for progressive failure analyses [115] where the mode was detected using the Hashin failure criterion [41] and shown to compare well with experiments. In the discrete ply discounting method, ply properties are reduced almost to zero when failure is detected (it is set to a

small value to avoid numerical singularities in the analysis). However, in reality the properties do not go to zero. The actual degradation depends on the level of micro-cracking. Simple laminate analysis cannot capture micro-cracking. As a result, the degradation level is a source of model uncertainty. Including more detailed micro-mechanics or physics based progressive failure models can help to reduce this uncertainty.

4.0.2 Modeling Uncertainty Included in Progressive Failure Robustness and Predictability Investigations

In our investigation of the effects of model uncertainty on progressive failure predictability and robustness, we included the parameter uncertainty in the biaxial stress interaction term F_{12}^{*} and the stiffness degradation factor (E_m) for stiffness terms after matrix and matrix-shear failure modes and the model uncertainty in stresses when the ply is predominantly loaded in shear. The range in which different parameters that contribute to model uncertainty were varied was based on results from the Tsai-Wu progressive failure model [111]. The uncertainty in the interaction term of the Tsai-Wu failure criteria was modeled using a uniform distribution in the interval -0.1 to -0.6. The commonly used (or nominal value) is -0.5. The matrix degradation factor that is used to model the reduction of transverse and shear stiffness is assumed also to have a uniform distribution ranging from 0.01 to 0.15. This implies that strength reductions can range from 85% when the degradation factor is equal to 0.15 and 99% when the degradation factor is equal to 0.01. Failure envelopes have shown to be particularly sensitive to changes in this parameter. A small model uncertainty is added to the ply level stress predictions. It is assumed that the uncertainty in the ply stresses are small when the ply level loading is in plane, with

normal stresses in the fiber and transverse to fiber direction. For this case we add a small uniformly distributed uncertainty within ±1% of its present value. When ply loading is predominant in shear, a uniformly distributed uncertainty of ±5% is introduced. The values assumed for the investigations are conservative estimates of the variations observed in the test-model correlation results.

Two options are available for implementing the above model uncertainties. The first option is to vary the model uncertainties every time a new laminate is analyzed. The second option is to vary the model uncertainties every time a stress calculation is performed or ply failure is checked and plies are degraded within a laminate. The first option assumes that the model uncertainty is a material property and does not change with stacking sequence. The latter approach accounts for the in situ variations of failure behavior and material stiffness degradation. Both methods are implemented and compared in our investigation. In both cases the stress uncertainty is varied from ply to ply.

4.1 Laminate Designs Optimized for Predictable Failure in the Presence of Design Variability

In our previous research [12, 112] we investigated the effects of ply angle variability on progressive failure predictability and energy absorption robustness of laminate designs. Here we briefly review the demonstration problem chosen, the optimization performed, reliability analysis procedures used, and the designs obtained.

Table 4.1: Elastic Properties of AS4/3501-S Graphite-Epoxy Material

Elastic Properties of the Material	(GPa)
Elastic Modulus in the fiber direction ($E1$)	126
Elastic Modulus in the matrix direction ($E2$)	11
Poissons ratio (ν_{12})	0.28
Shear Modulus ($G12$)	91.5

Table 4.2: Maximum Strengths of AS4/3501-S Graphite-Epoxy Material

Maximum Strengths of the Material	(Mpa)
Maximum tensile stress in the fiber direction (σ_1^T)	1738.8
Maximum compressive stress in the fiber direction (σ_1^C)	1486.8
Maximum tensile stress in the matrix direction (σ_2^T)	48.4
Maximum compressive stress in the matrix direction (σ_2^C)	220
Maximum shear stress in the 1-2 plane (τ_{12}^F)	136

4.1.1 Laminate Design Problem Chosen for Investigation

The progressive failure of a 48-ply symmetric and balanced composite laminate subjected to uniaxial tensile strain was chosen as an example for failure predictability investigation. A progressive failure analysis procedure was developed to compute the load versus strain history and energy dissipated by the progressive failure of the laminate plies. Details of the progressive failure methodology used are presented in Reference [12]. The properties of AS4/3501-S graphiteepoxy material used for the calculations are listed in Tables 4.1 and 4.2. The ply thickness is assumed to be 0.125 mm.

The effects of small random design variations, namely the changes in ply angles, on robustness of energy absorption and predictability of the failure sequence were investigated. Robustness was calculated by performing a Monte Carlo simulation (MCS). The MCS generates 1000 random variations of the design in which ply orientation angles are perturbed by small normally distributed random amounts. Progressive failure analyses are carried out for the 1000 samples. In the progressive failure analyses, the degraded stiffness

properties are reduced to 0.1% of their original values. The changes in the progressive failure response (failure sequence) are quantified by the changes in energy absorbed (or dissipated) during progressive failure. The mean, the standard deviation and the fifth percentile value of the energy absorbed by the 1000 samples are computed. The fifth percentile value of the energy absorption ($E_{0.05}$) corresponds to the fiftieth smallest energy absorption from the 1000 samples. This value when used as a design limit ($E \geq E_{0.05}$) will be satisfied with 95% reliability.

4.1.2 Optimum Designs of Laminates for Predictable Failure Under Ply Angle Variability

Figure 4.1 presents a summary of the energy absorption performance of different optimized designs for ply angle variations with zero mean and standard deviations of 0.1° and 1.0°. The variations in energy absorption are assumed to reflect the variations in laminate progressive failure sequence. The analyses of the designs in Figure 4.1 were performed using a degradation scheme that reduces failed ply properties to 0.1% of their original values.

To establish a reference case, a 48-ply quasi-isotropic laminate having a stacking sequence $[(0/30/60/90/-60/-30)_4]_s$ was chosen for the progressive failure analysis (design 1, Figure 4.1). The variability of the energy dissipated during failure remains low when small random variations are introduced to ply angles. The energy absorbed by the nominal design (no variability) was lower than the mean value of the energy absorbed by the designs with imperfections. The laminate stacking sequence of the 48 ply balanced symmetric laminate was optimized for maximum energy using a genetic algorithm [12].

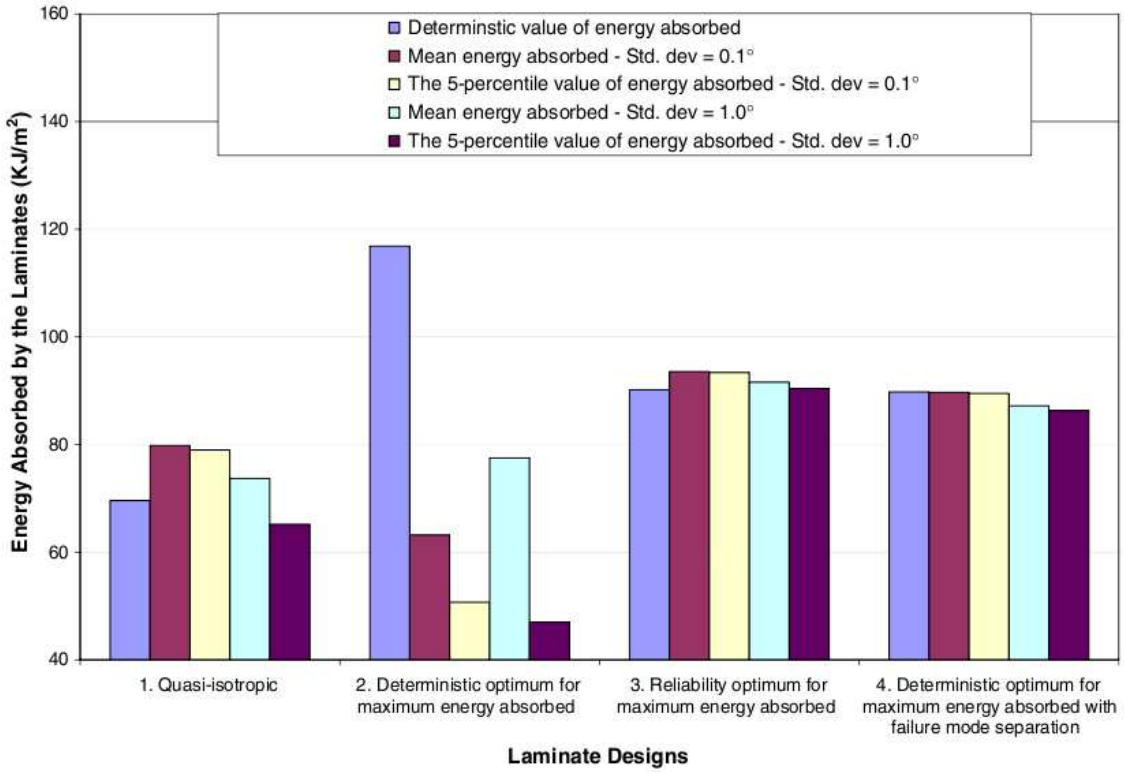

Figure 4.1: Summary of the energy absorption characteristic of different laminate design when subjected to ply angle variations of different magnitude

The optimum design found with stacking sequence $[\pm 15_7/\pm 30_4/\pm 45]_s$ (design 2, Figure 4.1) exhibited multiple bifurcations in the progressive failure sequence and led to different competing failure paths (Figure 5, Venkataraman and Salas [12]). Investigating the cause for bifurcations revealed that the optimization coalesced multiple failure modes, which resulted in competing failure paths and bifurcations in the progressive failure response. A deterministic optimization to maximize energy and separate competing failure paths was performed using a constraint that enforced a specified minimum strain increment between consecutive failures of different modes during the progressive failure. The optimum design obtained had a stacking sequence of $[0_{16}/\pm 30_3/90_2]_s$ (design 4, Figure 4.1). The use of a strain separation constraint to eliminate competing failure modes was found to be effective in eliminating competing failure paths and led to predictable failure response and

robust system response. The failure response of this design was compared with a design optimized for robustness using a reliability optimization (design 3, Figure 4.1). The reliability optimization maximized the 5th percentile value of energy absorption found using a Monte Carlo simulation of sample size 100, where ply angles are randomly varied (with zero mean and a standard deviation of 1.0°). The reliability optimization found an optimal laminate with stacking sequence $[0_{18}/\pm 30/\pm 45/\pm 60]_s$. It was determined that failure mode strain separation was a sufficient but not necessary condition to eliminate competing failure modes.

4.2 Reliability Analysis of Laminates with Ply Angle Variations and Model Uncertainty

In this section we present the results of the reliability analysis of laminates subjected to material uncertainties and ply angle variations. The various designs from the previous section that were either analyzed with ply angle variations or optimized for ply angle variations are analyzed here including model uncertainties. The goal is to understand the effect of model uncertainty on the robustness and predictability of the progressive failure response and to understand its interaction with design variability (ply angle variations). To investigate the effect of model uncertainty on progressive failure response, a Monte Carlo simulation with 1000 samples was performed. Design variability was considered in the form of ply angle variation having zero mean and standard deviation of 1.0°. The model uncertainties were treated as uniformly distributed random variables as discussed in Section **??**. Two options of varying model uncertainties, namely varying the biaxial stress interaction term F_{12}^* and the stiffness degradation factor E_m from laminate

to laminate and from ply to ply were implemented and compared. For the first case random values of the uncertainty in the stress interaction term F_{12}^{*} and the matrix stiffness degradation factor E_m were generated at the beginning of a laminate analysis and kept constant for all plies within the laminate. In the latter, random values for F_{12}^{*} and E_m were generated for each ply. Small uncertainties were introduced to each ply stress prediction, as discussed in Section **??**, regardless of the type of approach used (model uncertainties varied for each laminate or for each ply) and only depended on the nature of the lamina stresses.

4.2.1 Quasi-Isotropic Laminate

In the earlier analysis it was shown that the quasi-isotropic laminate exhibited little sensitivity to small ply angle variations and resulted in robust and predictable progressive failure. Figure 4.2 shows the statistics of the energy absorption for the quasi-isotropic laminate when subjected to individual and combined model uncertainties and ply angle variations. In comparing the response of the laminate when subjected to ply angle variations (Figure 4.1) with that when subjected to model uncertainties (Figure 4.2), it was found that although the laminate is slightly more sensitive to model uncertainties, the overall failure response does not significantly change.

Varying model uncertainties at the laminate level lead to larger variances in the energy absorption statistics. This is because when the model uncertainties are varied at the ply level within a laminate, the effect of the variations of ply level model uncertainties can cancel each other, whereas when the model uncertainty is kept constant for all plies it tends to over amplify the effect. A surprising result in Figure 4.2 is that of the effect of stiffness degradation uncertainty. The baseline laminate was analyzed with a degradation

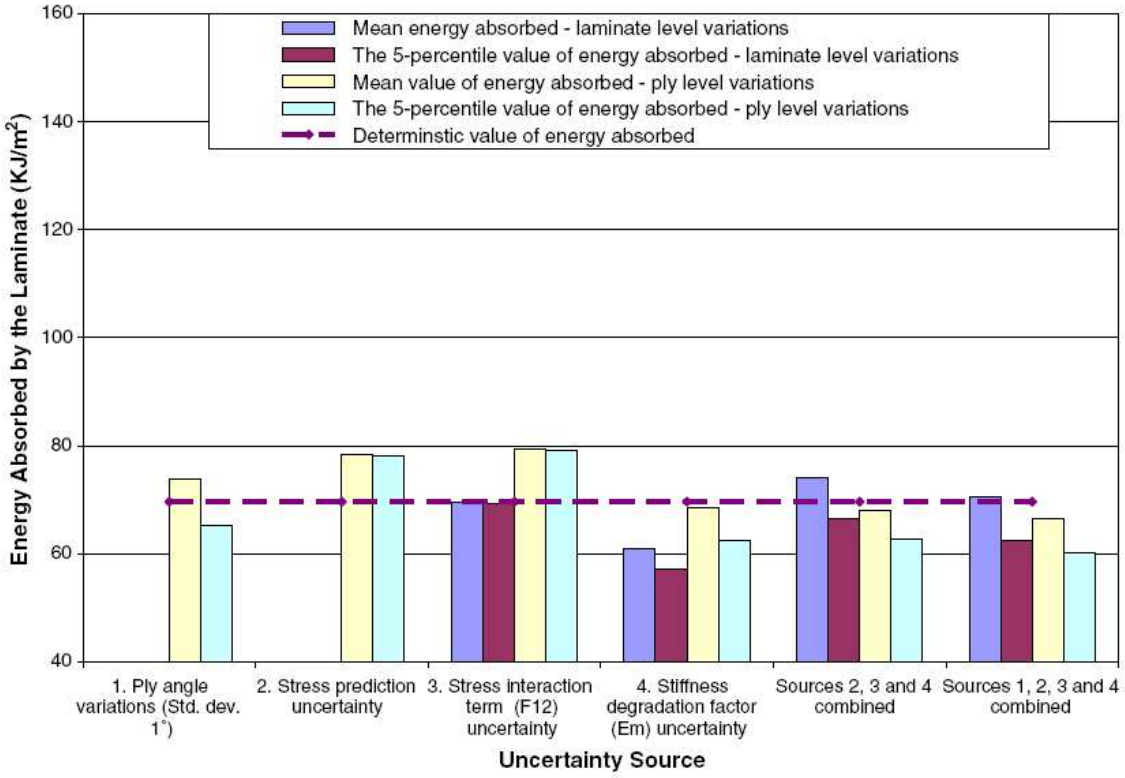

Figure 4.2: Effect of model uncertainties on the progressive failure energy absorption characteristic of a $\pi/6$-quasi-isotropic laminate

scheme that reduces the stiffness properties of the failed plies to 0.1% of their original values. However, for the investigations into model uncertainty, the ply stiffness degradation factor is only varied from 1% to 15%. This degradation scheme results in greater residual ply stiffness for the laminates analyzed for model uncertainty compared to the laminate in the baseline deterministic analysis. The higher elastic stiffness usually leads to increased energy, except in this case where it leads to lower mean energy and 5th percentile value. The uncertainty in ply level stresses has a significant effect on this design. This is because the laminate has many off axis plies that have significant shear loading, for which the ply level stresses were assumed to have uncertainties.

The variance of the energy absorption increases as more uncertainties are included, indicating that they have an additive effect on the variability of the progressive

failure response. However, this is not the case with the 5th percentile energy absorption or the mean. Small ply angle variations and stress uncertainties lead to increases in the mean energy absorbed, while the stress interaction uncertainty and the stiffness degradation uncertainty lead to decreases in mean energy absorption. It is more important that uncertainties are well-characterized when they have cancelling effects, than when they are additive because the response that appears to be more robust is now sensitive to the uncertainty assumptions made. The quasi-isotropic laminate is a robust laminate design and the effect of model uncertainties and ply angle variations on the energy absorption are small. In the next section we analyze a laminate whose progressive failure response is more sensitive to design variations and model uncertainty.

4.2.2 Laminate Obtained from Deterministic Optimization for Maximum Energy Absorption

When investigating effects of model uncertainties and design variability (e.g. ply angle variations) it is desirable to have a laminate that is sensitive to both sources of uncertainties. A design that is sensitive to small changes amplifies the effects of uncertainties and variability and makes it easier to understand the mechanisms and physics that lead to different failure responses. For this reason we choose from our previous study [12] a laminate that was optimized deterministically for maximum energy absorption in progressive failure. Here we investigate the effect of model uncertainties on this design.

Figure 4.3 shows the statistics of energy absorption for the deterministically optimized laminate when it is subjected to individual and combined model uncertainties and ply angle variations. Figure 4.4 shows the progressive failure of the laminate when

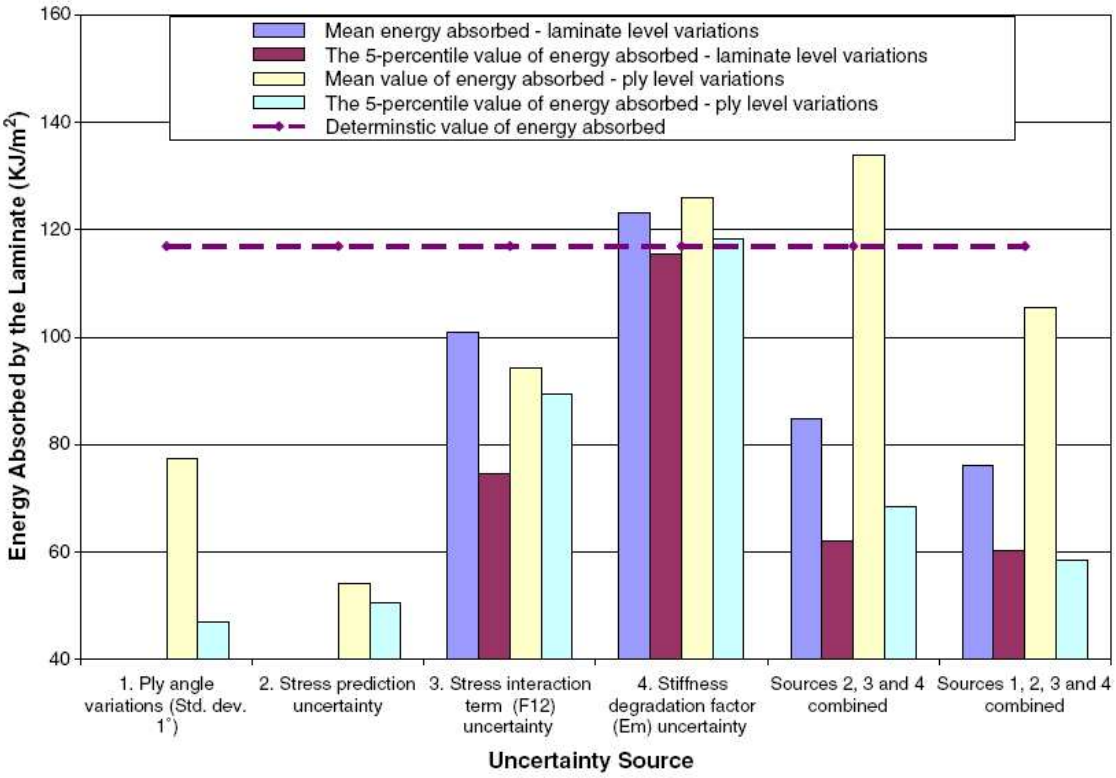

Figure 4.3: Effect of model uncertainties and design variations on energy absorption statistics for the laminate deterministically optimized for maximum energy absorption

individual and combined model uncertainties are introduced.

The design is sensitive to all model uncertainties, showing the most sensitivity to stress uncertainty followed by stress interaction term (F_{12}^{*}) uncertainty. The stress and terms uncertainties change the order of failure of the competing plies, leading to different failure sequences and load distributions and therefore different energy absorptions. The stiffness degradation factor E_m uncertainty has the least effect. In this example, the mean energy absorption of the laminate increases by a small amount when the E_m uncertainty is introduced. This can be explained as follows. The stiffness degradation uncertainty has smaller effect on the change in the failure sequence. The variations in energy absorption are a result of the change in the residual stiffness of the failed plies after matrix and shear failures. The change in stiffness does not change the failure sequence but affects the

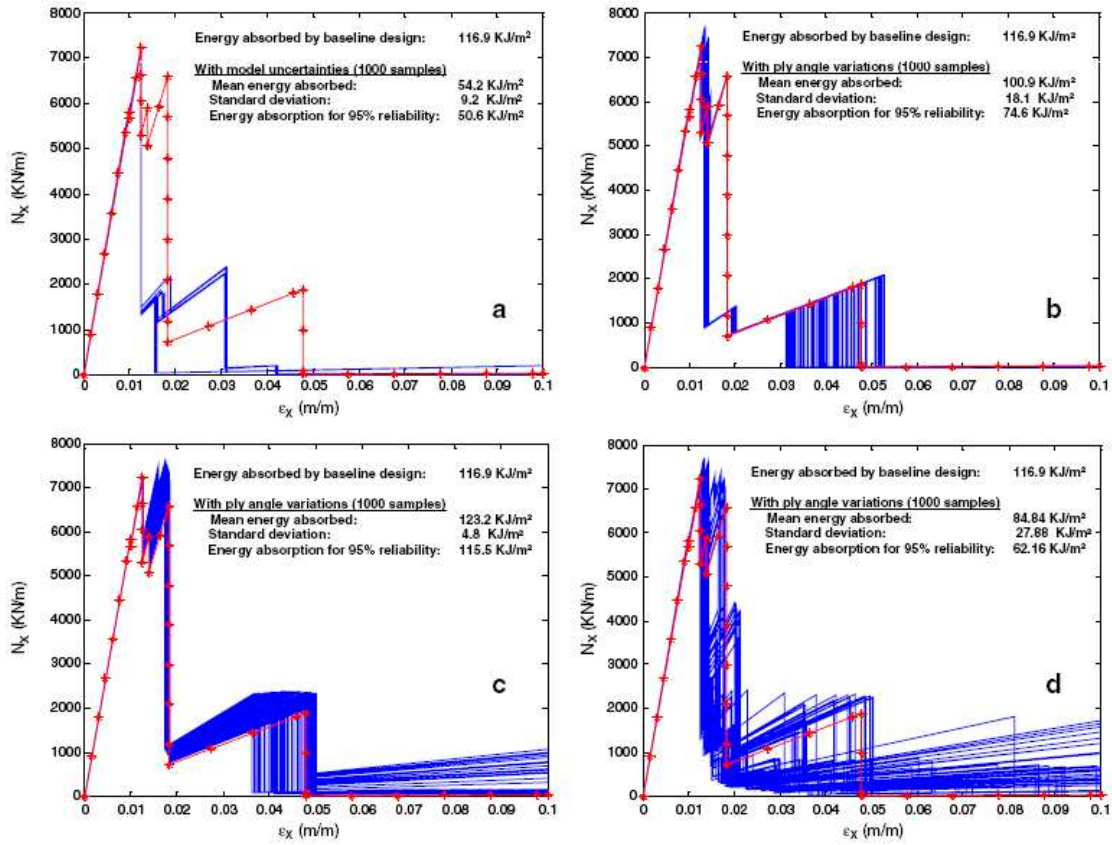

Figure 4.4: Progressive failure history for laminate optimized for maximum energy absorption with model uncertainties (varied from laminate to laminate). The progressive failure response of 100 MCS samples is shown for the design analyzed with (a) ply stress uncertainties (b) Failure criterion interaction term F12 uncertainties (c) stiffness degradation factor Em uncertainties (d) all model uncertainties combined. The line with asterisk marks represents the progressive failure of the design without any model uncertainty. The solid lines represent the progressive failure of 100 laminates analyzed with model uncertainties

resulting load redistributions after failures. This affects the load or laminate strain level at which next failure occurs. The improvement in energy absorption is due to the fact that, for the baseline design, the stiffness degradation used reduced the stiffness properties corresponding to the failure modes to almost zero (0.1% of the original properties value to avoid numerical problems). For the reliability analysis, the stiffness degradation factor was assumed to be a random variable that ranges from 0.01 to 0.15. The degraded stiffness ranges from 1% to 15% of the original values. The degradation performed for the baseline

design is a worst case degradation scenario. When all the sources of model uncertainties are combined, the statistics of the progressive failure response of the laminate (mean and 5th percentile value) are bounded by the values obtained by varying the ply stresses (lower bound) and the matrix degradation factor (upper bound) independently. This indicates that the effects of individual model uncertainties and design variability can negate each other.

Figure 4.5 shows the strain energy history of the deterministic optimum laminate when subjected to all model uncertainties varied at the laminate and ply level. The energy absorption histories indicate that there are at least two or three clusters of final energy absorption response. Many laminates also reach ultimate failure (lines ending vertically in the energy history) before reaching the 10% strain when model uncertainties are introduced. This was not the case when only ply angle variations were investigated.

In general, varying the modeling uncertainty in F_{12}^{*} and E_m at the ply rather than laminate level leads to smaller variance in the progressive failure energy absorption response. This is because when F_{12}^{*} and E_m are varied at the ply level, contributions of extreme variations are restricted to a single ply and therefore have a smaller effect. Further, the effect of uncertainties in the plies may have negating effect on each other thereby providing a robust laminate response. When model uncertainties are kept constant for all plies as in the case when variations occur at the laminate level, the extreme values of the model parameters that are encountered during the Monte-Carlo Simulation are applied to all plies. This amplifies the effect of model uncertainties. Varying model uncertainties at the ply level leads to a smaller variance. However, the presence of competing failure paths becomes more evident (Figure 4.5b).

Another important point is to correctly characterize the effect of each model

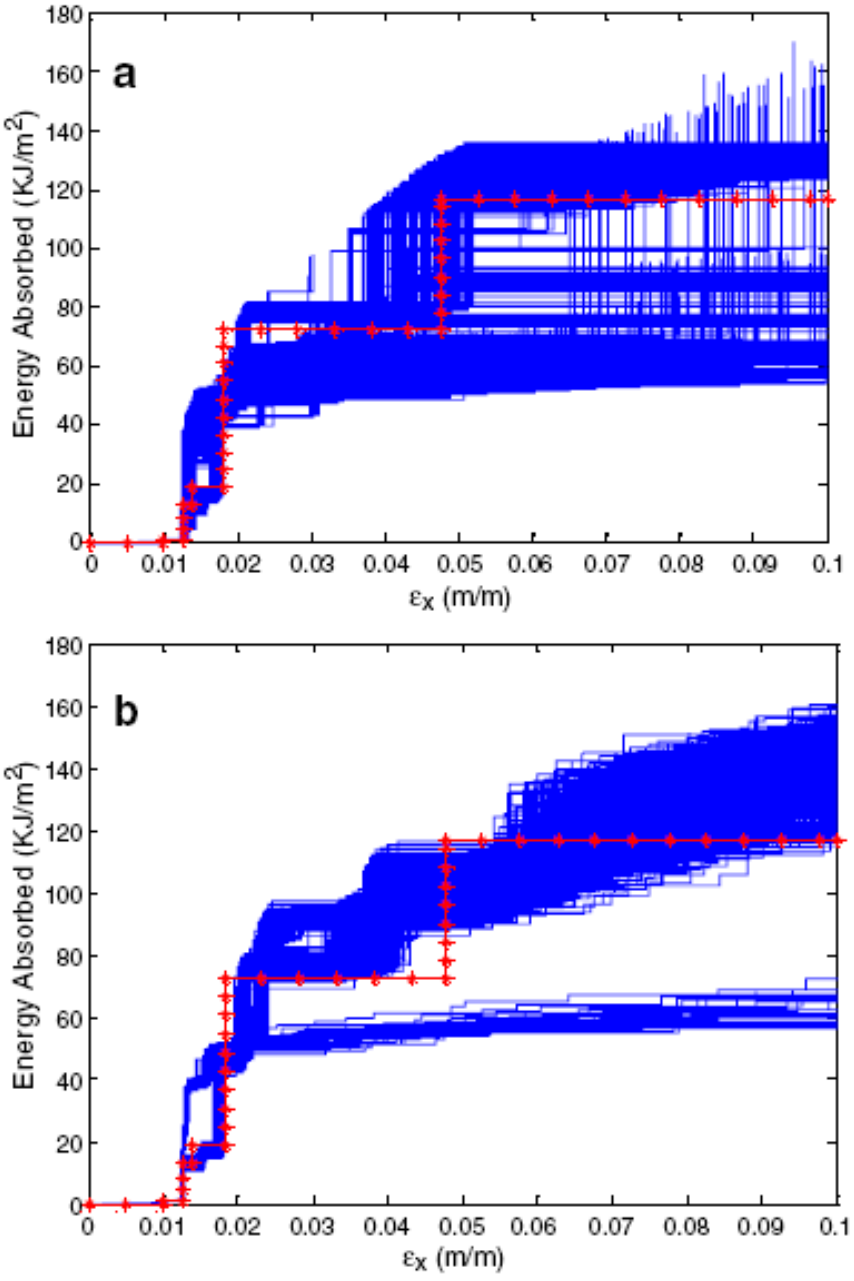

Figure 4.5: Strain energy absorption history for laminate optimized for maximum energy absorption with all model uncertainties included varied from (a) laminate to laminate (b) ply to ply. The line with asterisk marks represents the strain energy absorption of the design without any model uncertainty. The solid lines represent the strain energy absorption of 100 laminates analyzed with model uncertainties

uncertainty source individually. As seen from Figure 4.3, not all model uncertainties have an additive effect. Some model uncertainties have cancelling effects on each other when combined together. For the examples investigated in this section, the robustness and predictability of progressive failure response when subjected to all model uncertainties and variability combined is better than when subjected to some of the individual uncertainties, which means that for this case in particular, model uncertainties must be well characterized, since a false sense of security may arise by judging only their combined effect. Focusing exclusively on improving model and analysis capabilities is not enough. Model uncertainties must be correctly characterized and their effects must be taken into account in the design process.

4.2.3 Laminate Obtained from Optimization for Maximum Energy Absorption at 95% Reliability

In the previous section we analyzed a design that was known to be sensitive to small variations. Here we analyze a design that was shown to be insensitive to small variations. The example chosen here is a laminate obtained from a reliability optimization. The optimization maximized the 5th percentile value of energy absorption calculated from a 100 sample Monte-Carlo simulation. The design was optimized for random variation in the ply angles (zero mean and 1° standard deviation). In addition to having a high value for its 5th percentile energy absorption, the resulting laminate also had a very small variance for energy absorption when it was subjected to small random ply angle variations. This indicates that the laminate has no competing paths and provides a progressive failure response that is robust and predictable. Here we investigate the effect

of model uncertainties on a design that was optimized for robustness and predictability in the presence of design variability.

Figure 4.6 shows the statistics of energy absorption for the laminate when subjected to individual and combined model uncertainties and ply angle variations. The reliability optimization design for maximum energy absorption continues to exhibit predictable and robust progressive failure when model uncertainties are introduced. For this design the stress uncertainty has a small effect on the variability of energy absorption. The stress interaction term F_{12}^{*} uncertainty varied at laminate level leads to a large variance in energy absorption. Although the progressive failure response has a higher standard deviation when model uncertainties are introduced, the 5th percentile value of energy absorption is comparable to that of the deterministic response indicating a robust energy absorption response. For this particular case, optimizing the laminate design for ply design variability also protects it against model uncertainties. The presence of a large number of plies with the same orientation (0° plies) may explain the low variability in the energy absorption that results from the failure of the remaining plies.

Table 4.3 lists the probability of the progressive failure events in the same order as for the deterministic response. To calculate the probability of the failure sequence events the laminate was first analyzed under deterministic conditions and the failure events and their sequence were noted (e.g. the first failure event consisted of ±60° plies failing in matrix mode, followed by ±45° plies failing in matrix mode and so on). Next the laminate was analyzed with model uncertainties and variations in ply angles (1.0° standard deviation) for the 1000 Monte-Carlo samples. From these samples, at each failure the probability of the failure event being the same as that of the deterministic response is calculated. The first sets of events have 100% probability, indicating highly

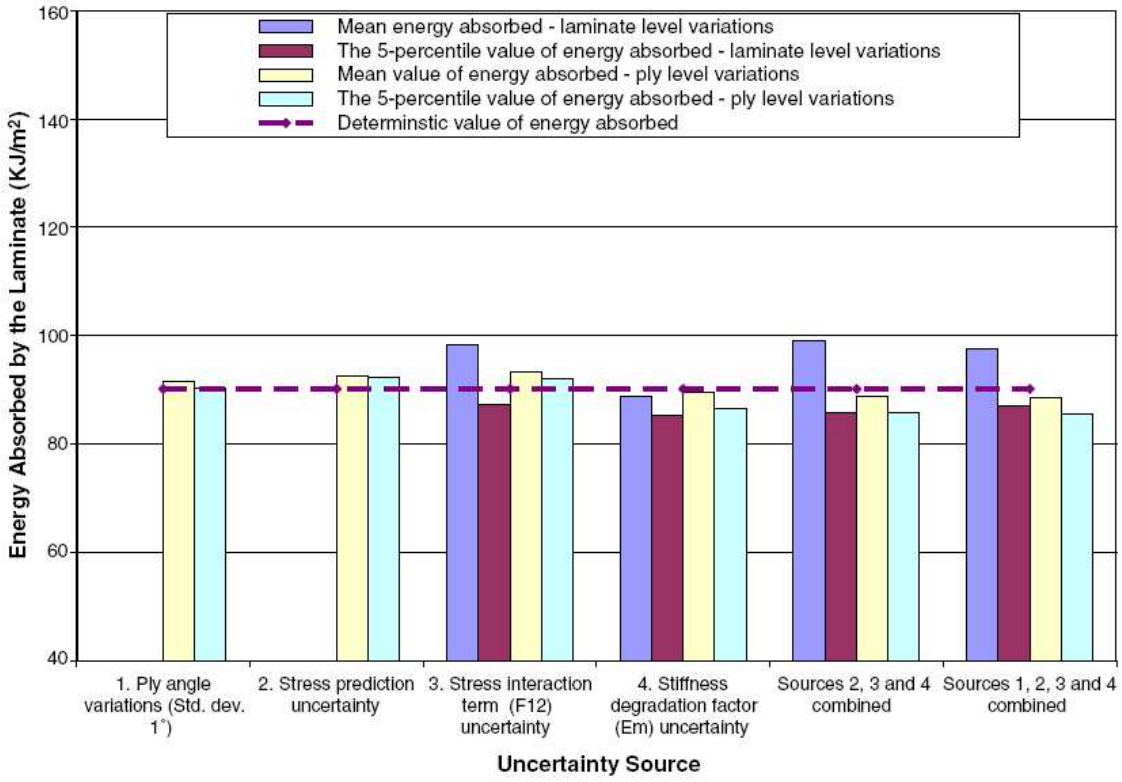

Figure 4.6: Effect of model uncertainties on energy absorption statistic for reliability optimization laminate optimized for maximum energy absorption and analyzed with model imperfections

predictable failures at the beginning. But, as small changes in stiffness degradations accumulate, they lead to changes later on in failure sequences. For example, in the presence of model uncertainties, shear failure of the $\pm 60^\circ$ plies precedes the 0° fiber failure. In this case, the degradation resulting from the earlier shear failure of the 60° plies does not significantly affect the stress levels in the remaining plies, so the responses have similar energy absorptions. However, if the laminate is used for testing to validate models or extract material parameters, its failure sequence predictability must also be high.

Table 4.3: Probability of failure events following the deterministic failure sequence when subjected to model uncertainties and ply angle variations (1° standard deviation) for the reliability optimization design

Deterministic failure sequences	Failure mode	Probability of failure in same mode and sequence when mode uncertainties are introduced (%)
±60°	matrix	100
±45°	matrix	100
±30°	shear	100
±45°	shear	99.8
0°	fiber	88.9
±60°	shear	0.1
±30°	fiber	70.0
±45°	fiber	22.5

4.2.4 Laminate Obtained from Optimization for Maximum Energy with Constraints for Failure Mode Separation

In our previous investigation into robustness and predictability of progressive failure response of a laminate in the presence of ply angle variations, we found that eliminating competing failure resulted in robust and progressive failure. This was accomplished by introducing a constraint that ensures that there is a small strain increment between any two laminate failures in distinct modes. Comparing the progressive failure response of the laminate design obtained with that response of the design obtained using reliability optimization revealed that the strain separation requirement was a sufficient but not a necessary condition to ensure robust and predictable failure. The laminate was optimized with a 0.005 strain separation margin between failure modes. The laminate obtained was found to provide a robust and predictable failure when ply angle variations were introduced. Here we investigate how the laminate optimized with strain separation performs in the presence of model uncertainties.

Figure 4.7 shows the statistics of the energy absorption for the laminate op-

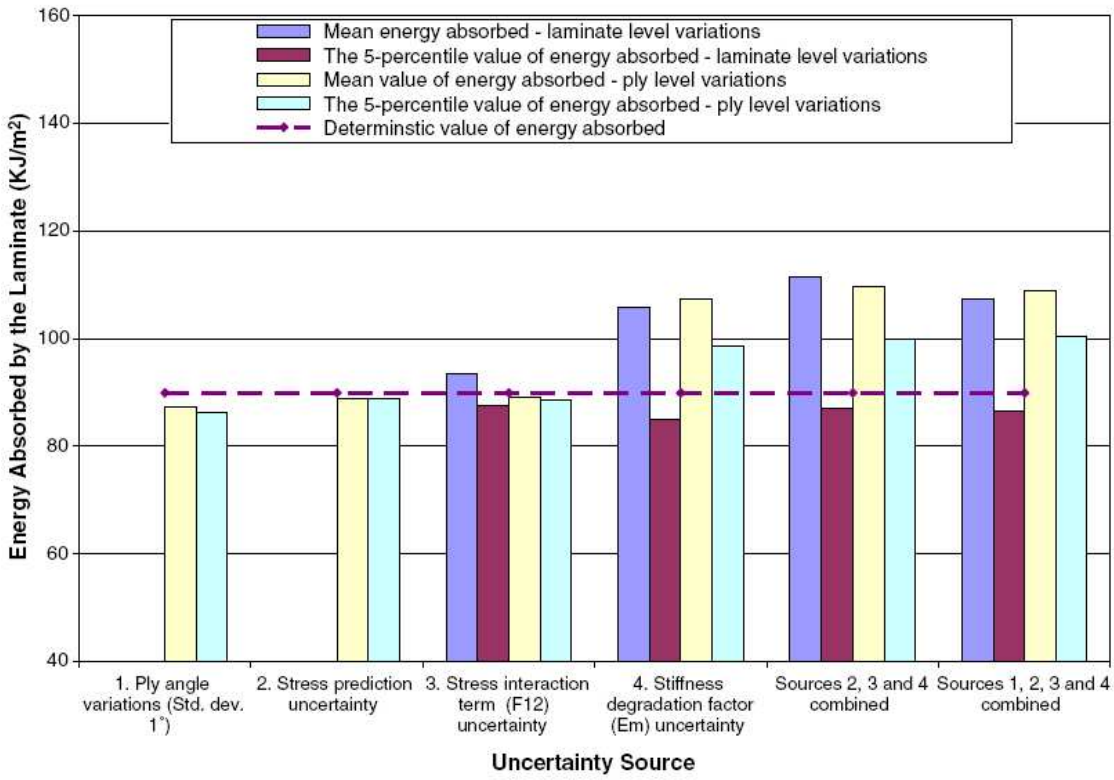

Figure 4.7: Effect of model uncertainties on energy absorption statistic for laminate deterministically optimized for maximum energy absorption with constraints for strain separation between consecutive failures in different modes analyzed with model imperfections

timized deterministically for maximum energy absorption with failure mode separation constraints when subjected to individual and combined model uncertainties and ply angle variations. The matrix stiffness degradation factor is the most significant among the model uncertainties. The variations in the residual stiffness of the plies resulting from the variations in the stiffness degradation factor lead to changes in amount of strain separation between consecutive failures in different modes.

The presence of competing modes leads to different alternate failure sequences that lead to different energy absorptions. However, since the deterministic analysis was performed using the worst case stiffness degradation, the mean value of the energy absorbed by the designs in the reliability analysis is usually higher. Laminates optimized

Table 4.4: Probability of failure events following the deterministic failure sequence when subjected to model uncertainties and ply angle variations (1° standard deviation) for the laminate deterministically optimized for maximum energy absorption with failure mode separation constraints

Deterministic failure sequences	Failure mode	Probability of failure in same mode and sequence when mode uncertainties are introduced (%)
±90°	matrix	100
±30°	shear	12.8
0°	fiber	67.3
±30°	fiber	3.3

for robustness against ply angle variations are less sensitive to ply stress uncertainty and failure criterion interaction term uncertainty. However, they are more sensitive to uncertainty in the stiffness degradation factor. The laminate optimized with 0.005 strain between consecutive failures in different modes does not provide robust and predictable failure when model uncertainties are introduced. Optimization of the laminate with increased (doubled) strain separation (0.01) between consecutive failures in different modes led to a design with all zero degree plies. The mechanisms that lead to competing failure modes are different in the case of model uncertainties. A deeper understanding of the mechanisms is necessary in order to devise a deterministic surrogate measure that can provide robust and predictable failure in the presence of model uncertainties and ply angle variations. The lack of predictability in the presence of model uncertainties can be better quantified by the failure sequence probabilistic analysis presented in Table 4.4.

4.3 Reliability Optimization of Laminates with Ply Angle Variations and Model Uncertainty

From the previous analysis of different laminates we found that the laminate optimized for robustness and predictability in the presence of ply angle variations (Section 4.2.3) is also very robust when model uncertainties in the ply stresses and failure criterion interaction term are included. For all cases, matrix stiffness degradation factor uncertainty contributes to the most variation in the energy absorption response of the laminate. However, since the deterministic response was calculated using a worst case degradation model, the mean and 5th percentile energy absorption of the designs analyzed with stiffness degradation factor uncertainty was higher or comparable to the deterministic predictions. It was shown that although the energy absorption robustness was satisfactory the design does not have a high failure sequence predictability. It is particularly important to improve the failure predictability and robustness of laminates used in experimental tests and validation. Laminates that have unpredictable failure sequences cannot provide good information on failure modes. It is necessary to have a predictable response of the test specimens in order to extract useful information from experimental tests. Obtaining empirical constants or validating material phenomenological models from such tests requires having a robust progressive failure response.

In this section we optimize the laminate stacking sequence using a reliability optimization with model uncertainties and ply angle variations. The model uncertainties are varied at the laminate level as this was found to create larger variability in the progressive failure energy absorption response. The 5th percentile value of energy absorption calculated using a 100 sample Monte Carlo simulation is maximized using a genetic algo-

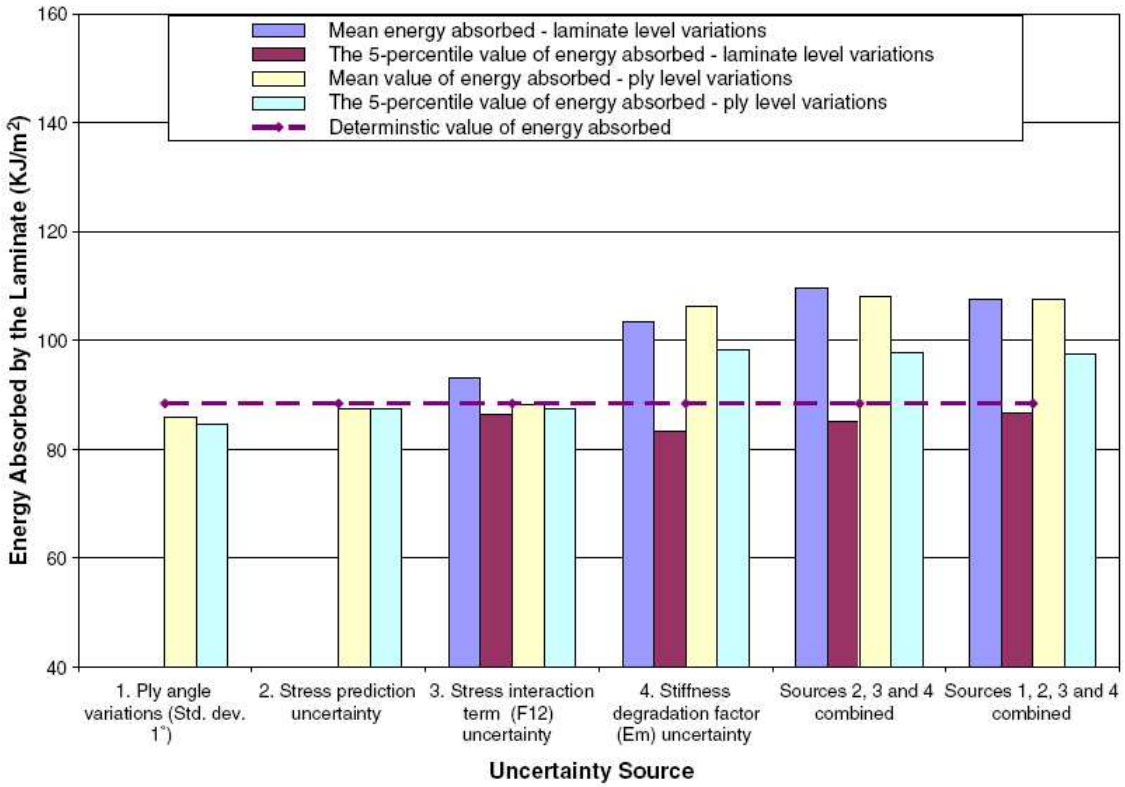

Figure 4.8: Effect of model uncertainties on energy absorption statistics for reliability optimization laminate optimized for maximum 95% reliability value of energy absorption in the presence of ply angle variations and model uncertainties

rithm. The discrete ply angles from 0 to 90° in increments of 15° are the design variables. The stacking sequence of the optimum design is $[0_{14}/\pm 15/\pm 30_3/90_2]_s$. This stacking sequence is similar (but not identical) to that obtained from the deterministic optimization $[0_{16}/\pm 30_3/90_2]_s$. The difference is that one pair of zero plies have been replaced with a $\pm 15°$ ply stack. However, this small change seems to make a significant difference in robustness and predictability. Figure 4.8 shows the statistics of energy absorption of the design when analyzed with individual and combined model uncertainties and ply angle variations.

The energy absorption statistics indicate that the design is less sensitive to model uncertainties and provides a robust energy absorption response. As seen before in other

Table 4.5: Probability of failure events following the deterministic failure sequence when subjected to model uncertainties and ply angle variations (1° standard deviation) for the laminate obtained from reliability optimization in the presence of model uncertainties and ply angle variations

Deterministic failure sequences	Failure mode	Probability of failure in same mode and sequence when mode uncertainties are introduced (%)
±90°	matrix	100
±30°	shear	98.8
±15°	fiber	96.5
0°	fiber	99.5
±30°	fiber	12.9

designs, the stiffness degradation factor has the most significant effect on the variance of the progressive failure response. The variations are smaller when model uncertainties are varied at the ply level. Analysis of the probability of failure events (Table 4.5) indicates that the design is also predictable in its failure. It must be remembered that this design differs from the previous design by only one set of plies (modified from 0° to 15° orientation). This small change leads to increased robustness and predictability.

It was shown that some model uncertainties have cancelling effects on each other. Therefore, it is important to understand and correctly characterized the effect of each individual model uncertainty before designing for safety taking into account all model uncertainties included. The laminates that were optimized for maximum energy absorption and robustness in the presence of ply angle variations showed a very robust performance when subjected to variations in the ply stresses and the failure criterion interaction term. However, some laminates were sensitivity to variations in the matrix degradation factor. The stiffness degradation factor was the most significant source of variation among the model uncertainties. The laminate stacking sequence was optimized to achieve max-

imum energy absorption at 95% reliability in the presence of ply angle variations and model uncertainties. The stacking sequence of the resulting design is similar to the design deterministically optimized for robustness with just ply angle variations. However, the predictability in the failure sequence of the laminate was greatly improved. This is particularly important if data obtained from experimental tests wants to be used to validate analysis models and extract empirical parameters. Optimizing for the effects of ply angle variations provided a design with robust energy absorption even when model uncertainties were introduced, but in order to obtain a design with predictable progressive failure sequence, the laminate had to be optimized with both model uncertainties and design variability. Eliminating the energy absorption variability was not possible even when the laminate was optimized with model uncertainties. The effect of matrix degradation factor uncertainties needs to be better understood to reduce its influence. It is important to include model uncertainties along with design variability to obtain robust and predictable progressive failure response. Failure predictability can be improved even with the use of poor models if the model inaccuracies are well characterized and their effect is taken into account in the design process.

In this section, a simple point load progressive failure example was used, which made possible to carry out the extensive probabilistic analysis necessary to quantify the variability of the composite response. However, for high velocity impact of composites, it is not quite possible to capture all the physics of the coupled failure mechanisms and nonlinear response by using such simplified models. Instead, higher system level tests such as ballistic impact tests are needed in order to represent the complex failure response. Likewise, appropriated computational models are needed in order to numerically reproduce such tests. In the next section, the implementation of an analytical composite

model for high strain rates using finite element methods is described in detail; the model will be used for the uncertainty analysis investigation of composite laminates subjected to high loading conditions.

Chapter 4, in full, is a reprint of the material as it appears in Laminate Optimization Incorporating Analysis and Model Parameter Uncertainties for Predictable Failure. Pablo Salas and Satchi Venkataraman. Structural & Multidisciplinary Optimization, Vol. 37, No. 6, February 2009, p. 541-555. The dissertation author was the primary investigator and author of this paper.

Chapter 5

Composite Model Implementation

In order to investigate and quantify the effect of model uncertainties in the response of composite laminates upon impact, it was first necessary to implement a constitutive material model that could be used to simulate the nonlinear and strain rate sensitive response of the composite under different strain rates. The main objective was to implement an efficient composite model that could be used in our investigation for model quantification. In modeling the impact response of the composite, it is critical to account for the nonlinear and strain rate dependent effects introduced by the polymer material. The Goldberg et al. [23] polymer model was used to simulate the polymer response in the composite model.

The implementation of computational models into finite element codes has proven to be an important tool in the design and validation process of engineering structures. For transient dynamic problems, explicit finite element codes such as LS-DYNA are greatly suitable for these applications. The composite model was defined as a user material routine (UMAT) in LS-DYNA, which allows the implementation of user defined material

constitutive equations into the finite element code. The implementation of efficient algorithms for solving the nonlinear visco-plastic equations on Goldberg's polymer model was a critical aspect in the composite model implementation. Additionally, a phenomenological fiber model and a simplified micromechanical model for computing the resultant stresses in the composite are described. The overall goal was to implement a robust computational model that could be effectively used for the model uncertainty quantification effort.

5.1 Numerical Implementation of Polymer Model

Goldberg et al. [23] visco-plastic model is used to simulate the response of the matrix material. The following sections describe in detail the numerical implementation of Goldberg's nonlinear rate dependent visco-plastic material model. First, Goldberg's model basic equations are presented followed by the details on the model discretization scheme employed and the nonlinear numerical solvers used.

5.1.1 Goldberg's Model

Hydrostatic stresses have shown to have a significant effect on the nonlinear deformation of polymer materials [116]. Their effect (which unlike metals can not be neglected) was incorporated in the model by using the Drucker-Prager yield criterion [25]

$$f = \sqrt{J_2} + \alpha\sigma_{kk} \tag{5.1}$$

where J_2 is the second invariant of the deviatoric stress tensor and α is a state variable used to control the influence of the hydrostatic stresses. From classical plasticity theory,

the inelastic strain rate $\dot{\epsilon}^I_{ij}$ is defined from an associative flow rule as

$$\dot{\epsilon}^I_{ij} = \dot{\lambda}\frac{\partial f}{\partial \sigma_{ij}} \tag{5.2}$$

where $\dot{\lambda}$ is a strain rate multiplier. Introducing the effective inelastic strain rate $\dot{\bar{\epsilon}}^I$, deviatoric stress σ'_{ij}, and the effective deviatoric stress $\bar{\sigma} = \sqrt{3J_2}$, the inelastic strain rate can be alternatively defined as

$$\dot{\epsilon}^I_{ij} = \sqrt{3}\dot{\bar{\epsilon}}^I \left(\frac{\sqrt{3}\sigma'_{ij}}{2\bar{\sigma}} + \alpha\delta_{ij} \right) \tag{5.3}$$

The Bodner-Partom visco-plastic model [24], traditionally employed to represent the visco-plastic deformation of metals, is modified to model the effective inelastic strain rate $\dot{\bar{\epsilon}}^I$ as

$$\dot{\bar{\epsilon}}^I = \frac{2}{\sqrt{3}} D_o \exp\left[-\frac{1}{2}\left(\frac{Z}{\sigma_e} \right)^{2n} \right] \tag{5.4}$$

The rate of change of the state variables α and Z, needed to update the variables at every time step, is defined as $\dot{Z} = q(Z_1 - Z)\dot{\bar{\epsilon}}^I$ and $\dot{\alpha} = q(\alpha_1 - \alpha)\dot{\bar{\epsilon}}^I$ respectively. The effective stress σ_e is expressed as $\sigma_e = \sqrt{3}f = \bar{\sigma} + \sqrt{3}\alpha\sigma_{kk}$. D_0 , q, Z_1 and α_1 are material constants. Finally, the resultant stress rate is

$$\dot{\sigma}_{ij} = 2G\left(\dot{\epsilon}'_{ij} - \dot{\epsilon}^{I\prime}_{ij} \right) + B\left(\dot{\epsilon}_{kk} - \dot{\epsilon}^I_{kk} \right)\delta_{ij} \tag{5.5}$$

where G and B are the shear and the bulk modulus respectively.

5.1.2 Implementation Background - Backward Euler Integration

Backward Euler integration is used to integrate the polymer model constitutive equations. For explicit finite element calculations, the time step size is limited by two stability criteria. The first is the classical Courant condition, which states that the time step size must be less than the time required for a wave to propagate across any element in the calculation. The second restriction is imposed by the material models. Some models, such as those used for explosives, require a small time step because of the rate at which they introduce energy into the system. A material model may, however, impose a time step limit based solely on the stability requirements of the algorithm used to integrate the constitutive equations. This limit may also apply to quasi-static finite element calculations, where the amount of deformation that can occur during a step is restricted by the stability of the material model. Unconditionally stable integration methods are therefore generally preferred for material models, the most common one being the backward Euler integration method.

For a model ordinary differential equation,

$$\dot{y} = Y(y, t) \tag{5.6}$$

where y is the solution variable and t is time, the backward Euler integration method advances the solution in time according to

$$\frac{y^{n+1} - y^n}{\triangle t} = Y(y^{n+1}, t) \tag{5.7}$$

which can be re-written as

$$y^{n+1} = y^n + \triangle t Y(y^{n+1}, t). \tag{5.8}$$

The superscript refers to the time step number and $\triangle t$ is the time step size. This method can also be applied to a vector $\boldsymbol{y}$,

$$\boldsymbol{y}^{n+1} = \boldsymbol{y}^n + \triangle t \boldsymbol{Y}(\boldsymbol{y}^{n+1}, t) \tag{5.9}$$

In general, Equations 5.8 and 5.9 are nonlinear algebraic equations that must be solved with iterative methods. The cost of solving nonlinear equations increases rapidly with the number of equations, and guaranteeing that the iteration scheme will converge is difficult. However, provided that an interval bounding the solution is known, there are methods guaranteed to converge for a single equation.

5.1.3 Model Discretization Scheme

The discretized form of Equation 5.4 was solved to compute the increment in inelastic strain over each time step,

$$f(\triangle \bar{\epsilon}^I) = 0 = \triangle \bar{\epsilon}^I - \frac{2D_o \triangle t}{\sqrt{3}} \exp\left[-\frac{1}{2}\left(\frac{Z^{n+1}(\triangle \bar{\epsilon}^I)}{\sigma_e(\triangle \bar{\epsilon}^I)}\right)^{2n}\right] \tag{5.10}$$

The implementation is motivated by the radial return method used for integrating the equations for J_2 elasto-plasticity. The direction of the increment in the inelastic strain is therefore chosen to be defined by the deviatoric trial stress,

$$\triangle\epsilon_{ij}^{I} = \sqrt{3}\triangle\bar{\epsilon}^{I}\left(\frac{\sqrt{3}\sigma_{ij}^{tr}}{2\bar{\sigma}^{tr}} + \alpha\delta_{ij}\right) \tag{5.11}$$

$$\sigma_{ij}^{tr} = \sigma_{ij}'^{n} + 2G\triangle\epsilon_{ij}'. \tag{5.12}$$

Substituting Equation 5.11 into Equation 5.5 results in an expression for the final stress in terms of the increment in inelastic strain $\triangle\bar{\epsilon}^{I}$,

$$\sigma_{ij}^{n+1} = \left(1 - 3G\frac{\triangle\bar{\epsilon}^{I}}{\bar{\sigma}^{tr}}\right)\sigma_{ij}^{tr} + \left(\hat{\sigma}^{tr} - 3\sqrt{3}B\alpha^{n+1}\triangle\bar{\epsilon}^{I}\right)\delta_{ij} \tag{5.13}$$

where $\hat{\sigma}^{tr} = \frac{1}{3}{\sigma_{kk}}^{n} + B\triangle\epsilon_{kk}$. The effective stress defined in Goldberg's model description is therefore expressed in terms of the increment of the inelastic strain,

$$\sigma_e = \bar{\sigma}^{tr} + 3\sqrt{3}\alpha^{n+1}(\triangle\bar{\epsilon}^{I})\hat{\sigma}^{tr} - (3G + 9(\alpha^{n+1}(\triangle\bar{\epsilon}^{I}))^2 B)\triangle\bar{\epsilon}^{I}. \tag{5.14}$$

The state variables Z and α are also updated using backwards Euler integration,

$$Z^{n+1} = \frac{Z^{n} + q\triangle\bar{\epsilon}^{I}Z_1}{1 + q\triangle\bar{\epsilon}^{I}} \tag{5.15}$$

$$\alpha^{n+1} = \frac{\alpha^{n} + q\triangle\bar{\epsilon}^{I}\alpha_1}{1 + q\triangle\bar{\epsilon}^{I}} \tag{5.16}$$

The nonlinear Equation 5.10 is solved using Ridder's method, described below. During each iteration, Equations 5.14, 5.15 and 5.16 are evaluated before evaluating the function f in Equation 5.10. Once the increment in the inelastic strain is known, the final stress

is calculated,

$$s = \left(1 - 3G\frac{\triangle\bar{\epsilon}^I}{\bar{\sigma}^{tr}}\right) \tag{5.17}$$

$$\hat{\sigma}^{n+1} = \hat{\sigma}^{tr} - 3\sqrt{3}B\alpha^{n+1}\triangle\bar{\epsilon}^I \tag{5.18}$$

$$\sigma_{ij}^{n+1} = s \cdot \sigma_{ij}^{tr} + \hat{\sigma}^{n+1}\delta_{ij} \tag{5.19}$$

5.1.4 Ridder's Method

The backward Euler method applied to solve the inelastic strain evolution results in an implicit equation (Equation 5.10) which requires an iterative solver. In this implementation, Ridder's Method [117] is used to solve Equation 5.10 for the increment of the inelastic strain over the time step. Ridder's method is a very robust method that works well for a wide variety of problems, including solving for the increment in equivalent plastic strain in strongly nonlinear plasticity models. The method was further popularized by the book Numerical Recipes: The Art of Scientific Computing [118]. Ridder's method, like the Bisection method, is guaranteed to converge. It requires an initial interval containing the solution, $[u_L, u_R]$ where u_L and u_R are the values on the left and right boundaries of the interval. The interval contains at least one solution if $f(u_L).f(u_R) < 0$. The function is evaluated two times for every iteration. The first evaluation is at the midpoint of the interval,

$$u_M = \frac{1}{2}(u_L + u_R) \tag{5.20}$$

$$f_M = f(u_M) \tag{5.21}$$

The location of the solution is a function of the two endpoints and the midpoint:

$$u = u_M + (u_M - u_L)\frac{sign|f_L - f_R|f_M}{\sqrt{f_M^2 - f_L f_R}} \tag{5.22}$$

The method updates the interval using u in the same manner as the Bisection and Regula Falsi methods [119]. In terms of pseudo-code, Ridder's method can be written as:

$f_L = f(u_L)$

$f_R = f(u_R)$

do $i = 1, n$

  $u_M = (u_L + u_R)/2$

  $f_M = f(u_M)$

  $u = u_M + (u_M - u_L)\frac{\text{sign}|f_L - f_R|f_M}{\sqrt{f_M^2 - f_L f_R}}$

  if $(|f(u)| > \epsilon)$ then

    $f_{\text{avg}} = f(u)$

    if $(f_{\text{avg}} \cdot f_L \geq 0)$ then

      $u_L = u$

      $f_L = f_{\text{avg}}$

    else

      $u_R = u$

      $f_R = f_{\text{avg}}$

    endif

  else

    exit loop

endif

enddo

A simple modification has been added to the implementation which seems to significantly increase the robustness of the method and slightly improve the speed of convergence. A second update is performed on the interval using u_M if $f(u_M).f(u) < 0$. Only two iterations are typically needed for convergence with the polymer model. The initial interval for the inelastic strain increment is specified to be $[0, \beta \triangle t\dot{\bar{\epsilon}}]$, where β is a constant greater than 1.0 to account for the fact that inelastic strain occurs even if the overall strain increment during a time step is zero. The values of f are evaluated at the ends of the interval. If they don't have opposite signs, the right boundary is adjusted until they do.

5.1.5 Rate Dependence of Elastic Modulus

The polymer material elastic modulus is assumed to be strain rate independent at small effective strain rates. Beyond a critical value $\dot{\bar{\epsilon}}_o$ the material exhibits strain rate sensitivity. In this implementation a logarithmic dependence of strain rate sensitivity is assumed and is defined by the following model:

$$E = \begin{cases} E_o \left(1 + c_1 \log(\dot{\bar{\epsilon}}/\dot{\bar{\epsilon}}_o)\right) & \text{if } \dot{\bar{\epsilon}} > \dot{\bar{\epsilon}}_o \\ E_o & \text{otherwise} \end{cases} \tag{5.23}$$

where c_1 is a scaling parameter to control the strain rate dependency. The effective deviatoric strain rate $\dot{\bar{\epsilon}}$ is defined as

$$\dot{\bar{\epsilon}} = \sqrt{\frac{2}{3}\dot{\epsilon}'_{kl}\dot{\epsilon}'_{kl}} \tag{5.24}$$

5.1.6 Damage Model

Beyond the limit strain $\bar{\epsilon}_o$, the material becomes damaged and it is therefore softened. A continuum damage model is defined as

$$\Omega = 1 - \exp\left[\left(1 - \left(\bar{\epsilon}/\bar{\epsilon}_o\right)^m\right)/m\right] \tag{5.25}$$

but it is integrated from its rate form instead of being evaluated directly. The damage Ω progressively reduces the strength of the material. At the end of each update, the stress used to calculate the element force is multiplied by $1 - \Omega$,

$$\sigma^{n+1} = (1 - \Omega^{n+1})\sigma^{n+1} \tag{5.26}$$

and the stress passed to the constitutive subroutine at the beginning of the time step is divided by $1 - \Omega$ to recover the actual stress prior to its update.

5.1.7 Verification of Polymer Model Implementation

Experimental data from Goldberg et al. [23] was used to qualitatively validate the numerical implementation of the polymer material model. Stress-strain curves for tensile and shear tests at medium and high strain rates are provided for toughened epoxies 977-2 and PR520.

The comparisons between experimental and computed responses are shown in Figure 5.1 and Figure 5.2 for PR520 and Figure 5.3 and Figure 5.4 for 977-2. According

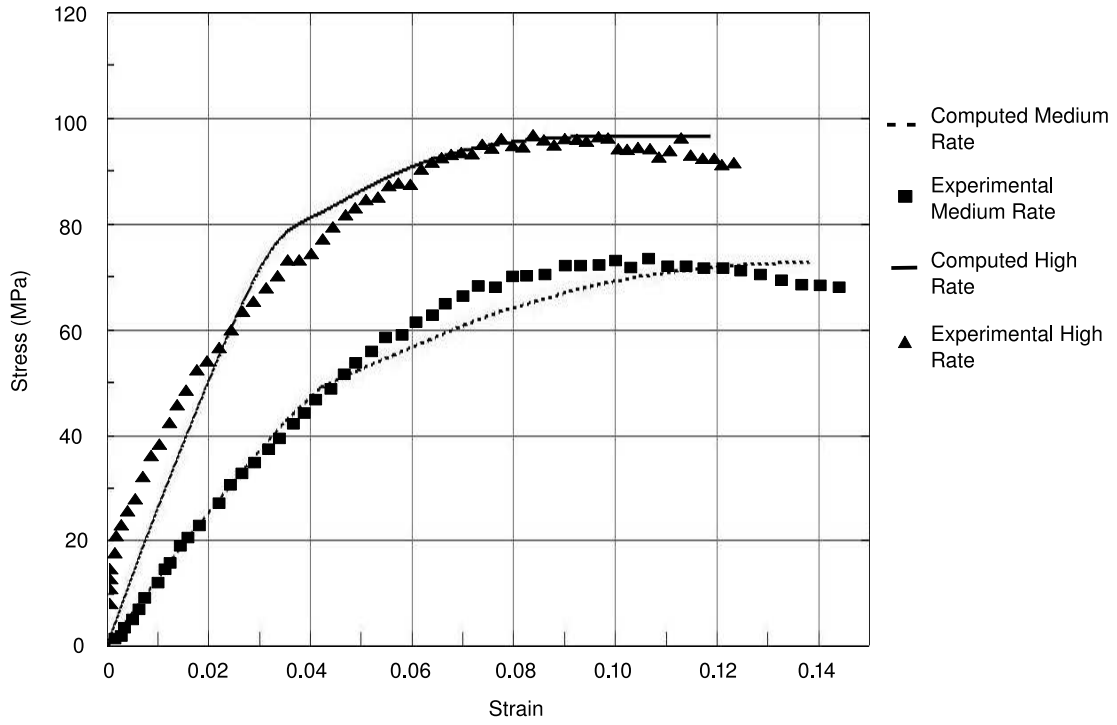

Figure 5.1: Experimental and computed shear response for PR520 resin at medium (1.76/sec) and high (420/sec) strain rates

to Goldberg et al. [23], the sharp increase in stress at the onset of loading seen in both materials experimental data sets for tension at high strain rates can be attributed to the lack of stress equilibrium at the start of loading, which may explain why both sets of simulations were found to under predict the stresses. Also, the oscillations observed in the high strain rate tensile response for 977-2 are due to the coupon specimen geometry. The geometry of the specimen was changed for the PR520 high strain rate tensile test, which is given as the reason why the response for PR520 is free of oscillations.

5.2 Fiber Orthotropic Model

The fiber response is modeled as elastic orthotropic while the fiber's stiffness degradation is obtained by using a simple phenomenological model. As shown in Figure

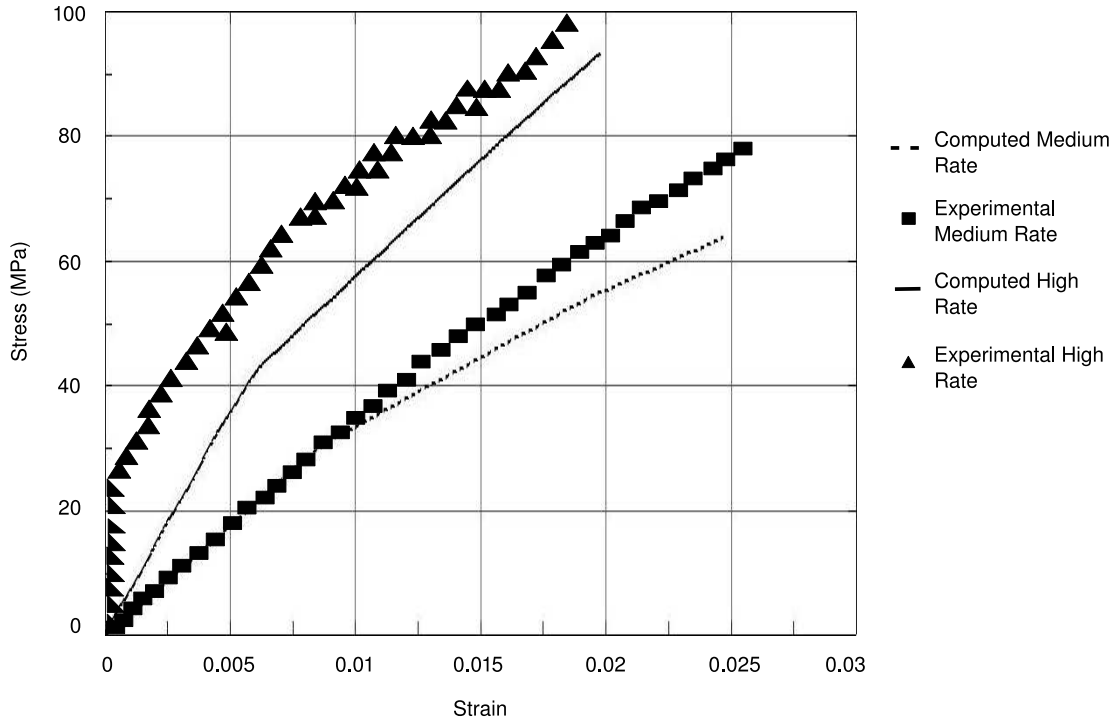

Figure 5.2: Experimental and computed tensile response for PR520 resin at medium (1.4/sec) and high (510/sec) strain rates

5.5, the fiber model response consists of two parts: the first is linearly elastic,

$$\{\sigma\} = [C]\{\epsilon\} \tag{5.27}$$

where [C] is the 6 by 6 elastic material matrix defined for orthotropic materials. The second part defines the fiber softening due to damage. A stress-strain curve for the softening portion of the fiber can be defined in the LS-DYNA input file. Once the fiber strain exceeds the critical softening strain ϵ_P, the stresses are computed by interpolating stress values from the phenomenologically defined softening curve. The curve is typically obtained from experimental uniaxial tensile and compression tests. The stress value at which softening is assumed to initiate is defined by the first value in the curve, $\Sigma(0)$, and the corresponding critical softening strain in the longitudinal direction at such stress level

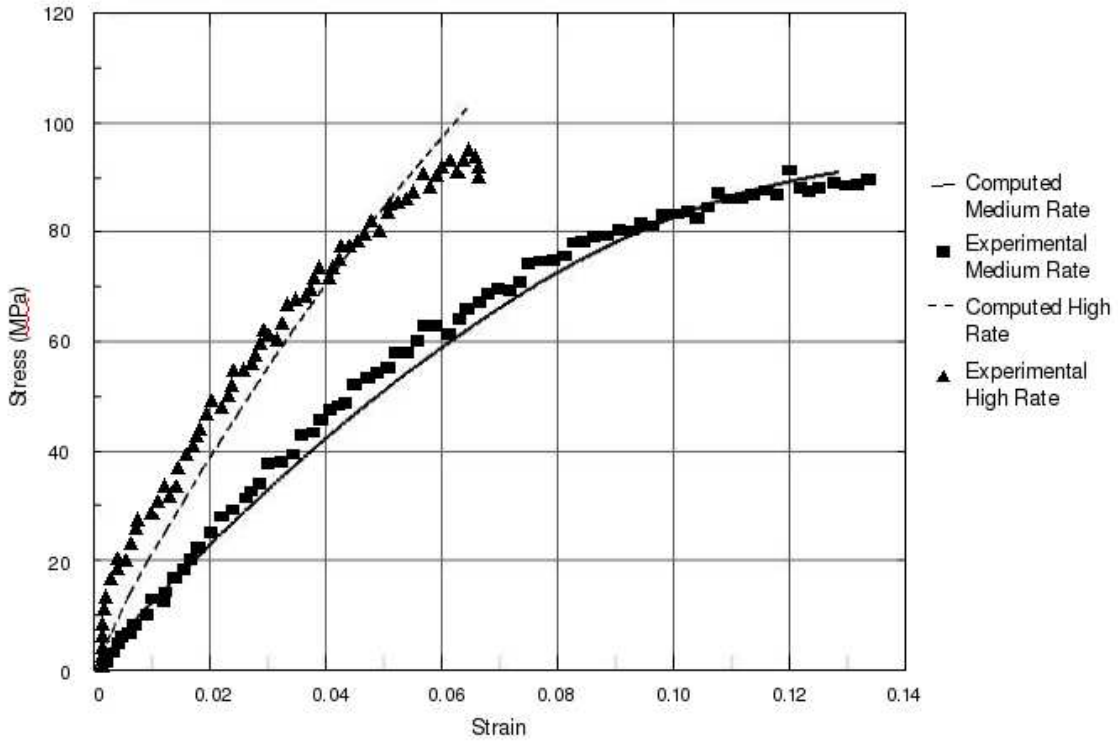

Figure 5.3: Experimental and computed shear response for 977-2 resin at medium (1.91/sec) and high (518/sec) strain rates

, ϵ_P, is defined as

$$\epsilon_P = \Sigma(0)/E_1 \tag{5.28}$$

Once softening begins ($\epsilon_1 > \epsilon_P$), the corresponding longitudinal stress σ_1 is interpolated directly from the load curve,

$$\sigma_1 = \Sigma(\epsilon_1 - \epsilon_P). \tag{5.29}$$

Once the stress σ_1 is known, the degraded elastic modulus E_1 can be computed by solving the stress-strain constitutive relation Equation 5.30 for orthotropic linear elastic materials in terms of E_1.

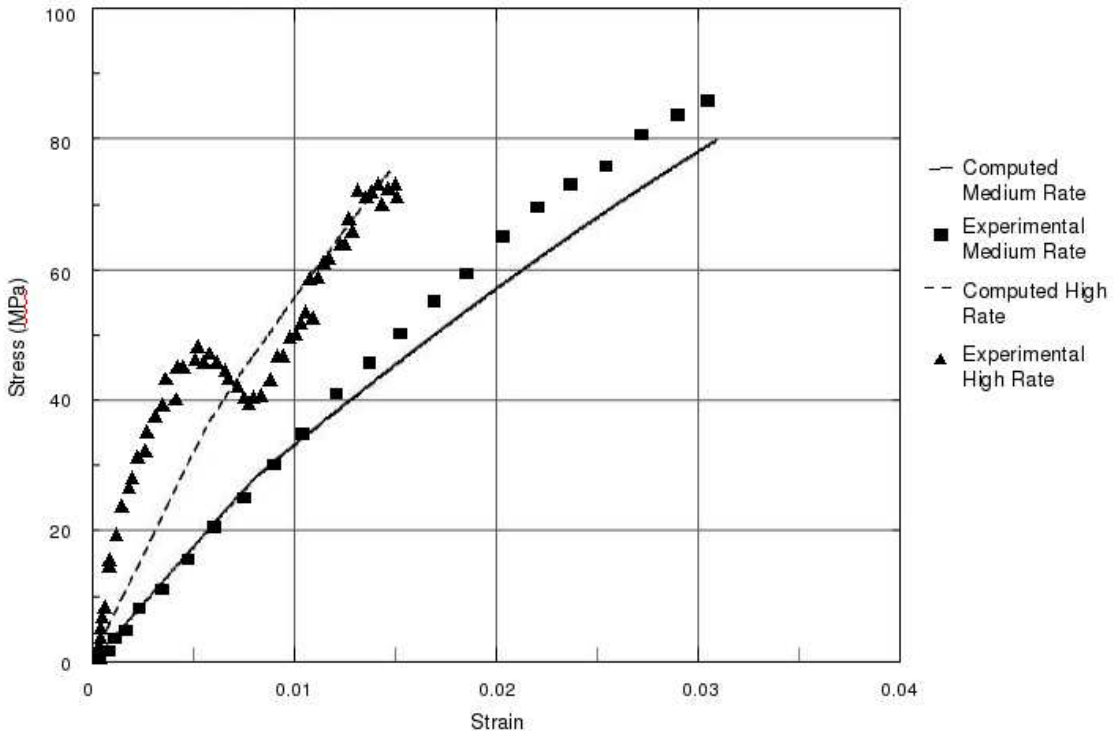

Figure 5.4: Experimental and computed tensile response for 977-2 resin at medium (1.31/sec) and high (365/sec) strain rates

$$\sigma_1 = C_{11}(E_1)\epsilon_1 + C_{12}(E_1)\epsilon_2 + C_{13}(E_1)\epsilon_3 \tag{5.30}$$

The rest of the stress components can then be obtained by using Hooke's law for orthotropic linear elastic materials,

$$\begin{Bmatrix} \sigma_2 \\ \sigma_3 \\ \sigma_4 \\ \sigma_5 \\ \sigma_6 \end{Bmatrix} = \begin{bmatrix} C_{21} & C_{22} & C_{23} & 0 & 0 & 0 \\ C_{31} & C_{32} & C_{33} & 0 & 0 & 0 \\ 0 & 0 & 0 & C_{44} & 0 & 0 \\ 0 & 0 & 0 & 0 & C_{55} & 0 \\ 0 & 0 & 0 & 0 & 0 & C_{66} \end{bmatrix} \begin{Bmatrix} \epsilon_2 \\ \epsilon_3 \\ \epsilon_4 \\ \epsilon_5 \\ \epsilon_6 \end{Bmatrix} \tag{5.31}$$

When unloading or reloading below ϵ_{max}, the response is elastic with the new

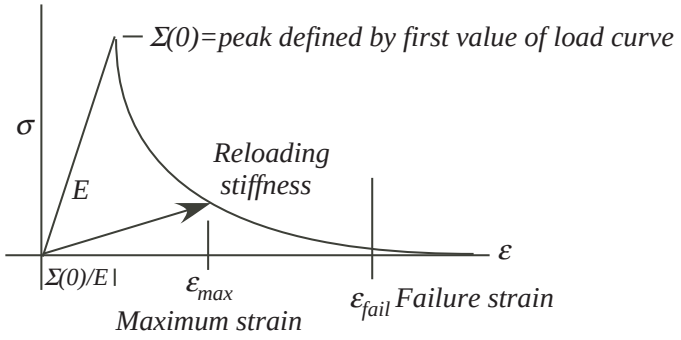

Figure 5.5: Elastic response of the fiber followed by softening

computed elastic modulus E_1. No residual strains are considered in the material. The same model is implemented for compressive loading, where a softening stress-strain curve for compression can be defined if necessary. Fiber failure occurs when either ϵ_1 reaches the specified failure strain ϵ_{fail}, or the matrix fails while the fiber is in compression (i.e. fiber buckling).

5.3 Composite Material Model

A micromechanical model was implemented to model the response of unidirectional composite laminas. The equations of the micromechanical model are described in detail in Goldberg [120]. The response of the unidirectional composite lamina was computed using the response of the individual constituents, namely, polymer matrix and fiber materials. The polymer matrix response was computed using the polymer viscoplastic material model defined by Goldberg et al [23], as described in Section 5.1.1. The fiber was assumed to be linear elastic, and details of the implementation are given in Section 5.2.

As described in Chapter 2, micromechanical models typically rely on representative volume elements to define the appropriate relationships between constituents. There-

fore, a composite unit cell was defined to represent the lamina behavior. A standard mechanics of materials approach was used to define the micromechanical equations. As mentioned previously, the model was implemented for unidirectional composite laminas. The composite unit cell was defined based on a periodic, standard square package configuration. Only a quarter of the unit cell was modeled due to symmetric conditions. The unit cell was discretized into four rectangular sections or subcells: one section for the fiber material and the remaining three sections (surrounding the fiber) for the polymer material. The cross-sectional area of the fiber section was assumed to be equal to the fiber volume fraction of the composite lamina.

Three-dimensional strains and stresses were considered when modeling the response of the composite unit cell. The full strain tensor of the composite unit cell was assumed to be known (strain load control), along with the polymer matrix subcell inelastic strains, which were computed using the polymer model. The response of both the polymer matrix and the fiber material can be determined by expressing the total strain in the corresponding subcell as the sum of elastic and inelastic strains:

$$\{\epsilon\} = [S]\{\sigma\} + \left\{\epsilon^I\right\} \tag{5.32}$$

where $\{\epsilon\}$ and $\left\{\epsilon^I\right\}$ represent the subcell total and inelastic strain tensors respectively, $\{\sigma\}$ represents the subcell stress tensor and $[S]$ represents the material compliance matrix. For the polymer model, $[S]$ is isotropic and $\left\{\epsilon^I\right\}$ nonzero. For the fiber material, $[S]$ is assumed to be transversely isotropic with zero $\left\{\epsilon^I\right\}$.

Mechanics of materials assumptions were made to compute the resultant unitcell stresses. Subindices $1, 2$ and 3 denote fiber direction, transverse to fiber "in-plane lamina"

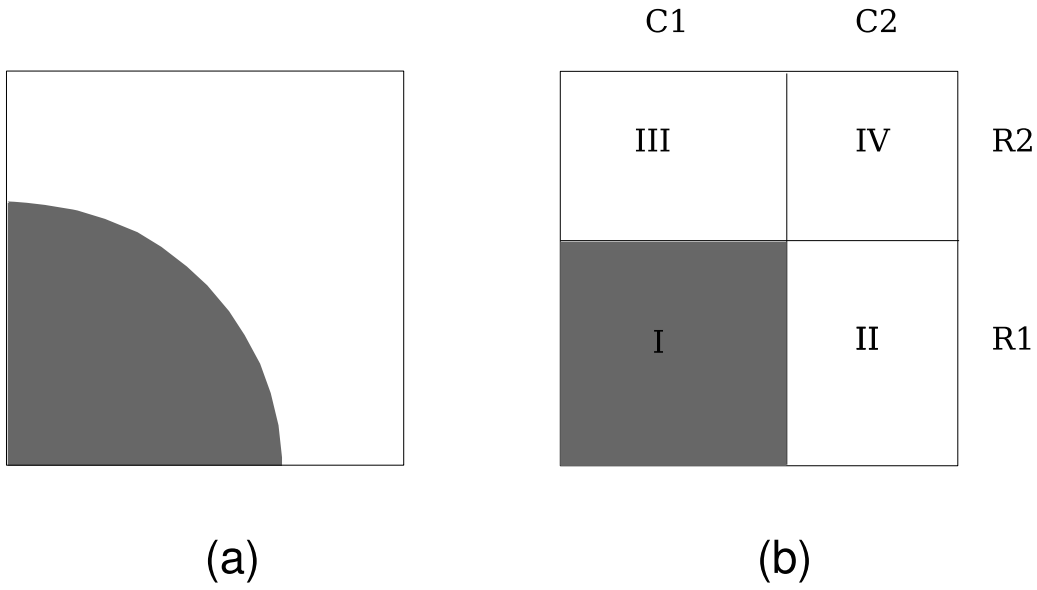

Figure 5.6: Schematic representation of composite lamina micromechanical unitcell. (a) Quarter of the micromechanical unitcell. (b) Discretized representation of the micromechanical unitcell

direction and transverse to fiber "out of plane lamina" direction respectively. Each subcell was denoted with a subscript ranging from (I) to (IV) as depicted in Figure 5.6. Subcell (I) is comprised of only fiber material; subcells $(II), (III)$ and (IV) consist of polymer material. Adjacent subcells are paired up in rows $R1$ and $R2$ and columns $C1$ and $C2$. The cross sectional area of each subcell in terms of percentage is denoted by V_i, for $i = (I), (II), (III), (IV)$. The cross sectional area of each row or column of subcells in terms of percentage is denoted by V_j, for $j = (R1), (R2), (C1), (C2)$.

In the longitudinal direction (fiber direction), uniform normal strains were assumed in all subcells, while the resulting unitcell normal stress σ_1 is obtained by taking the volume average of all the subcell normal stresses:

$$\begin{aligned}
&\epsilon_1 = \epsilon_{1(I)} = \epsilon_{1(II)} = \epsilon_{1(III)} = \epsilon_{1(IV)} \\
&\sigma_1 = V_{(I)}\sigma_{1(I)} + V_{(II)}\sigma_{1(II)} + V_{(III)}\sigma_{1(III)} + V_{(IV)}\sigma_{1(IV)}
\end{aligned} \tag{5.33}$$

The opposite assumptions are made to obtain the unitcell shear transverse strain ϵ_{23} and stress σ_{23}:

$$\begin{aligned}
&\sigma_{23} = \sigma_{23(I)} = \sigma_{23(II)} = \sigma_{23(III)} = \sigma_{23(IV)} \\
&\epsilon_{23} = V_{(I)}\epsilon_{23(I)} + V_{(II)}\epsilon_{23(II)} + V_{(III)}\epsilon_{23(III)} + V_{(IV)}\epsilon_{23(IV)}
\end{aligned} \tag{5.34}$$

In the transverse directions (perpendicular to fiber), normal stresses at each row and column of subcells are assumed to be uniform while the resultant normal strains are obtained by volume averaging of the subcell strains. The resultant unitcell transverse normal strains are obtained by assuming uniform strains between rows $R1$ and $R2$, and uniform strains between columns $C1$ and $C2$. The resultant unitcell transverse normal stresses are obtained by taking the volume average of rows $R1$ and $R2$ respective stresses or columns $C1$ and $C2$ respective stresses. For example, the corresponding strains in the transverse direction 2 are obtained as follows:

$$\begin{aligned}
&\epsilon_{2(R1)} = V_{(I)}\epsilon_{2(I)} + V_{(II)}\epsilon_{2(II)} \\
&\epsilon_{2(R2)} = V_{(III)}\epsilon_{2(III)} + V_{(IV)}\epsilon_{2(IV)} \\
&\epsilon_2 = \epsilon_{2(R1)} = \epsilon_{2(R2)}
\end{aligned} \tag{5.35}$$

while the corresponding stresses in the transverse direction 2 are:

$$\begin{aligned}
&\sigma_{2(R1)} = \sigma_{2(I)} = \sigma_{2(II)} \\
&\sigma_{2(R2)} = \sigma_{2(III)} = \sigma_{2(IV)} \\
&\sigma_2 = V_{(R1)}\sigma_{2(R1)} + V_{(R2)}\sigma_{2(R2)}
\end{aligned} \tag{5.36}$$

The same procedure is used to obtain the normal and shear strains ϵ_3, ϵ_{12} and ϵ_{13}, and normal and shear stresses σ_3, σ_{12} and σ_{13}. Combining strain and stress assumptions (Equations 5.33 to 5.36) with the corresponding constituent material Equation 5.32, all subcell and unitcell stresses can be computed. The detailed equations for all six components of stress and strain of the unitcell and general procedure for their implementation are given in Goldberg [120].

5.4 Composite Model Results

Experimental data from Goldberg et al [23] was used to qualitatively validate the composite micromechanical model. Experimental stress-strain curves are provided for uniaxial tensile tests at medium and high strain rates for various IM7/977-2 composite lamina orientations (10, 45 and 90 degree orientation). The comparisons between experimental and computed responses are shown in Figures 5.7, 5.8 and 5.9.

The computed stress-strain curves match reasonably well the computed curves presented by Goldberg et al [23]. Qualitatively speaking, the composite model captures the response of the composite lamina at medium strain rates for almost all fiber orientations reasonably well, except for the 10 degree lamina case, where the model was found to overpredict the stresses. For high strain rates, the model was found to capture the response of the lamina at higher strain values (near the failure point), but not for lower strain values, where stresses were under-predicted (particularly for matrix dominated response cases, e.g. 45 and 90 degree laminas). The slight oscillation observed in the computed response at high strain rates was caused by slight vibrations in the modeled specimens due to the high deformation rates. Details of issues with the experimental data regarding

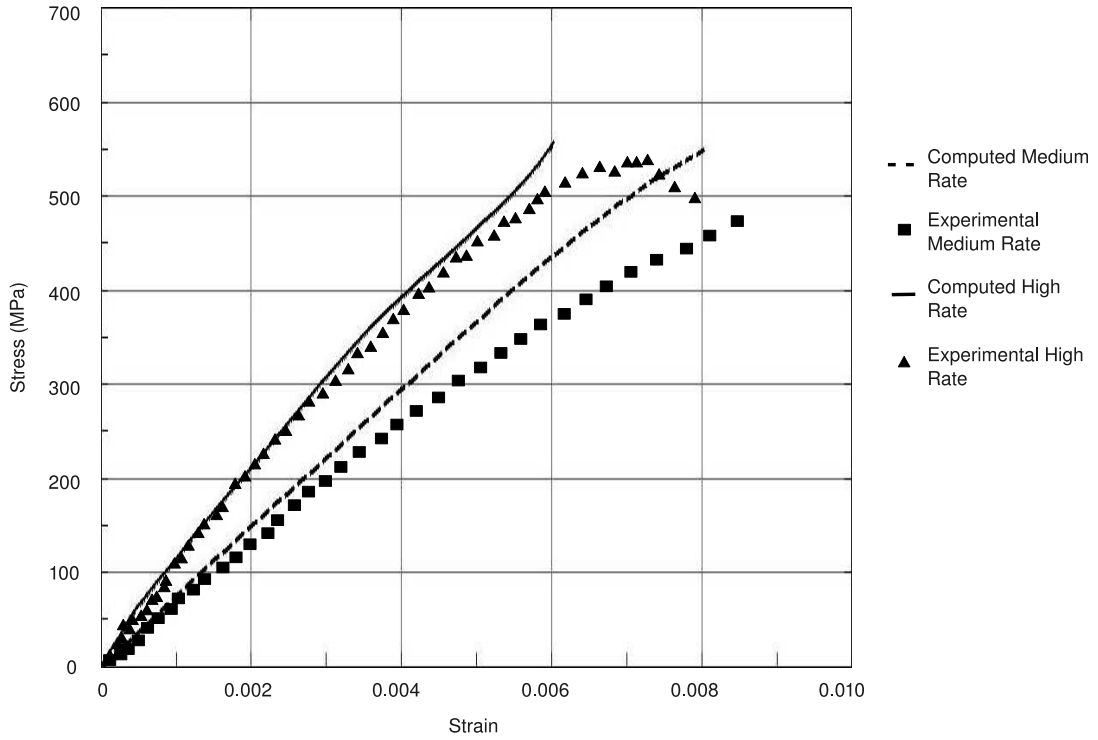

Figure 5.7: Experimental and computed response for IM7/977-2 [10 degree] composite lamina at medium (0.56/sec) and high (320/sec) strain rates

the composite lamina validation tests are given in Reference [23].

Chapter 5, in full, is a reprint of the material as it appears in Numerical Implementation of Polymer Visco-plastic Equations for High Strain Rate Composite Models. Pablo Salas, David J. Benson, Satchi Venkataraman, Matti Loikkanen. ASCE Journal of Aerospace Engineering, Vol. 22, No. 3, p. 304-310, July 2009. The dissertation author was the primary investigator and author of this paper.

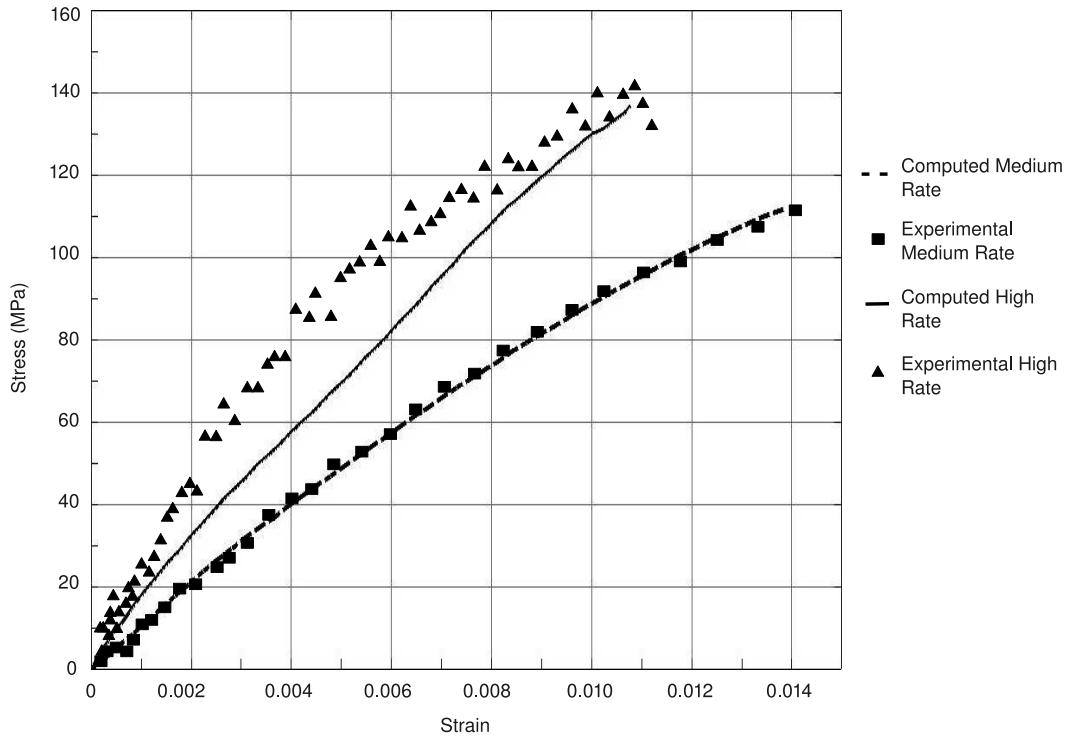

Figure 5.8: Experimental and computed response for IM7/977-2 [45 degree] composite lamina at medium (1.2/sec) and high (405/sec) strain rates

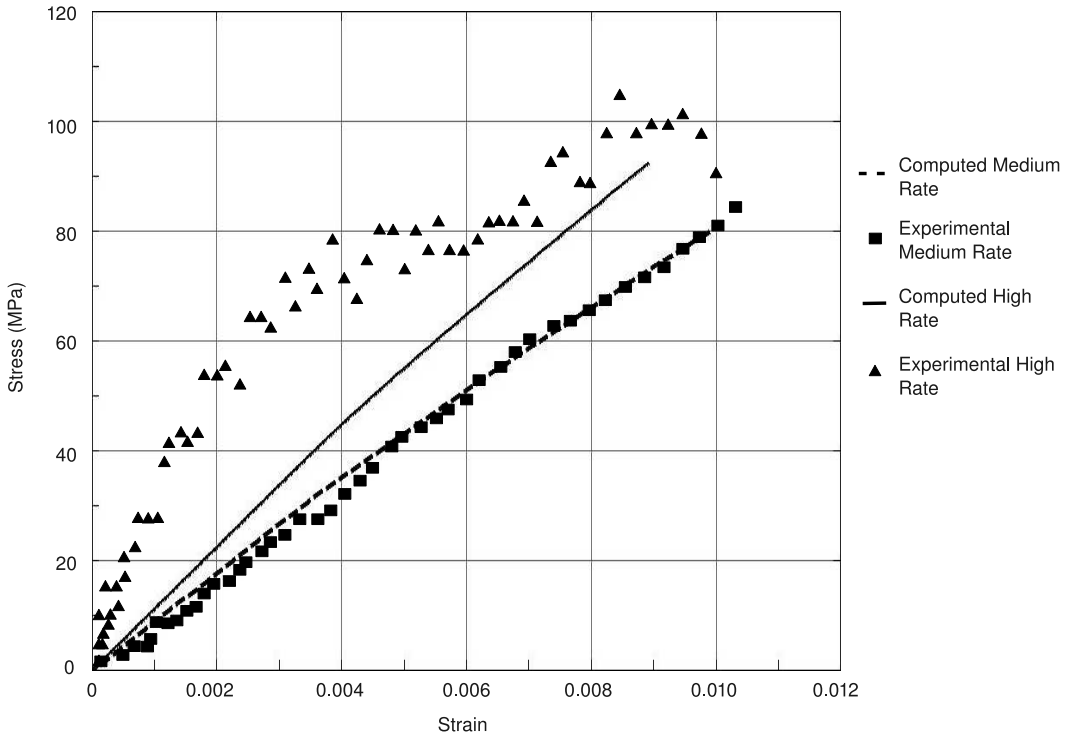

Figure 5.9: Experimental and computed response for IM7/977-2 [90 degree] composite lamina at medium (1.09/sec) and high (405/sec) strain rates

Chapter 6

Bayesian Network Implementation

Increasingly, numerical simulations are used to partially replace full scale experimental tests that are expensive to perform. In such cases, the models used for simulating the response of the full scale system need to be validated using subsystem and component level tests. Bayesian based approaches such as the ones described in Section 3.2 can be used to quantify the effect of physical and numerical uncertainties at each level and to understand how uncertainties are propagated from lower system levels (e.g. coupon tests) to more complex ones (e.g. ballistic impact tests).

As described in the previous chapter, an analytical material model for response prediction of impact on composite materials was implemented in the LS-DYNA commercial finite element code [35]. The analytical model will be used along with Bayesian based validation approaches for the model uncertainty quantification of ballistic impact response of composite laminates. In the next section, a brief overview of Bayesian network theory and their numerical implementation is presented. In the last two sections of the chapter, two algebraic examples are presented to outline the model error estimation methodology.

6.1 Bayesian Networks

As discussed in Section 3.2, Bayes theory has been widely used for uncertainty propagation and estimation of uncertain model parameters. The Bayes factor, a validation factor that stems from Bayes theory, has been used as a validation metric to help estimate how well available experimental data fits model predictions [93]. Bayesian updating methods such as Bayes network models [121] update the reliability estimate of an overall system as more tests from different system levels become available. The approach can be useful in quantifying the contribution of different sources of uncertainty in a system.

Preliminary model validations are often carried out at the component system level, were is easier to perform tests under well controlled environments. However, for higher system level validation, experimental data might be scarce or more difficult to obtain. Bayesian networks can be used to update the posterior distributions of higher system level components in the network given any new data or information for lower component levels in the network. Likewise, different sources of error may be quantified given new evidence at any subsystem level.

6.1.1 Bayes Network Theory and Gibbs Sampling

Uncertainty introduced by physical variability and numerical discrepancies at various levels in a multilevel system problem can be propagated using Bayesian networks. Typically, systems can be divided into subsystem levels. Such levels can be represented as nodes in the Bayesian network. Each node represents a random quantity (e.g. a component level response, an input parameter or material property) and is therefore associated with a probability density function (pdf). The conditional relation among

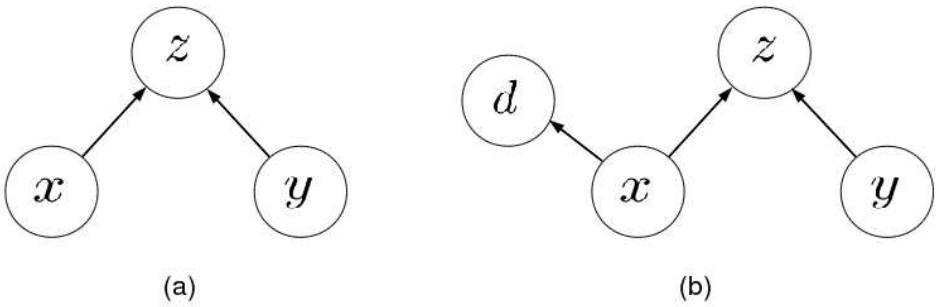

Figure 6.1: Bayes network schematic representation

nodes is established by arcs that graphically represent how nodes depend on each other, as illustrated in Figure 6.1. Therefore, a network will typically consist of a population of parents and its respective children. The full joint probability function or joint pdf of the entire system depicted on Figure 6.1(a) can then be computed by taking the product of all the node's probability density functions in the network, as follows [121]:

$$p(x, y, z) = p(x)p(y)p(z|x, y) \tag{6.1}$$

The marginal pdf of any node (including the system response if it is included in the network) can then be determined by integrating the join pdf of the entire system (Equation 6.1) over the values of all the remaining nodes:

$$p(x) = \int p(x, y, z)dydz \tag{6.2}$$

If a new set of evidence becomes available and it is included in the network as a new node, the joint pdf of the system can be updated. For example, if a new node d representing new experimental data available for node x is added to the network (Figure 6.1(b)), the joint pdf can be updated as follows

$$p(x, y, z, d) = p(x)p(y)p(z|x, y)p(d|x) \tag{6.3}$$

Once the full joint probability density function has been updated, it can be integrated to obtain the probability density function for any given node. Obtaining an exact or analytical solution for the integral of the joint pdf is typically not feasible. Markov Chain Monte Carlo methods (MCMC) [122] can be used to obtain samples from the multivariate joint pdf and estimate the posterior distribution of the system response. MCMC methods generate new random samples from the joint pdf by using the previously sampled values, i.e. generating a Markov chain. Several schemes are available to carry out the MCMC sampling [123]. Gibbs sampling [124] is one of the easiest to implement.

Instead of sampling directly n random variables from a more complicated joint probability density function, the Gibbs sampler estimates n random variables from n univariate conditional distributions, which are easier to sample. Instead of trying to estimate the marginal probability of each node in Figure 6.1(a) (i.e. $p(x), p(y), p(z)$) by integrating in turn the joint pdf with respect to the remaining variables (e.g. $p(x) = \int p(x, y, z)dydz$), univariate conditional distributions (e.g. $p(x|y, z)$) are sampled sequentially. All variables are initialized to starting values x_o, y_o, z_o and the marginal pdf's are estimated as follows

$$\begin{aligned}
&\text{Repeat n times } (i = 1 \text{ to n}) \\
&x_i \sim p(x|y_{i-1}, z_{i-1}) \\
&y_i \sim p(y|x_i, z_{i-1}) \\
&z_i \sim p(z|x_i, y_i) \\
&i = i + 1
\end{aligned} \tag{6.4}$$

If conditional density functions are not available (e.g. $p(x|y, z)$), they can be con-

structed by taking the product of terms containing the variable of interest (e.g. $p(x|y,z) = p(x)p(z|x,y)$) and using a rejection sampling technique [123] to obtain a variable sample. The marginal distribution for the variable of interest (e.g. x) can be obtained by collecting all sampled values of the respective variable. The n random sample values for each node are typically drawn from the conditional pdf's after a burn-in period to eliminate the effect of the initial selected values. The Gibbs sampler has a convergence of order $0(n)$. The available data for any node (e.g. d) can be incorporated in the network by defining a likelihood function. As described in [93], the likelihood of the model can be represented as

$$f(d|x) \sim N(x, \sigma_{\epsilon_{exp}}) \tag{6.5}$$

where x represents the model prediction, d the experimental observations, and $\sigma_{\epsilon_{exp}}$ the experimental measurement error standard deviation. If multiple experimental observations are available, the likelihood is obtained by taking the product of $f(d|x)$ evaluated at each available data point. The open source version of BUGS (Bayesian inference Using Gibbs Sampling) software, OpenBugs [125] was used to perform the Gibbs sampling. In the next section, a simple example problem will be used to illustrate how to introduce and update different sources of error given experimental data.

6.2 Single Level Algebraic Example

A simple algebraic example was developed to demonstrate the procedure used to quantify different sources of uncertainty and error using Bayesian networks. The example was used to help understand the general uncertainty quantification procedure before

moving on to the more complex impact response composite problem. The example test problem true response was assumed to be given by the next algebraic expression

$$y_{true} = (2a)log(1 + x) \tag{6.6}$$

where $a = 500.0$ represents the model input parameter and x represents the independent variable with value $x = [0 : 1]$. The algebraic expression y_{true} was assumed to be unknown. Only the analytical expression (model) used to predict the phenomenon represented by y_{true} was assumed to be known

$$y_{mod} = 1000x - ax^2 \tag{6.7}$$

Figure 6.2 shows the response of both the model simulation y_{mod} and the true response y_{true} across x. Both y_{mod} and y_{true} plotted in Figure 6.2 represent the true values for the simulation and data respectively.

The true response y_{true} and the predicted response y_{mod} are affected by different sources of variability and error that introduce uncertainty in the respective responses. The true response y_{true} (unknown) can only be estimated from experimental observations. The experimental observations suffer from experimental errors. The measured (observed) response y_{meas} exhibits uncertainty due to the experimental measurement error ϵ_{exp}. As described in [93], the true response y_{true} can be expressed as

$$y_{true} = y_{meas} + \epsilon_{exp} \tag{6.8}$$

The measurement error ϵ_{exp} can be modeled as $\epsilon_{exp} \sim N(0, \sigma_{\epsilon_{exp}})$, assuming ϵ_{exp}

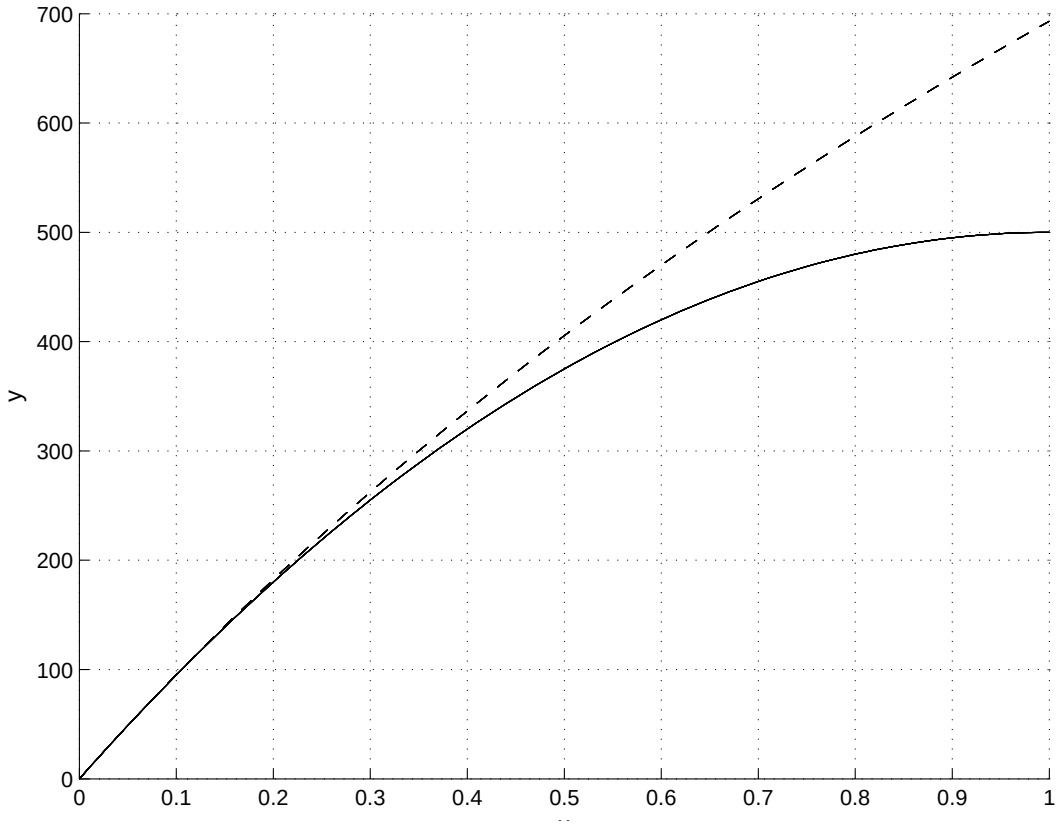

Figure 6.2: Analytical example predicted response y_{mod} (solid line) and true response y_{true} (dash line)

is random with no bias error in measurement. Using Equation 6.8 and assuming normal distributed measurement errors, the measured response y_{meas} can be written as a random variable that follows a normal distribution with mean given by the true response y_{true} and standard deviation given by $\sigma_{\epsilon_{exp}}$,

$$y_{meas} \sim N(y_{true}, \sigma_{\epsilon_{exp}}) \tag{6.9}$$

The experimental error standard deviation $\sigma_{\epsilon_{exp}}$ was assumed to have a value of 2% with respect to y_{true}. Another source of uncertainty that affects the true and simulated responses is the physical variability in the input parameter a. The parameter a is a random

variable that exhibits aleatory uncertainty. The variability in the input parameter a typically corresponds to variation of material properties encountered from experimental sample to sample and uncontrollable manufacturing conditions. The variability of a can be represented by assuming a random distribution (e.g. normal distribution) with mean μ_a and standard deviation σ_a,

$$a \sim N(\mu_a, \sigma_a) \tag{6.10}$$

In order to estimate the parameters of the random distribution in Equation 6.10, it is necessary to compute μ_a and σ_a from measured values of a. If a finite number of measurements for a are taken, the estimated value of a, referred to as $\hat{a}$, can be expressed as

$$\hat{a} \sim N(\hat{\mu_a}, \hat{\sigma_a}) \tag{6.11}$$

where $\hat{\mu_a}$ and $\hat{\sigma_a}$ denote the estimated mean and standard deviation of the distribution obtained by computing the statistics of the group of measured values of a. If enough samples of a are collected, then $\hat{\mu_a} \rightarrow \mu_a$ and $\hat{\sigma_a} \rightarrow \sigma_a$. In the example, the true values for the distribution parameters of a were assumed to be known ($\mu_a = 500.0$, $\sigma_a = 10.0$). The physical variability of a introduces variation in the true response, i.e. $y_{true} = f(a, x)$. Likewise, the variation in the response caused by a has to be taken into account in the predicted response y_{mod}. The predicted response y_{mod} can then be written as

$$y_{mod} = 1000x - \hat{a}x^2 \tag{6.12}$$

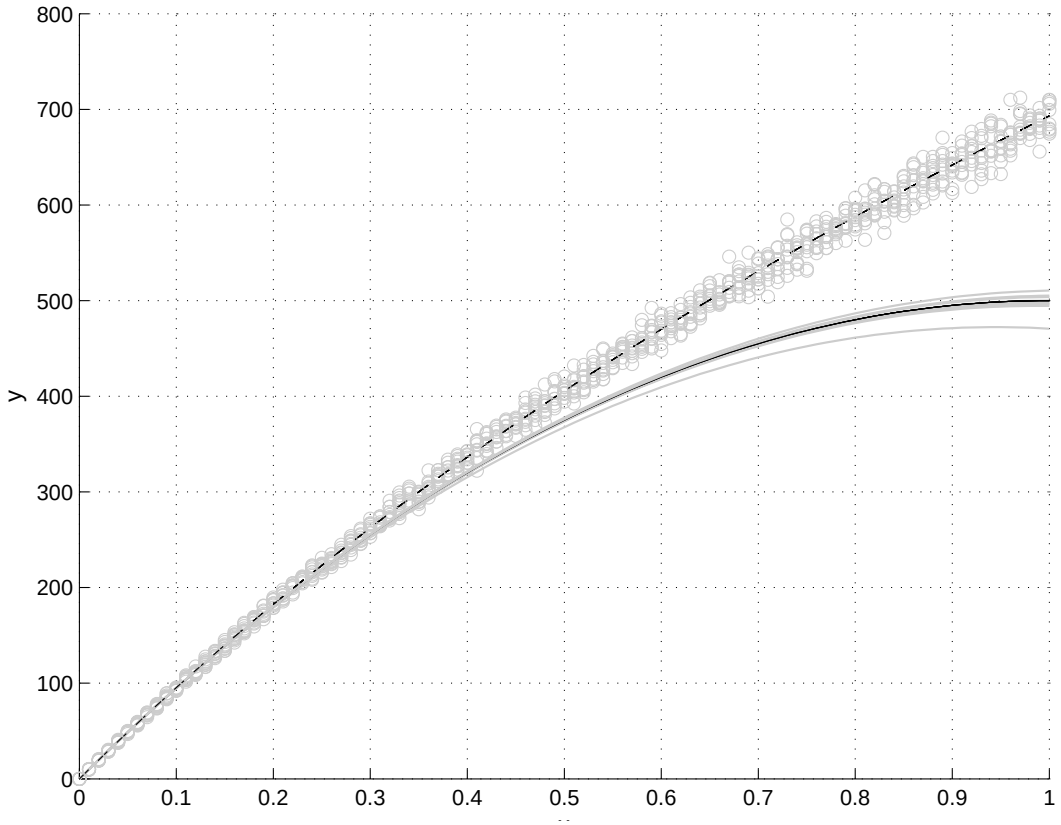

Figure 6.3: Analytical example true and predicted responses. The predicted response y_{mod} (solid lines), mean of the true response y_{true} (dash line) and measured response y_{meas} (circle marks) once variability in a and error ϵ_{exp} were incorporated are shown

The y_{true} and y_{mod} responses once variability in a was introduced are shown in Figure 6.3. The measured response y_{meas}, which includes the measurement error ϵ_{exp}, is also shown in Figure 6.3.

The predicted response y_{mod} also suffers from errors, such as numerical discretization errors introduced by approximations in the spatial and temporal discretization schemes (e.g. finite element methods), numerical truncation errors introduced by sampling methodologies such as response surface methods and model errors introduced by the model formulation itself. The prediction error ϵ_{pred} represents the error corresponding to numerical error ϵ_{num} and model errors ϵ_{mod} combined, i.e. $\epsilon_{pred} = \epsilon_{num} + \epsilon_{mod}$. The true

response y_{true} can also be written as a function of the predicted response [93]

$$y_{true} = y_{mod} + \epsilon_{pred} \tag{6.13}$$

For the simple algebraic example, the numerical error ϵ_{num} was assumed to be sufficiently small to be neglected. Therefore, the prediction error ϵ_{pred} was assumed to be equal to the model error ϵ_{mod}:

$$y_{true} = y_{mod} + \epsilon_{mod} \tag{6.14}$$

The model error ϵ_{mod} quantifies the discrepancy between the true prediction model (no numerical errors) and the true experimental observations (no experimental error). Many possibilities exist for how one can incorporate this source of error into the uncertainty quantification process. An obvious choice will be to express the model error ϵ_{mod} as a function of the variables that influence the response, i.e. $\epsilon_{mod} = f(x_i)$. Assuming a polynomial type approximation with n coefficients, the model error for the univariate algebraic problem can be expressed as

$$\epsilon_{mod} = \beta_0 + \beta_1 x + \beta_2 x^2 + ... + \beta_{n-1} x^{n-1} \tag{6.15}$$

The model error coefficients β_i represent random variables to be estimated through the Bayesian update. Therefore, prior distributions need to be provided for each one of the model error coefficients, for example:

$$\beta_i \sim uniform(a, b) \tag{6.16}$$

In preliminary studies, it was found that attempting to quantify all sources of uncertainty simultaneously (i.e. ϵ_{exp}, a and ϵ_{mod}) led to incorrect posterior distributions for the updated variables. Bayesian network theory does not provide a formal framework that allows to correctly partition the total uncertainty among the different sources of uncertainty. For instance, the measured experimental response y_{meas} includes the effect of both the experimental measurement error ϵ_{exp} and the variation of y_{true} due to the input parameter a. Although it would be desirable to separate the sources of uncertainty that affect the measured response y_{meas}, it is necessary to further investigate how to do so in practice.

For the sake of illustration, the experimental error ϵ_{exp} was assumed to reflect the variation in data due to measurement error ϵ_{exp} and physical variability of a combined. A general methodology that allows to incorporate and update all sources of uncertainties in a single theoretical framework will be investigated as part of the future work. For the current work, each source of uncertainty was estimated separately. The uncertainty due to measurements errors ϵ_{exp} and variability of a were estimated first given the available experimental data. Once ϵ_{exp} and a were estimated, the model error ϵ_{mod} was computed.

To illustrate the general procedure, it was assumed 10 measured responses y_{meas} were experimentally collected. Each response contains 10 data points, where each data point was measured at equally spaced discrete intervals of 0.1 on x. It was also assumed 10 values of the input parameter a_{meas} were experimentally measured as well. The statistics of the distribution parameters for the experimental error ϵ_{exp} and the input parameter a were estimated separately by obtaining corresponding prior distributions. For the illustration example, the statistics of the distributions for the mean and standard deviation of y_{meas} (y_{true}, $\sigma_{\epsilon_{exp}}$) and a ($\hat{\mu_a}, \hat{\sigma_a}$) were computed by performing bootstrapping sampling

Table 6.1: Estimated mean values for $\hat{\mu_a}$ and $\hat{\sigma_a}$ μ_a

$\hat{\mu_a}$	$\hat{\sigma_a}$
504.7	10.16

Table 6.2: Estimated mean values for the mean and standard deviation of y_{meas} (y_{true}, $\sigma_{\epsilon_{exp}}$) and y_{mod} ($\mu_{y_{mod}}$, $\sigma_{y_{mod}}$)

x	y_{true}	$\sigma_{\epsilon_{exp}}$	$\mu_{y_{mod}}$	$\sigma_{y_{mod}}$
0.1	95.09	1.533	94.95	0.1016
0.2	181.9	3.926	179.8	0.4065
0.3	260.8	4.139	254.6	0.9147
0.4	335.6	3.837	319.3	1.626
0.5	403.0	4.739	373.8	2.541
0.6	466.5	9.915	418.3	3.659
0.7	522.9	11.27	452.7	4.98
0.8	588.0	15.77	477.0	6.505
0.9	635.7	11.19	491.2	8.232
1.0	690.2	12.04	495.3	10.16

with replacement [126] over the available data, i.e. the 10 measured responses y_{meas} and the 10 measured values of a respectively. The estimated mean values for $\hat{\mu_a}$ and $\hat{\sigma_a}$ are presented in Table 6.1. Using Equation 6.12, the statistical parameters of the distribution of y_{mod} can also be computed. The mean values of the distribution parameters for y_{meas} and y_{mod} are presented in Table 6.2

Once the priors for the measurement error ϵ_{exp} and a were estimated, the Bayesian update was carried out to estimate the coefficients β_i of the model error ϵ_{mod}. The model error coefficients β_i were found to exhibit poor convergence when updated simultaneously. Systematically updating each model error coefficient β_i in turn was found to improve the convergence of the solution considerably. The estimated distributions for coefficients β_i at a given update were used as prior distributions for the next update. If the Bayesian update is denoted by a subscript, then ${\beta_1}^n$ refers to the n Bayesian update of coefficient β_1. Following that convention, the coefficients β_i were updated as follows:

$$
\begin{array}{lllllll}
1^{\underline{o}} \text{ update} & {\beta_0}^1 = {\beta_0}^0 & & & & & \\
2^{\underline{o}} \text{ update} & {\beta_0}^2 = {\beta_0}^1, & {\beta_1}^2 = {\beta_1}^0 & & & & \\
3^{\underline{o}} \text{ update} & {\beta_0}^3 = {\beta_0}^2, & {\beta_1}^3 = {\beta_1}^2, & {\beta_2}^3 = {\beta_2}^0 & & & \\
\vdots & \vdots & \vdots & \vdots & \ddots & & \\
n^{\underline{o}} \text{ update} & {\beta_0}^n = {\beta_0}^{n-1}, & {\beta_1}^n = {\beta_1}^{n-1}, & {\beta_2}^n = {\beta_2}^{n-1}, & \ldots & , {\beta_{n-1}}^n = {\beta_{n-1}}^0 &
\end{array}
\tag{6.17}
$$

The number of Bayesian updates should at least equal the number of coefficients β_i to update. For the algebraic example, the number of model error terms (Equation 6.15) used was $n = 5$. The prior distributions for the model error coefficients β_i are presented in Table 6.3. For the first Bayesian update, only the first term in Equation 6.15 was included and the model error coefficient ${\beta_0}^0$ updated. For the second Bayesian update, both constant and linear terms in Equation 6.15 were included. The distribution of β_0 obtained in the first update was used as prior for the second update. The prior distribution ${\beta_1}^0$ was also updated. The remaining Bayesian updates were sequentially carried out in the same way until all coefficients β_i were updated. The statistics for the estimated posterior distributions corresponding to β_i are presented in Table 6.4. All the estimated model error coefficients approximately follow normal distributions. The predicted response once model errors were estimated is shown in Figure 6.4 along with the real response y_{true}. Confidence bounds for 95% reliability are also shown for both the true response y_{true} and the predicted response (diamond marks). Error estimation for multilevel and hierarchical models constitutes a more complex problem. For such type of systems, limited data may be available for only a few subsystem levels. Such type of scenario was investigated in the Bayesian update of the multilevel algebraic example

Table 6.3: Prior distributions for model error coefficients β_i

${\beta_0}^0 \sim$ unif(-50.00,50.00)
${\beta_1}^0 \sim$ unif(-300.0,300.0)
${\beta_2}^0 \sim$ unif(-300.0,300.0)
${\beta_3}^0 \sim$ unif(-300.0,300.0)
${\beta_4}^0 \sim$ unif(-300.0,300.0)

Table 6.4: Mean μ and standard deviation σ of posterior distributions for model error coefficient β_i

	μ	σ
${\beta_0}^5$	0.050	1.633
${\beta_1}^5$	-6.239	17.92
${\beta_2}^5$	52.08	50.03
${\beta_3}^5$	158.5	68.87
${\beta_4}^5$	-9.673	40.80

presented in the next section.

6.3 Multilevel Example Problem

In this section, the simple algebraic example presented in the previous section was expanded to a multi-level hierarchical system of algebraic functions. The schematic representation of the entire hierarchical system can be seen in Figure 6.5. The subsystem levels depicted in Figure 6.5 were modeled by the following functions

$$y_1 = 1000x_1 - ax_1^2 \tag{6.18}$$

$$y_2 = bx_2 \tag{6.19}$$

$$z_1 = \frac{1}{100}(0.1y_1)^3 + y_2 \tag{6.20}$$

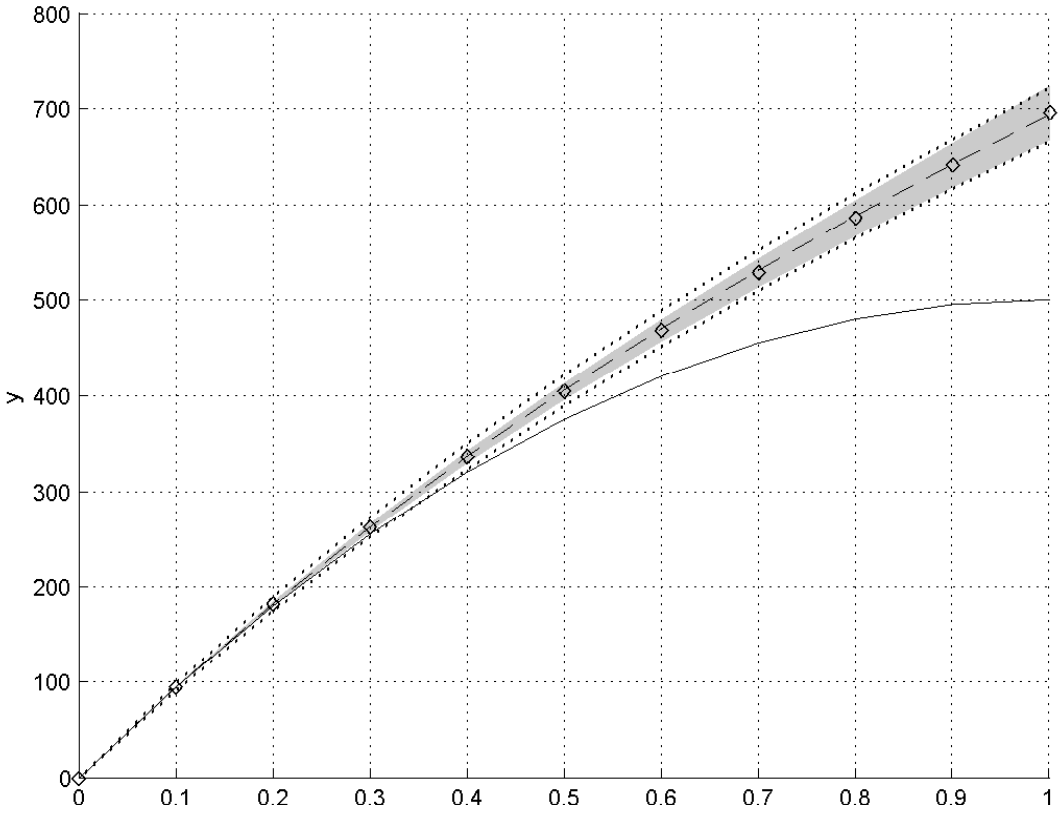

Figure 6.4: Model prediction y_{mod} (solid line), mean of true response y_{true} (dash line) and updated prediction (diamond marks). The dotted lines represent the 95% confidence intervals for y_{true}. The shaded area represents the 95% confidence intervals for the update prediction (diamond marks)

$$z_2 = y_1 + \frac{c}{100} x_3 y_2 \tag{6.21}$$

$$w = \frac{1}{1000} z_1 (5000 - z_2) \tag{6.22}$$

where $x_1 = [0:1], x_2 = [0:10], x_3 = [0:100]$ represent the independent variables and a, b, c represent the model input parameters. As discussed in the previous section, experimental errors ϵ_{exp} and physical variability of input parameters were either assumed to be known or enough information was assumed to be available to estimate their prior

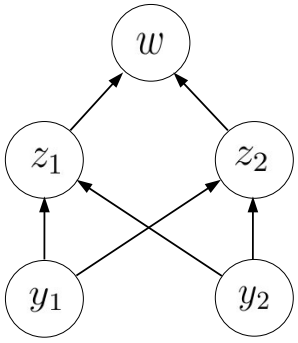

Figure 6.5: Schematic representation of hierarchical algebraic system example

distributions. The distributions for the input parameters were assumed to be approximately known, with normal distributions given by $a \sim N(500, 5), b \sim N(50, 0.5)$ and $c \sim N(5, 0.05)$. The true responses at each level were assumed to be functions of the algebraic expressions in Equations 6.18 to 6.22, with added extra terms as follows:

$$\begin{aligned} y_{1_{true}} &= y_1 + \beta_1^{(1)} y_1 + \beta_2^{(1)} y_1^2 \\ y_{2_{true}} &= y_2 + \beta_1^{(2)} y_2 + \beta_2^{(2)} y_2^2 \\ z_{1_{true}} &= z_1 + \beta_1^{(3)} z_1 + \beta_2^{(3)} z_1^2 \\ z_{2_{true}} &= z_2 + \beta_1^{(4)} z_2 + \beta_2^{(4)} z_2^2 \\ w_{true} &= w + \beta_1^{(5)} w + \beta_2^{(5)} w^2 \end{aligned} \tag{6.23}$$

with the added model error coefficient values $\beta_1 = [0.2, 0.0, 0.0, 0.25, 0.0]$ and $\beta_2 = [0.0, 0.0005, 0.0, 0.0, 0.0]$. A circumscribed central composite design [127] was used to obtain representative samples of each level response over the entire design space. Central composite designs (CCD) are used to sample the design points needed to fit response surface models. For a full quadratic response surface model, CCD provide enough points to estimate all the model coefficients. The responses obtained using Equation 6.23 over the sampled values of x_1, x_2 and x_3 are presented in Table 6.5. A circumscribed central composite design uses points outside the design space (e.g. $x_1 = 1.34$) to obtain good

Table 6.5: Sampled values of $y_{1_{true}}$, $y_{2_{true}}$, $z_{1_{true}}$, $z_{2_{true}}$ and w_{true} over the design space

x_1	x_2	x_3	$\mathbf{y_{1_{true}}}$	$y_{2_{true}}$	$z_{1_{true}}$	$z_{2_{true}}$	$\mathbf{w_{true}}$
0.0	0.0	0.0	0.0	0.0	0.0	0.0	0.0
0.0	0.0	100.0	0.0	0.0	0.0	0.0	0.0
0.0	10.0	0.0	0.0	625.0	625.0	0.0	3125.0
0.0	10.0	100.0	0.0	625.0	625.0	3906.2	683.5
1.0	0.0	0.0	600.0	0.0	2160.0	750.0	9180.0
1.0	0.0	100.0	600.0	0.0	2160.0	750.0	9180.0
1.0	10.0	0.0	600.0	625.0	2785.0	750.0	11836.0
1.0	10.0	100.0	600.0	625.0	2785.0	4656.2	957.3
-0.34	5.0	50.0	-478.8	281.2	-816.4	280.4	-3853.1
1.34	5.0	50.0	530.2	281.2	1772.3	1541.7	6129.2
0.5	-3.4	50.0	450.0	-155.9	755.3	75.2	3719.8
0.5	13.4	50.0	450.0	895.2	1806.4	3360.0	2962.6
0.5	5.0	-34.0	450.0	281.2	1192.5	-36.7	6006.3
0.5	5.0	134.0	450.0	281.2	1192.5	2919.5	2480.9
0.5	5.0	50.0	450.0	281.2	1192.5	1441.4	4243.6

estimates of second-order effects over the entire design space. For the illustrative multi-level simulation problem, it was assumed that only the true values for the y_1 and w levels were known. Therefore, the values of $y_{1_{true}}$ and w_{true} presented in Table 6.5 were assumed to represent the available data $y_{1_{data}}$ and w_{data}. The experimental error ϵ_{exp} distribution was also assumed to be known a priori. It follows a normal distribution with zero mean and standard deviation of 1% with respect to the values of $y_{1_{true}}$ and w_{true} presented in Table 6.5.

Figure 6.6 shows the Bayes network representation of the hierarchical system example depicted in Figure 6.5. The true responses were estimated by adding modeling errors to the model predictions at each level. For the single variable algebraic example presented in the last section, the model error ϵ_{mod} was expressed as a function of the independent variables, i.e. $\epsilon_{mod} = f(x)$. For a multivariate problem, if a polynomial type model is used to capture the error dependency of the problem variables, the number of terms in the polynomial model becomes too many. Therefore, the model error ϵ_{mod}

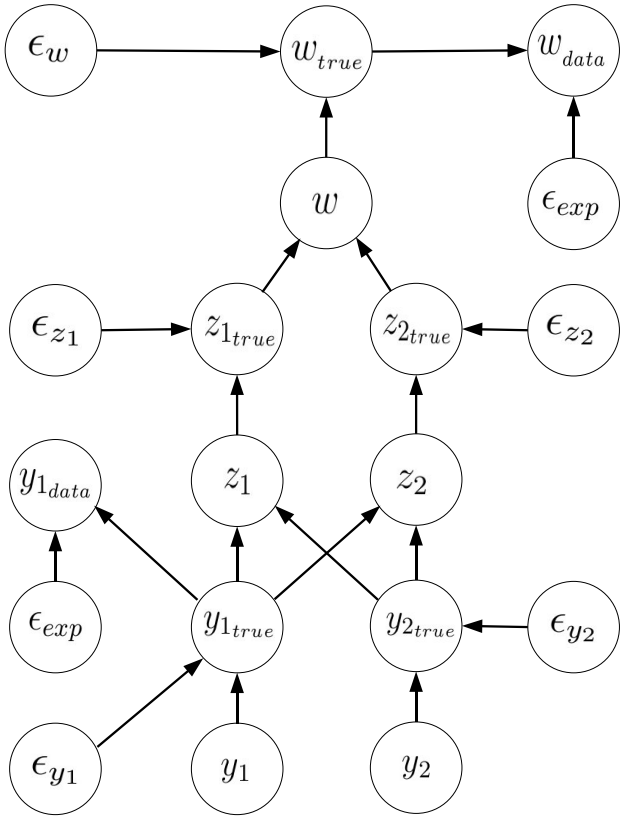

Figure 6.6: Bayes network representation of hierarchical algebraic system example

was expressed as a function of the model prediction, i.e. $\epsilon_{mod} = f(y_{mod})$. Assuming a polynomial type approximation leads to

$$\epsilon_{mod} = \beta_0 + \beta_1 y_{mod} + \beta_2 y_{mod}^2 + ... + \beta_{n-1} y_{mod}^{n-1} \tag{6.24}$$

Using the model error form presented in Equation 6.24, the model errors ϵ_{y_1}, ϵ_{y_2}, ϵ_{z_1}, ϵ_{z_2} and ϵ_w were estimated as shown in Equation 6.25. For the multivariate simulation problem, the Bayesian update exhibited instabilities when trying to estimate bias model error effects. Therefore, it was assumed that there was no bias error in the model prediction, i.e. $\beta_0 = 0.0$. The model error coefficients $\hat{\beta}_1$ and $\hat{\beta}_2$ represent unknown random variables that will be estimated via Bayesian update. The true values of $\hat{\beta}_1$ and

Table 6.6: Prior distributions for model error coefficient $\hat{\beta}_1$

$\hat{\beta}_1^{(1)} \sim unif(-0.40, 0.40)$
$\hat{\beta}_1^{(2)} \sim unif(-0.40, 0.40)$
$\hat{\beta}_1^{(3)} \sim unif(-0.40, 0.40)$
$\hat{\beta}_1^{(4)} \sim unif(-0.40, 0.40)$
$\hat{\beta}_1^{(5)} \sim unif(-0.40, 0.40)$

$\hat{\beta}_2$ (assumed to be unknown) are given by β_1 and β_2 in Equation 6.23.

$$\begin{aligned} \epsilon_{y_1} &= y_1 + \hat{\beta}_1^{(1)} y_1 + \hat{\beta}_2^{(1)} y_1^2 \\ \epsilon_{y_2} &= y_2 + \hat{\beta}_1^{(2)} y_2 + \hat{\beta}_2^{(2)} y_2^2 \\ \epsilon_{z_1} &= z_1 + \hat{\beta}_1^{(3)} z_1 + \hat{\beta}_2^{(3)} z_1^2 \\ \epsilon_{z_2} &= z_2 + \hat{\beta}_1^{(4)} z_2 + \hat{\beta}_2^{(4)} z_2^2 \\ \epsilon_w &= w + \hat{\beta}_1^{(5)} w + \hat{\beta}_2^{(5)} w^2 \end{aligned} \tag{6.25}$$

As discussed in the previous section, the number of Bayesian updates should at least equal the number of model error terms employed in Equation 6.15. As depicted in Tables 6.6 and 6.7, both model error coefficients $\hat{\beta}_1$ and $\hat{\beta}_2$ were given uniform distributions as priors. The prior distribution bounds were assigned based on reasonable value ranges within the level response. For the first Bayesian update, only linear terms associated with $\hat{\beta}_1$ were added to the Bayesian network. The prior distributions of $\hat{\beta}_1$ were then updated via the Bayesian procedure. For the second Bayesian update, both linear terms and second order terms associated with $\hat{\beta}_1$ and $\hat{\beta}_2$ were added to the network. The estimated $\hat{\beta}_1$ probability distributions computed in the first update were used as priors for the second Bayesian update. Both $\hat{\beta}_1$ and $\hat{\beta}_2$ estimated solutions were found to converge.

The statistics of the posterior distributions obtained via Bayesian update for $\hat{\beta}_1$ and $\hat{\beta}_2$ are presented in Tables 6.8 and 6.9. The posterior distributions for the model error

Table 6.7: Prior distributions for model error coefficient $\hat{\beta}_2$

$\hat{\beta}_2^{(1)} \sim unif(-0.001, 0.001)$
$\hat{\beta}_2^{(2)} \sim unif(-0.001, 0.001)$
$\hat{\beta}_2^{(3)} \sim unif(-0.001, 0.001)$
$\hat{\beta}_2^{(4)} \sim unif(-0.001, 0.001)$
$\hat{\beta}_2^{(5)} \sim unif(-0.001, 0.001)$

Table 6.8: Mean μ and standard deviation σ of posterior distributions for model error coefficient $\hat{\beta}_1$. The true values of $\hat{\beta}_1$ (assumed to be unknown) are also presented

	true value	μ	σ
$\hat{\beta}_1^{(1)}$	0.20	0.210	0.036
$\hat{\beta}_1^{(2)}$	0.00	-0.017	0.036
$\hat{\beta}_1^{(3)}$	0.00	-0.006	0.288
$\hat{\beta}_1^{(4)}$	0.25	0.233	0.232
$\hat{\beta}_1^{(5)}$	0.00	0.077	0.287

coefficients $\hat{\beta}_1$ and $\hat{\beta}_2$ can be seen in Figures 6.7 to 6.8. It can be seen from the statistics in Tables 6.8 and 6.9, that the estimated posterior distributions bound the true values β_1 and β_2. Some of the model error coefficients exhibit relatively large standard deviations, which reflects the lack of knowledge (data) regarding the true response of y_2, z_1 and z_2, as specified by the large priors given to the model error coefficients $\hat{\beta}_1$ and $\hat{\beta}_2$.

In the next chapter, the general methodology to implement the composite problem within the Bayesian network will be discussed. Following the methodology presented in the last two sections, it will be investigated if model errors can be estimated at different levels of the composite system problem.

Table 6.9: Mean μ and standard deviation σ of posterior distributions for model error coefficient $\hat{\beta}_2$. The true values of $\hat{\beta}_2$ (assumed to be unknown) are also presented

	true value	μ	σ
$\hat{\beta}_2^{(1)}$	0.0000	0.00e-4	5.76e-4
$\hat{\beta}_2^{(2)}$	5.0e-4	3.60e-4	2.70e-4
$\hat{\beta}_2^{(3)}$	0.0000	-0.56e-4	0.63e-4
$\hat{\beta}_2^{(4)}$	0.0000	0.26e-4	0.70e-4
$\hat{\beta}_2^{(5)}$	0.0000	0.30e-4	0.34e-4

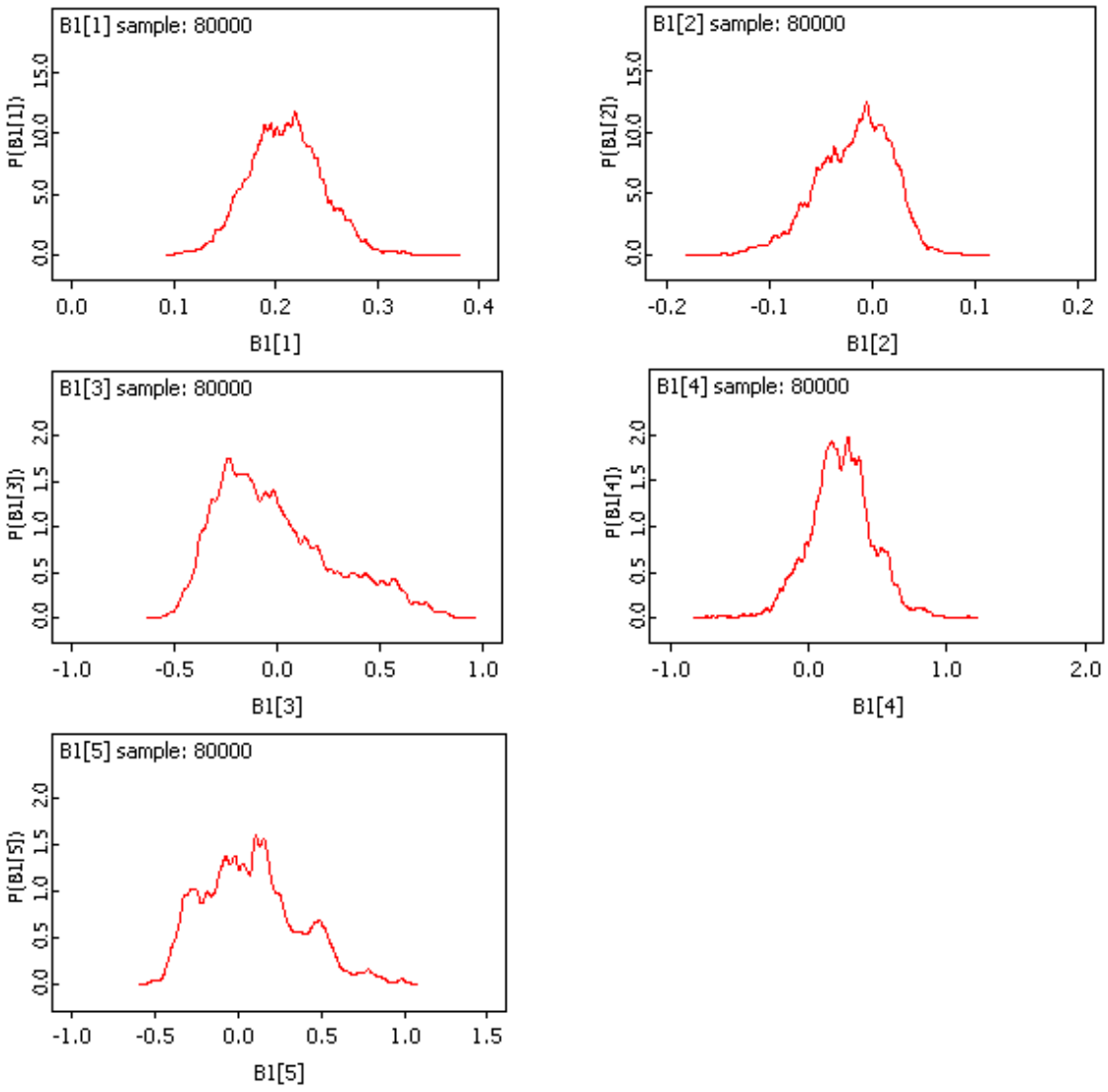

Figure 6.7: Estimated posterior distributions for model error coefficient $\hat{\beta}_1$

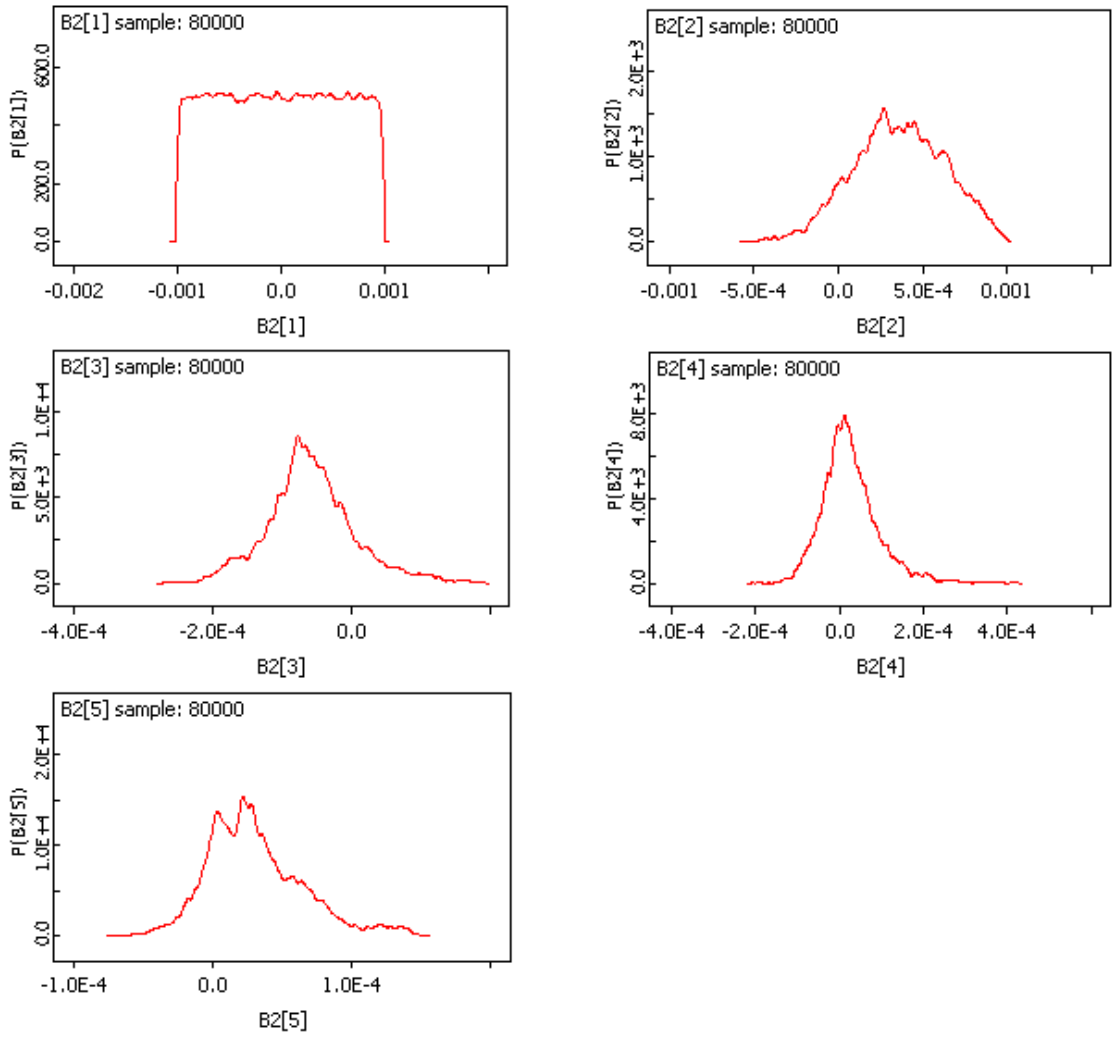

Figure 6.8: Estimated posterior distributions for model error coefficient $\hat{\beta}_2$

Chapter 7

Composite Multilevel & Hierarchical System Problem

Many sources of uncertainty and errors affect the response of complex engineering systems. As discussed in Chapter 3, uncertainties arise due to lack of knowledge regarding the behavior and inefficient characterization of a specific phenomenon as well as variation in material properties, manufacturing and operation conditions, while errors arise due to known assumptions introduced in order to simplify the analysis at hand and reduce computational time [128].

The impact response of engineering materials has been shown to exhibit sensitivity to physical variability resulting from small changes in boundary conditions, angle of impact, projectile velocity and material properties. Experimental impact tests of steel impactors hitting a viscoelastic foam-pad have shown that even if the test is repeated under the same initial conditions in a carefully controlled environment, peak accelerations measured upon impact can vary substantially [129].

Constitutive material model input parameters constitute one of the major sources of uncertainty in any numerical simulation. Propagation of input parameters uncertainty is well documented in the literature. Different techniques are available to estimate or bound the response variability due to input material parameters uncertainty. However, the inherent problem is that material parameters are often derived from simple experimental tests that don't necessarily exhibit a) the complex physics and b) the highly variable response of the target engineering application.

Experimental tests used for model parameters estimation typically account for only a subset of the physics shown by more complex problems [130]. A natural question that arises is how well can material parameters derived from simple tests account for material behavior under multiaxial loading, coupled failure modes and high sensitivity to small variations. Material models may require deriving material parameters at length scales for which experimental set up may be difficult (e.g. microscale); parameters are therefore estimated from tests performed at feasible length scales, such as the macroscale level. All these issues constitute sources of uncertainty and error in complex engineering problems.

In the presence of various sources of uncertainty (both physical and numerical), it is only logical to question the level of confidence of the predicted response. Accurate quantification of different type of uncertainties can help bound the response within realistic estimates. In the current chapter, the model error estimation methodology presented in Chapter 6 was applied to a ballistic impact test problem to quantify the individual sources of modeling error that affect the response of the composite test problem.

7.1 Sources of Modeling and Physical Uncertainties on Composite-Impact Problems

Any model validation exercise requires a systematic identification of sources of uncertainty. In the current section, the most common sources of uncertainty that affect prediction response of composite impact problems were identified. As described in Rebba et al [93], the main sources of error can be broken into the following major categories:

- Assumptions/measurements of input parameters
- Approximations in the spatial and temporal discretization schemes such as FEM
- Sampling methodologies such as Monte Carlo simulation and response surface methods
- Measurement of output quantities
- Model itself

A schematic representation of the different physical, modeling and numerical sources of uncertainty that affect the response of typical composite-impact problems is shown in Figure 7.1. Modeling errors in composite analytical models arise from assumptions and simplifications made at different scales of the material. Uncertainties at the constituent, ply and laminate level response arise in the modeling of the following physical phenomena:

- Nonlinearity and strain rate sensitivity of the polymer material.
- Initiation of damage, crack propagation, onset of plasticity and stiffness degradation of the polymer material.

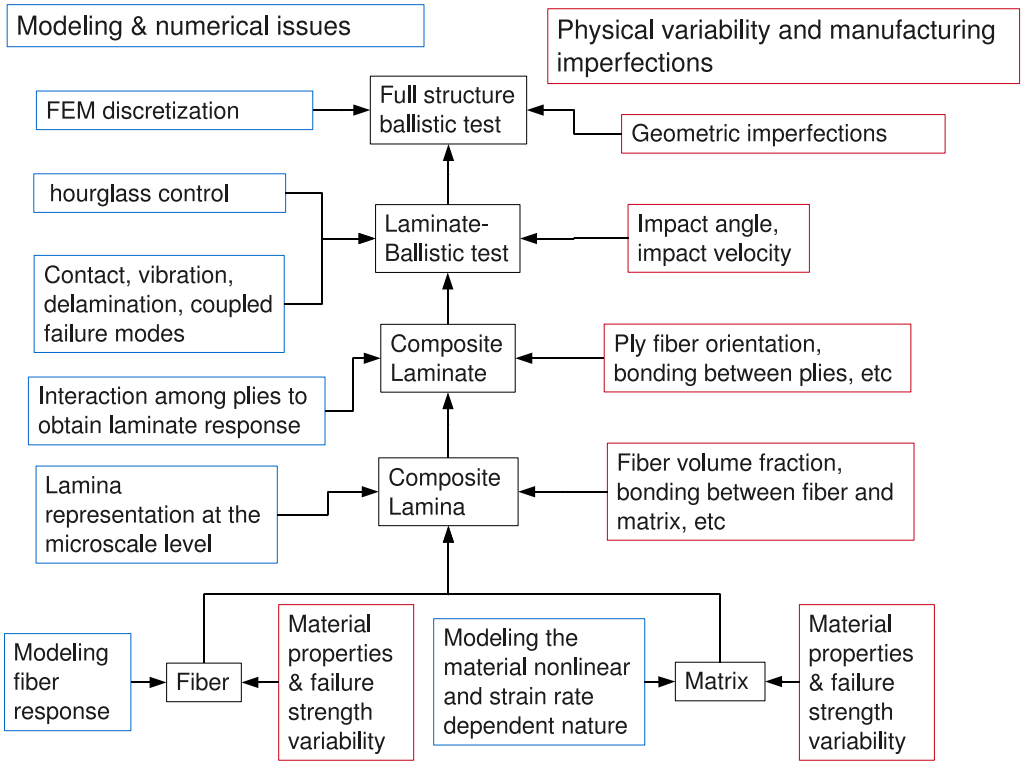

Figure 7.1: Schematic representation of sub-system and system main sources of physical, modeling and numerical uncertainty

- Fiber bundles/yarns response and fiber failure.

- Interaction of constituents at the micromechanical level. Typical assumptions on representative volume elements include uniform stresses and strains, and volume averaging of stresses and strains.

- Fibers distribution across composite cross-sectional area. Simplified fiber distributions (e.g. square packing and hexagonal packing) are typically used on representative volume elements.

- Multiple failure modes that ballistic impact response of composites exhibit. Failure modes observed on ballistic impact tests of composites include fiber breakage, fiber buckling, matrix cracking, indentation, fiber pullout, delamination and shear

plugging [7].

- Bonding between fiber and matrix. Some interface effects that arise due to the lack of perfect bonding between fiber and matrix include chemical bonding between fiber and matrix, mechanical bonding due to natural fiber roughness, micro-cracks in the fiber as a result of interfacial bonding and effects of moisture due to weak bonding interface [40].

- Thermal effects (such as residual stresses due to different matrix and fiber thermal coefficients), moisture, fatigue, creep.

- Material imperfections, such as voids and manufacturing defects.

- Contact between plies.

Sources of aleatoric uncertainty include:

- Variability of material properties. For example, effective mechanical properties of fiber yarns can vary from yarn to yarn due to fiber misalignment at the micro-scale level and rupture of fibers [131].

- Manufacture imperfections. Variations in the angle orientation of composite layers, layer thickness, constituent volume fractions, void content and imperfect bonding between fiber and matrix.

- Angle and location of bullet impact.

- Measurement experimental error.

Sources of numerical error include:

- Time and spatial numerical discretization of governing differential equations in finite element methods and finite element differences.

- Parallel decomposition schemes such as massive parallel processing (MPP).

Sources of uncertainty and error differ in nature and the challenge resides on accounting for their different effects in the uncertainty propagation process. Correctly characterizing modeling, numerical and experimental errors constitutes the ultimate goal of any model validation effort.

7.2 Composite Impact Problem Test

In the current section, the composite test problem used for the model validation investigation is described in detail. Multilevel systems and hierarchical systems are used exchangeably when referring to the composite test problem. Multilevel refers to the presence of two or more sub-levels (e.g. variables, equations, models) within the main system. For example, the composite problem can be broken into polymer, fiber, lamina, laminate and structural subsystems or sub-levels. Hierarchical refers to the dependence of one or more levels to one another, where typically lower levels feed information (input) to upper levels (output). For example, the inelastic response of the matrix-polymer material is needed in order to compute the response of the composite lamina. As the complexity of the system increases, it is likely that the number of levels and degree of dependency among each other will increase too.

A composite fuselage structure represents a good illustrative example of the type of systems of interest. In order to validate the response of the composite structure under impact, it is desirable to validate the model with available data at different sub-levels (e.g.

matrix, fiber, composite lamina and composite laminate). The model validation effort can help identify sources of large model discrepancy that can be targeted for more accurate model development.

The composite structural impact problem investigated exhibits failure response that requires models that can predict responses at various scales and integrate them into the system response prediction. A brief description of each subsystem level in the composite problem, the type of experiments simulated and used material properties are given next.

7.2.1 Polymer level

The response of the polymer material was simulated using the implemented polymer material model described in Section 5.1.1. The inelastic behavior of the polymer material exhibits nonlinearity and strain rate sensitivity. The polymer material inelastic strain ϵ_{ij}^{I} was passed on to the composite lamina level to compute the response of the unidirectional lamina.

A longitudinal tensile test simulation at high strain rate was carried out to measure the polymer stress, which was denoted by σ_x^{pol}. The strain rate used for the simulation was $\dot{\epsilon_x} = 365/sec$ [23]. The material properties X_{pol} for the polymer specimen were obtained from Reference [23] and are given in Table 7.1.

7.2.2 Fiber level

The fiber response was assumed to be linear elastic and transversely isotropic, until it reaches failure. The softening and stiffness degradation of the fiber material were given by the phenomenological model described in Section 5.2. The model was

Table 7.1: Polymer material model input parameters X_{pol}

Elastic Modulus (GPa)	6.33
Poisson's ratio	0.4
D_0 (1/s)	1.0e+06
n	0.85
q	150.5
Z_0 (MPa)	259.5
Z_1 (MPa)	1131.4
α_0	0.129
α_1	0.152

Table 7.2: Fiber material model input parameters X_{fib}

Longitudinal Modulus (GPa)	276.0
Transverse Modulus (GPa)	13.8
Longitudinal Poisson's ratio	0.25
Transverse Poisson's ratio	0.25
In-plane Shear Modulus (GPa)	20.0
Longitudinal Failure Strain	0.018

implemented within the composite lamina micromechanical formulation, so only the fiber input material parameters X_{fib} were passed to the composite lamina model. The material properties for IM7 fiber were obtained from Reference [23] and are listed in Table 7.2.

7.2.3 Composite Unidirectional Lamina level

The stresses of the composite lamina were computed in the fiber material local coordinate system, i.e. the fiber orientation angle is equal to zero. The resultant stresses in the composite lamina were obtained by using a micromechanical representative volume element, as described in Section 5.3. The linear elastic responses of the matrix and fiber materials are embedded within the micromechanical model formulation, so only the polymer inelastic strains ϵ_{ij}^I and fiber material properties were given as input to the composite lamina model. A uniaxial tensile test at high strain rates was simulated to compute the stress of the lamina in the fiber direction (denoted by $\sigma_x^{\theta=0^\circ}$). A strain rate

equal to $\dot{\epsilon_x} = 320/sec$ was assumed for the test. A fiber volume fraction of 0.6 was used for the composite material [23]. The fiber volume fraction represents the only material input parameter (denoted by $X_{\theta=0^\circ}$) for the composite lamina model .

7.2.4 Composite Lamina with Fiber Angle Orientation level

The stresses of the composite lamina were computed in the lamina global coordinate system, i.e. the fiber has a finite angle orientation, which involves a coordinate system transformation from fiber coordinate system (local material system) to lamina coordinate system (global material system). Similar to the previous composite lamina level, a uniaxial tensile test at high strain rates was carried out in LS-DYNA to measure the stress of a 10° lamina in the x direction $\sigma_x^{\theta=10^\circ}$. The test strain rate value $\dot{\epsilon_x} = 320/sec$ was taken from Reference [23]. The fiber angle orientation of the lamina (10 °) represents the only material level input parameter $X_{\theta=10^\circ}$ for the current level.

7.2.5 Ballistic Impact level

The final level in the composite example problem corresponds to the ballistic impact test of a balanced and symmetric composite laminate made out of eight plies with 10° fiber angle orientation. The velocity of the projectile V_p upon impact was measured in the simulated ballistic impact test. Details of the cohesive model law implementation can be found in Reference [35]. The material model input parameters for the ballistic impact test X_{bal} are listed bellow. The initial velocity and material properties of the cylindrical steel projectile used in the impact test simulation are given in Table 7.3.

A Bayesian network schematic representation of the composite test problem described in the current section is presented in Figure 7.2. The schematic representation

Table 7.3: Projectile input parameters

Elastic Modulus (GPa)	207.0
Poisson's ratio	0.30
Initial Velocity (m/s)	122.0

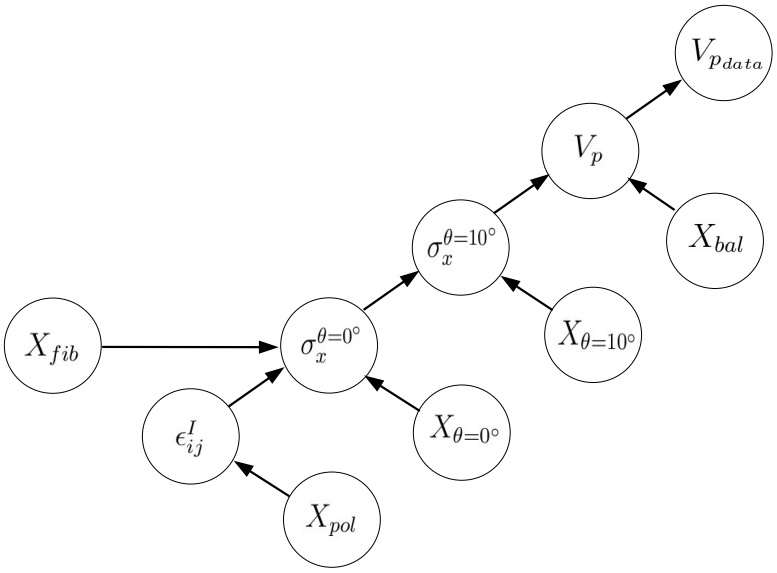

Figure 7.2: Schematic representation of the composite multilevel and hierarchical system

presented in Figure 7.2 provides a general idea of how the different levels within the network were structured along with the hierarchical nature of the system. The node $V_{p_{data}}$ represents ballistic test experimental data (projectile residual velocity). For some levels, such as the polymer level, the variables passed as input to the next level (inelastic strains), do not always correspond to the variables that get validated with measured data (polymer stresses). However, due to back propagation of uncertainty within the network, the prior distribution of the inelastic strain can be updated once data at any level becomes available. The general implementation procedure of the composite system within the Bayesian framework is outlined in the next section.

7.3 Bayesian Network Implementation using Response Surface Models

The OpenBugs software, which was used to conveniently carry out the Gibbs sampling updating, is not a programming language in the strict sense of the word. Conditional statements such as "if" statements or the sequential nature of traditional programming languages do not have any significance in OpenBugs. Therefore, it was not possible to implement any type of iterative or sequential algorithms within OpenBugs. Nodes can only be defined as explicit functions of other variables or nodes within the Bayes network.

Response surface methods have been used to simplify the analysis of complex problems and reduce the computational cost of large simulations. Basically, a simplified response surface is fitted to a discrete number of model runs to build an approximate function that can be evaluated at significantly less computational cost. Propagation of uncertainty can be carried out more efficiently in large models where the use of Monte Carlo simulations is prohibitively expensive. A review of issues associated with response surface approximations was given in Morgan et al. [132]. Linear and quadratic regression models, least square methods (polynomial, exponential, logarithmic), spline interpolation and Lagrange interpolation are commonly used to fit the response surface models.

Response surface models (RSM) [127] constitute a relatively simple way of explicitly specifying a given response as a function of its input parameters. Response surface models are multivariate polynomial models that include as many predictor variables $x_i (i = 1, ..., N)$ as necessary (e.g. higher order terms) in order to specify the response:

$$y(x) = b_0 + \sum_{i=1}^{N} b_i x_i + \sum_{i<j}^{N} b_{ij} x_i x_j + \sum_{i=1}^{N} b_{ii} {x_i}^2 + ... + \varepsilon \tag{7.1}$$

Quadratic response surface models are among the simplest to implement and provide an optimum level (maximum or minimum) for the response. The process of obtaining the response surface model coefficients b_i in Equation 7.1 is commonly refer to as model fitting or model calibration. Given a set of N predictor variables x_i, the number of model coefficients b_i to be determined is equal to $p = (N + 2)(N + 1)/2$. The vector y of m independent observations is related to the m by p effects matrix X as follows [133]:

$$y = Xb \tag{7.2}$$

where y and X are defined as

$$y = \left\{ \begin{array}{c} y_1 \\ y_2 \\ \vdots \\ y_m \end{array} \right\} \tag{7.3}$$

$$X = \left[\begin{array}{cccc} X_{11} & X_{12} & \dots & X_{1p} \\ X_{21} & X_{22} & \dots & X_{2p} \\ \vdots & \vdots & \ddots & \vdots \\ X_{m1} & X_{m2} & \dots & X_{mp} \end{array} \right] \tag{7.4}$$

The p effects X_{ij} for each observation y_i include an intercept, linear, interaction and squared terms that result from combining the predictor variables x_i as depicted in Equation 7.1. The error introduced by the response surface model was denoted by ε in

Equation [**?**]. The most common unbiased estimator for the b_i coefficients is given by:

$$b = (X^T X)^{-1} X^T y \tag{7.5}$$

Central composite designs (CCD's), also known as Box-Wilson designs [134], were used to calibrate the quadratic response surface models. The CCD's designs can estimate the $(N + 2)(N + 1)/2$ coefficients of a quadratic model with N factors more efficiently than a full factorial design. The general procedure to implement the polymer material model within OpenBugs is described in the next section. Emphasis was made in illustrating the transition between the FEM implementation and the Bayesian network implementation.

7.4 Composite System Implementation within the Bayesian Framework

As previously discussed, the composite model was implemented in the finite element code LS-DYNA. A schematic representation of the polymer material model implemented in LS-DYNA is shown in Figure 7.3. In the finite element implementation, all quantities were updated via time integration. The strain tensor components ϵ_{ij} and material model parameters were passed as inputs to the polymer material model, which in turn updated the stresses. The updated stress tensor components σ_{ij} were returned as input for the next time step calculation and subsequent increment in the strains.

Implementation of the polymer material model in the Bayesian network framework differs significantly from that on the finite element code. As mentioned earlier, only

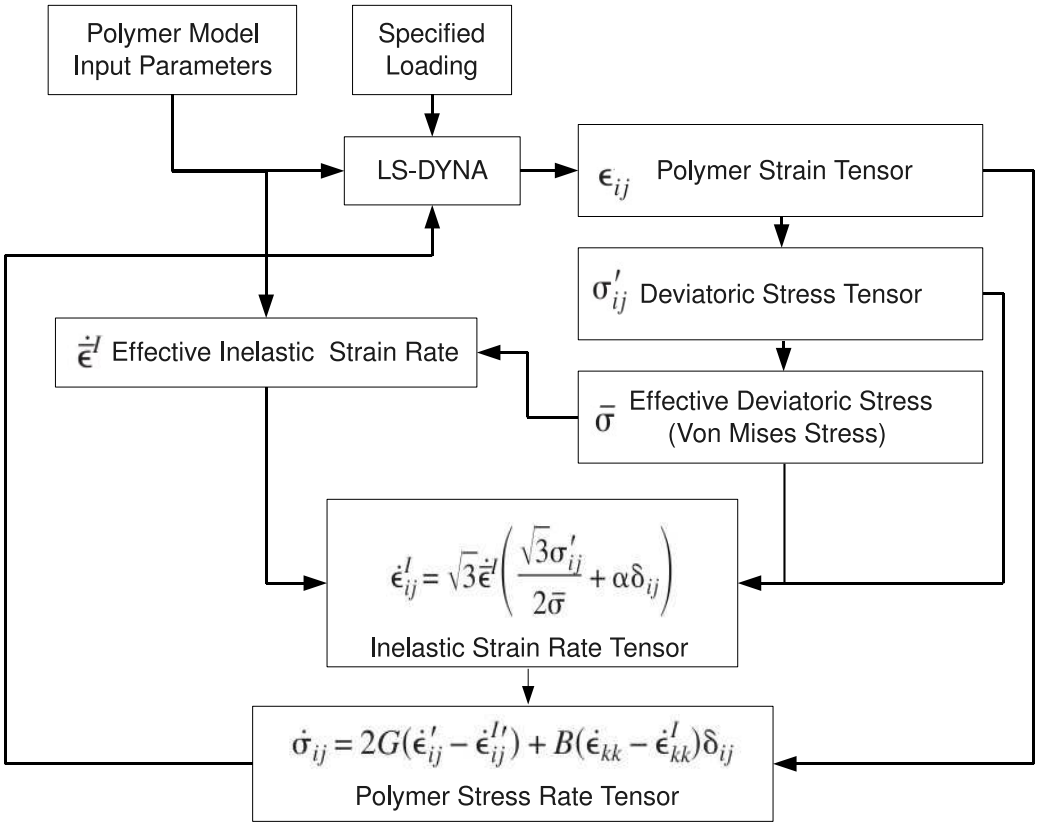

Figure 7.3: Schematic representation of Polymer Model FEM Implementation

explicit equations can be defined within OpenBugs. Implementing implicit equations that need to be solved using nonlinear implicit solvers or updating of model variables via time integration becomes an issue. Figure 7.4 shows the schematic representation of the polymer model as implemented within the Bayesian framework. Response surface models were used in different instances of the polymer model implementation:

- The inelastic strain ϵ^I_{ij} is a direct function of two quantities: the effective inelastic strain $\bar{\epsilon}^I$ and the stress σ_{ij}. The effective inelastic strain $\bar{\epsilon}^I$ was computed using the modified Bodner-Partom model, a nonlinear implicit equation. Likewise, the stress σ_{ij} was updated by integrating over time. RSM were used to explicitly defined the inelastic strain ϵ^I_{ij} as a function of model input parameters and specified loading

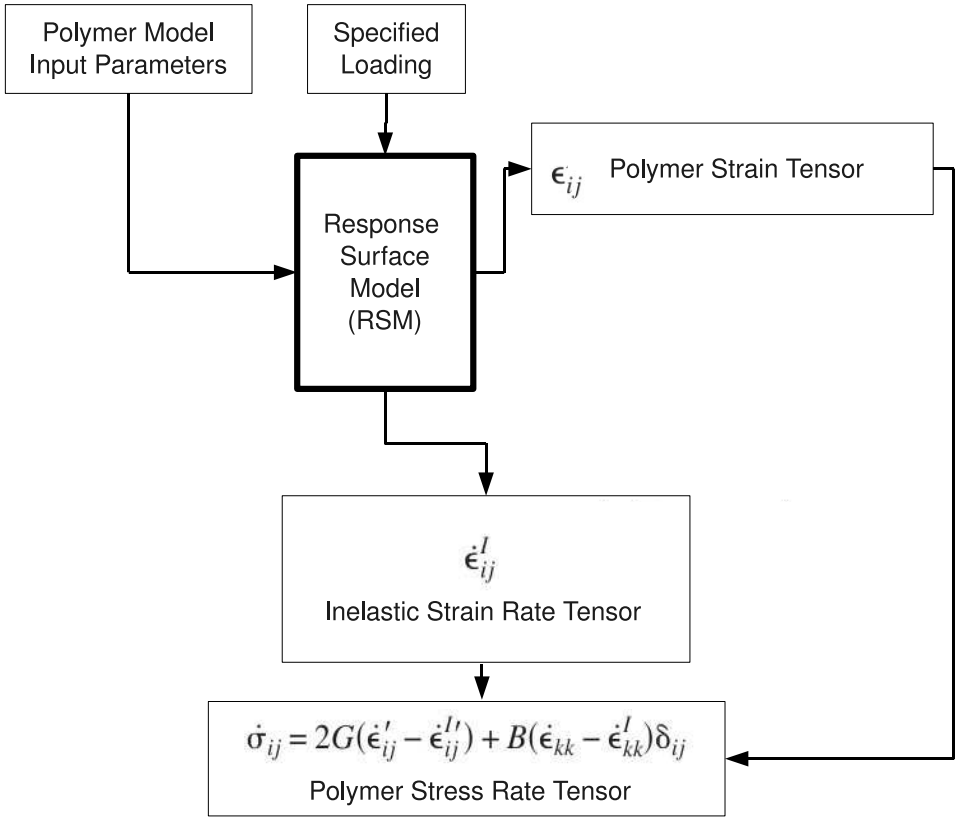

Figure 7.4: Schematic representation of Polymer Model OpenBugs Implementation

(e.g. strain load control).

- The updated strain ϵ_{ij} is passed by the finite element code as an input to the polymer material model along with the material model input parameters at each time step. Random perturbations of the material model input parameters result in variation of the strain ϵ_{ij}. RSM were used to explicitly simulate the variation of the strain ϵ_{ij} as a result of random variations in the polymer model input parameters.

Once the model variables were explicitly defined via RSM, the time history of each variable had to be defined within OpenBugs. For transient problems, validating the time dependent response of a material model may be of particular interest. Validating a material model solely on a single value type of response (e.g. the total strain energy

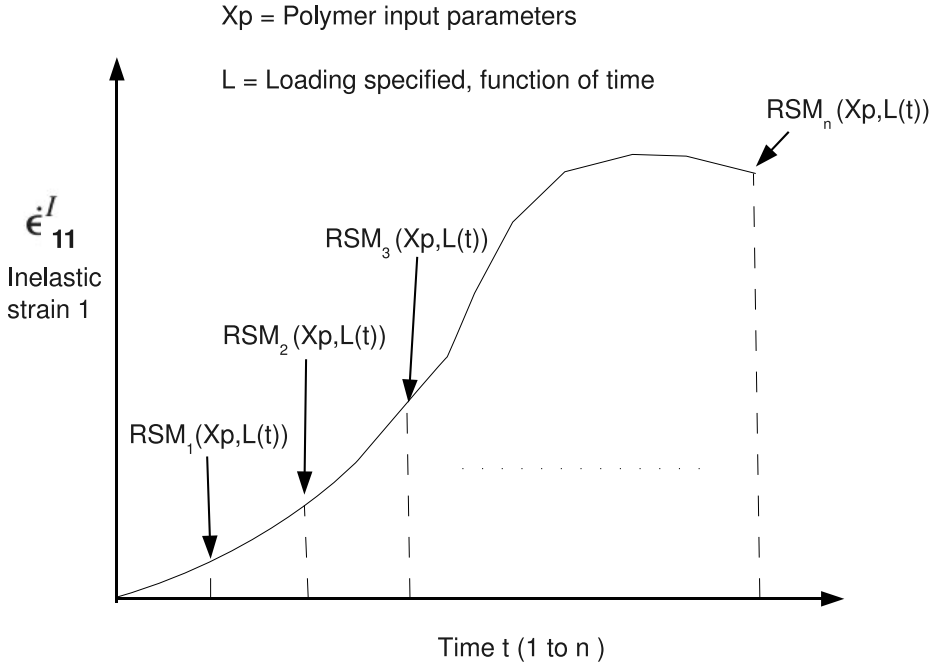

Figure 7.5: Time evolution of inelastic strain tensor component using response surface models

dissipated), may not provide an accurate estimate of the model predictive capabilities. For systems whose performance is load path dependent, it may be desirable to validate the model at different stages of the time loading history. The level of confidence in the predictions can be estimated by incorporating data over the entire loading history domain into the Bayes network.

The time evolution of the polymer material strains and stresses was modeled by representing the corresponding nodes in the network as vector arrays. If the time domain is discretized in n intervals, each node in the network can be visualized as a vector of size n that contains the corresponding variable value at each time interval. A "for loop" was used to step into each time interval in the node array. Furthermore, a response surface model was used to represent the value of each variable (e.g. inelastic strains) at each time interval, as seen in Figure 7.5.

The same procedure was used to implement the remaining subsystem levels in the composite test problem (i.e. response surface models were used to define the remaining nodes in the network). Figure 7.6 depicts the Bayesian network representation of the composite system as implemented using response surface models for every subsystem level. The numerical error ϵ_{RSM} (described in the next section) that results from using response surface models was incorporated into the network. The variable predictions obtained using response surface models were denoted with a RSM subindex. (e.g. $\epsilon^I_{ij_{RSM}}$ represents the inelastic strain computed using response surface models, while ϵ^I_{ij} represents the inelastic strain model prediction once the corresponding response surface model error ϵ^{pol}_{RSM} was incorporated). The next step will be to propagate uncertainty across the network due to different sources of error. Errors can be represented as additional nodes in the network. The next section describes the general procedure to incorporate modeling, numerical and experimental errors into the Bayes network.

7.5 Introducing Modeling, Numerical and Experimental Errors into the Bayesian Network

In general, errors can be broadly grouped into two major categories: prediction errors and experimental errors [93]. Prediction errors include all errors made as part of the analytical and computer simulation process, such as numerical errors and modeling errors. The numerical error that results from the surrogate model approximation (i.e. response surface models) constitutes a prediction error. Experimental errors correspond to errors in the measurement of experimental data. The different type of errors that were considered in the composite test problem are described next:

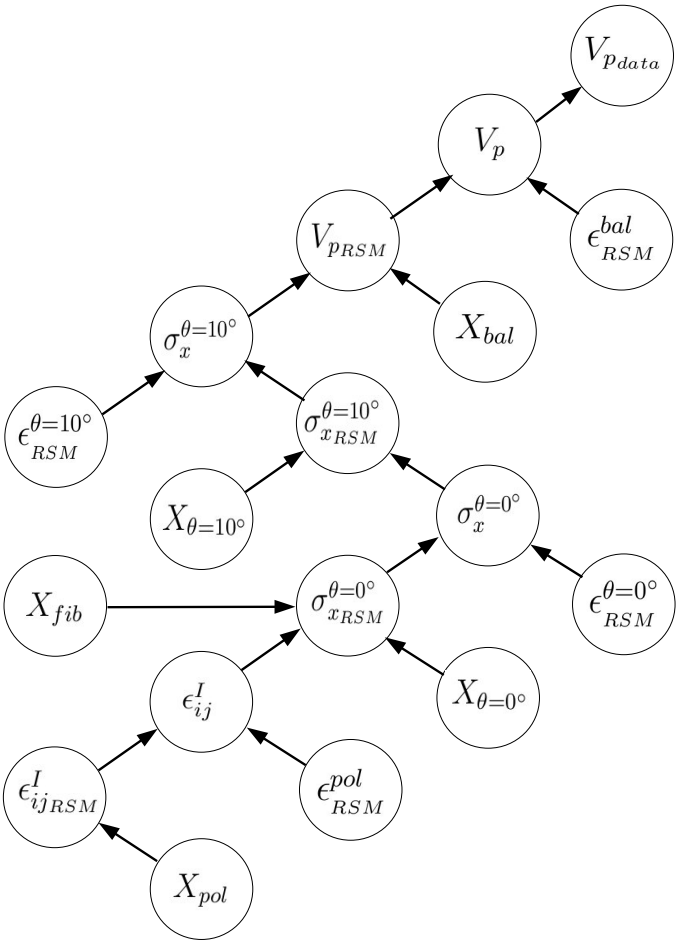

Figure 7.6: Schematic representation of the composite system with response surface models incorporated

- Response surface error ϵ_{RSM} : Corresponds to the truncation error introduced by response surface models. Multiresponse surface models are used to estimate the response of correlated response variables. If the same group of estimator effects X depicted in Equation 7.4 are used to fit each one of the response variables, the response surface model coefficients b_i do not depend on the response surface model error ε (Equation 7.1) and the best linear unbiased estimate of the model parameters b_i is given by Equation 7.5 [135]. The standard error of the predicted response $\sigma_{\bar{y}}$, assumed in this case to be similar to the response surface model truncation error, can be computed as defined in Myers et al [134]:

$$\sigma_{\bar{y}} = S\sqrt{\bar{x}(X^T X)^{-1}\bar{x}} \tag{7.6}$$

where $\bar{x}$ represents a vector of effects (e.g. for two design variables, the vector $\bar{x}$ can be defined as $\bar{x} = [1, x_1, x_2, x_1x_2, x_1^2, x_2^2]$) evaluated at a particular point in the design space and S represents the root mean squared error of the response surface model (an unbiased estimator of the variance of the response surface error), computed using the sum of the squared residuals:

$$S^2 = \frac{1}{m-N}(y - X\beta)^T(y - X\beta) \tag{7.7}$$

Equation 7.7 is valid for most general cases where the number of observations m is bigger than the number of predictor variables N. The response surface model error ϵ_{RSM} was modeled as a random variable that follows a normal distribution with zero mean and standard deviation $\sigma_{\bar{y}}$.

- Experimental error ϵ_{exp} : The error that results from measuring the output response is typically modeled as a random variable with zero mean and known or assumed variance. If enough data is available, the standard deviation of ϵ_{exp} may be approximated by estimating the variance of all the response measurements.

- Modeling error ϵ_{mod} : Represents the analytical error introduced by the model formulation itself. Assuming no numerical errors exist (or are small enough that can be neglected), the model error can be expressed as the difference between the true response y_{true} and the true model predicted response y_{mod}:

$$\epsilon_{mod} = y_{true} - y_{mod} \tag{7.8}$$

In general, limited data is available to estimate y_{true} and numerical errors affect y_{mod}. The model error estimation methodology presented in the last chapter was used to estimate the uncertainty in the prediction introduced by ϵ_{mod}.

As more data becomes available, the uncertainty in the various errors can be reduced. When limited data is available, errors can be formulated based on known characteristics of the response along with vague or noninformative prior distributions. Errors were incorporated as additional nodes in the composite system network. Figure 7.7 depicts the schematic representation of the Bayesian network for the entire composite system with model, numerical (RSM error) and experimental errors incorporated. An additional node representing the predicted true response (denoted by a *true* subindex) was added to each level in the network. The predicted true response was computed by adding the model error ϵ_{mod} to the corresponding level response prediction, as depicted in Equation [**?**]. With the network implementation finished, the model error estimation methodology presented in last chapter will be used to investigate if modeling errors can be estimated across multiple levels of the composite test problem.

7.6 Composite Multilevel Example

In Chapter 6, the basic error estimation methodology was illustrated via single level and multilevel (hierarchical) algebraic examples. In the current section, the error estimation procedure was carried out via Bayesian updating for the full composite system problem described in Section 7.2. For simplicity, additional forms of error such as input

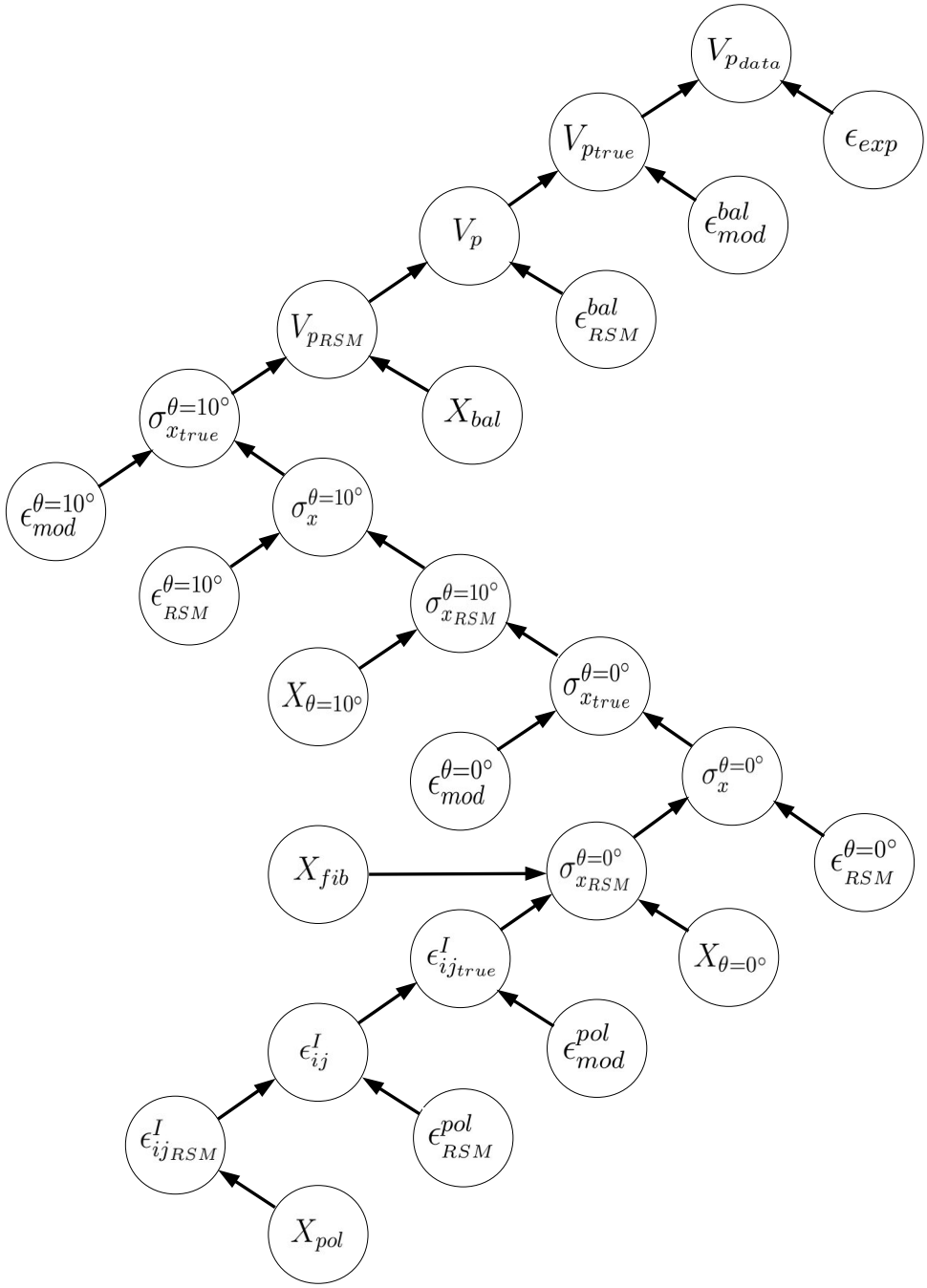

Figure 7.7: Schematic representation of Bayes network with all errors incorporated

data errors ϵ_{par} were not included. It was assumed the values for the material model input parameters presented in Section 7.2 accurately represent the parameter true values. Due to the extensive use of response surface models within the Bayesian network, numerical errors were assumed to arise mainly from the response surface model approximations.

Numerical errors due to FEM spatial discretization schemes were assumed to be negligible in comparison to the response surface model error.

For the hierarchical algebraic example presented in the previous chapter, data was assumed to be available at different subsystem levels in order to illustrate how to estimate modeling errors given limited experimental data. For the composite problem, it was not possible to find experimental data for all system levels. For illustration purposes, the true response was simulated by introducing known errors to the model predictions as follows:

$$y_{true} = y_{mod} + C_1 y_{mod} \tag{7.9}$$

where y_{mod} represents the finite element analysis prediction using the analytical composite model described in Chapter 5 and y_{true} represents the true response as described in Section 6.2. In the context of the current test problem, y_{mod} represents any quantity of interest that may exhibit error in its prediction, e.g. computed lamina stresses or projectile residual velocity. The added term in Equation 7.9 represents the model error in the prediction, which was assumed to be unknown. For the composite test problem, it was assumed only experimental data at the highest level was available, i.e. only data at the ballistic impact test level was provided. The experimental measurement error ϵ_{exp} and input data uncertainty ϵ_{par} were assumed to have been previously estimated. Only the model error ϵ_{mod} at each subsystem level was updated. Model errors were added at each level, starting with the unidirectional 0° lamina level. Using Equation 7.9, the true responses were obtained as follows:

Table 7.4: Available data for V_p (mt/sec)

$V_{p_{data}}$
121.92
113.30
103.20
97.70
96.75
96.33

$$\begin{aligned} \epsilon^I_{x_{true}} &= \epsilon^I_x + C_1^{(1)}\epsilon^I_x \\ \sigma^{\theta=0^\circ}_{x_{true}} &= \sigma^{\theta=0^\circ}_x + C_1^{(2)}\sigma^{\theta=0^\circ}_x \\ \sigma^{\theta=10^\circ}_{x_{true}} &= \sigma^{\theta=10^\circ}_x + C_1^{(3)}\sigma^{\theta=10^\circ}_x \\ V_{p_{true}} &= V_p + C_1^{(4)}V_p \end{aligned} \tag{7.10}$$

where the added terms were given values C_1 = [0.0, -0.30, -0.15, 0.10]. Once known errors were added to each level prediction as depicted in Equation 7.10, the true response at the ballistic impact test level was computed. The true projectile residual velocity $V_{p_{true}}$ was assumed to represent the true value of the available experimental data. The provided data for $V_{p_{true}}$ is shown in Table 7.4. Five data points (in addition to the prescribed initial velocity) were provided for the projectile residual velocity curve response. The relatively small number of points was chosen to reduce the computational time of the Bayesian update. The experimental error ϵ_{exp} distribution was assumed to follow a normal distribution with zero mean and standard deviation of 3% with respect to the data values presented in Table 7.4. As mentioned before, the data presented in Table 7.4 represents the only information available regarding the response of the composite multilevel system.

Given the ballistic impact test data shown in Table 7.4, it was investigated if the model errors added at each subsystem level (assumed to be unknown) can be correctly

estimated. The model error estimation approach described in Sections 6.2 and 6.3 was used to estimate the added model errors. The model error form used was a combination of the methodologies employed in the single and multilevel algebraic examples presented in Sections 6.2 and 6.3. Model errors at each level of the composite system example were defined as follows:

$$\begin{aligned} \epsilon_{mod}^{pol} &= \beta_1^{(1)} X^{(1)} + \beta_2^{(1)} {X^{(1)}}^2 \\ \epsilon_{mod}^{\theta=0^\circ} &= \beta_1^{(2)} X^{(2)} + \beta_2^{(2)} {X^{(2)}}^2 \\ \epsilon_{mod}^{\theta=10^\circ} &= \beta_1^{(3)} X^{(3)} + \beta_2^{(3)} {X^{(3)}}^2 \\ \epsilon_{mod}^{bal} &= \beta_1^{(4)} X^{(4)} + \beta_2^{(4)} {X^{(4)}}^2 \end{aligned} \tag{7.11}$$

All model error coefficients β_i at each level were given appropriate uniform prior distributions. The prior distributions for the model error coefficients β_i are given in Tables 7.5 and 7.6. The model error term X represents an independent variable scaled using the maximum value of the corresponding model prediction response $X = [0:1]max(y_{mod})$. Although no model errors were added at the polymer level (i.e. $C_1^{(1)} = 0.0$), the Bayesian update can propagate the uncertainty backwards in the network, updating all coefficients β_i at each level, including the polymer level model error coefficients $\beta_1^{(1)}$ and $\beta_2^{(1)}$. Any previous knowledge regarding the predicted response should be incorporated in the model error coefficient prior distributions. For example, it is reasonable to assume that $\sigma_{x_{true}}^{\theta=0^\circ}$ is mainly linear; therefore, the model error coefficient $\beta_2^{(2)}$ that introduces second order effects in the response was given a zero value. Another issue to consider when assigning prior distributions were the inherent constraints of employing response surfaces to propagate the response from level to level in the Bayesian update. The added model errors described in Equation 7.10 were given in ranges where the corresponding response (finite

Table 7.5: Prior Distributions for Model Error Coefficient β_1

$\beta_1^{(1)} \sim unif(-0.25, 0.25)$
$\beta_1^{(2)} \sim unif(-0.50, 0.00)$
$\beta_1^{(3)} \sim unif(-0.25.0.25)$
$\beta_1^{(4)} \sim unif(-0.25, 0.25)$

Table 7.6: Prior Distributions for Model Error Coefficient β_2

$\beta_2^{(1)} \sim unif(-0.025, 0.025)$
$\beta_2^{(2)} \sim unif(0.000, 0.000)$
$\beta_2^{(3)} \sim unif(-0.025, 0.025)$
$\beta_2^{(4)} \sim unif(-0.025, 0.025)$

element simulation) was found to be stable. For the lamina test cases, adding error terms that significantly increase $\sigma_x^{\theta=0^\circ}$ or $\sigma_x^{\theta=10^\circ}$ (as oppose to decrease the corresponding stress value as depicted in Equation 7.10) was found to lead to instabilities in the solution. The response surfaces were fitted to propagate values in the stable range of the response. Likewise, the prior distribution values had to be confined within the bounds of the response surface in order to guaranty convergence of the Bayesian update.

Two Bayesian updates were performed following the methodology presented in Sections 6.2 and 6.3. The estimated true responses for each level are shown in Figures 7.8 to 7.11. The same convention used to plot the level responses of the multilevel hierarchical example presented in Section 6.3 was used for the current problem. The solid lines represent the model predictions for $\epsilon_x^I, \sigma_x^{\theta=0^\circ}, \sigma_x^{\theta=10^\circ}$ and V_p. The dashed lines represent the true responses $\epsilon_{x_{true}}^I, \sigma_{x_{true}}^{\theta=0^\circ}, \sigma_{x_{true}}^{\theta=10^\circ}$ and $V_{p_{true}}$. The dotted lines represent the level prediction given the responses of all parent nodes were accurately predicted (e.g. the value of $\sigma_x^{\theta=10^\circ}$ providing ϵ_x^I and $\sigma_x^{\theta=10^\circ}$ were accurately estimated). The square marks represent the mean values of the level response once the model errors of the parent nodes were updated. The diamond marks represent the mean values of the level response once

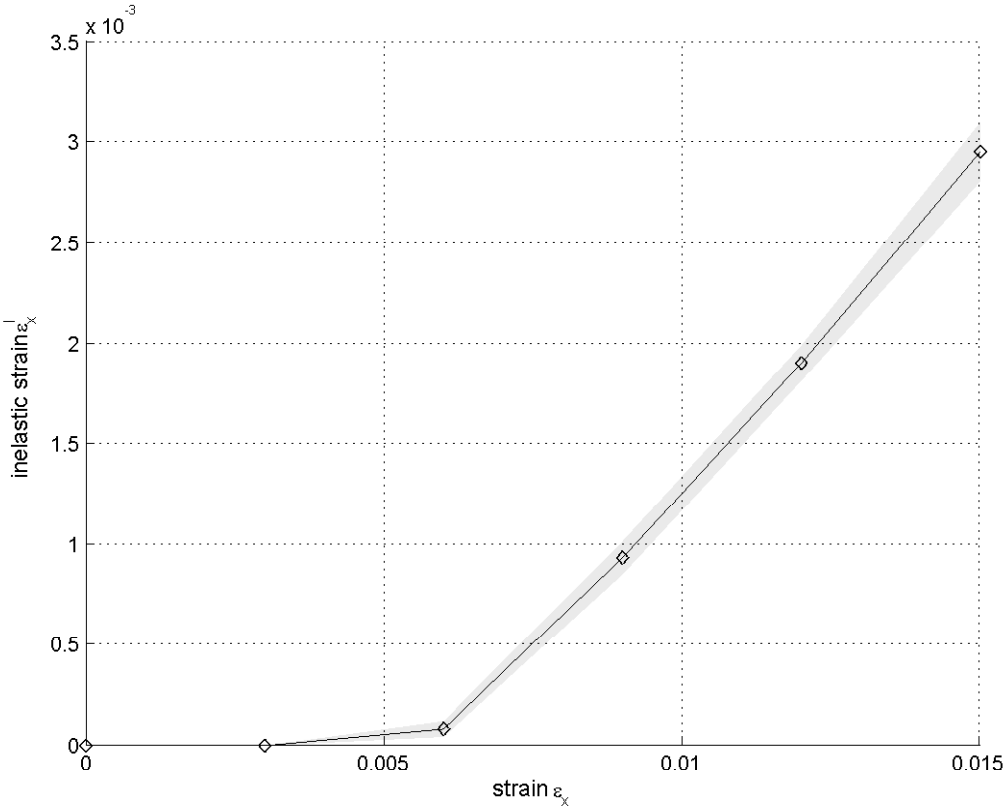

Figure 7.8: Inelastic strain true and predicted responses. The model prediction ϵ_x^I (solid line), true response $\epsilon_{x_{true}}^I$ (dash line) and updated prediction (diamond marks) were plotted. The shaded area represents the 99% confidence intervals for the updated prediction (diamond marks)

the model error of the current node was updated. The shaded area represents the 99% confidence intervals of the mean estimated response at each level (diamond marks).

From the updated predictions shown in Figures 7.8 to 7.11, it can be concluded that providing data for only one level was not enough to accurately estimate the model errors at all levels of the composite system, particularly for the composite lamina stresses $\sigma_x^{\theta=0^\circ}$ and $\sigma_x^{\theta=10^\circ}$. However, the provided data was enough for the Bayesian update to estimate reasonable confidence bounds for the uncertainty at each level. The response depicted in Figure 7.8 shows that ϵ_x^I was estimated reasonably well. On the other hand, the updated predictions for stresses $\sigma_x^{\theta=0^\circ}$ and $\sigma_x^{\theta=10^\circ}$ were found to deviate from their

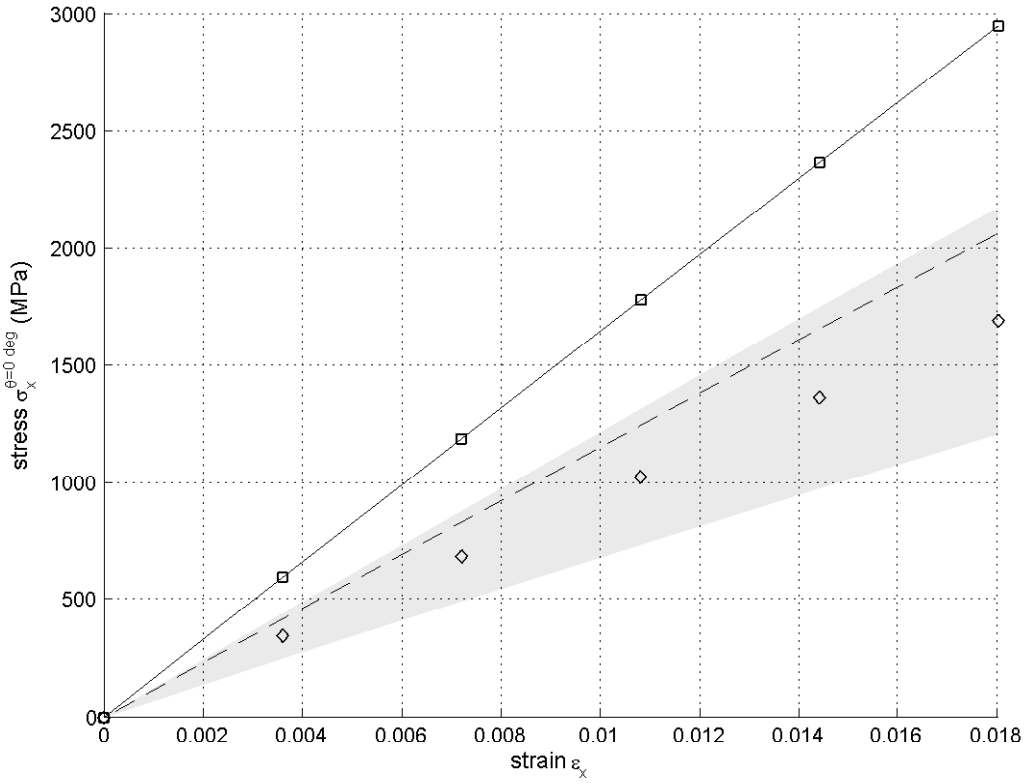

Figure 7.9: Composite lamina ($\theta = 0°$) true and predicted responses. The model prediction $\sigma_x^{\theta=0°}$ (solid line), true response $\sigma_{x_{true}}^{\theta=0°}$ (dash line), true prediction excluding $\epsilon_{mod}^{\theta=0°}$ (dotted line), updated prediction excluding $\epsilon_{mod}^{\theta=0°}$ (square marks) and updated prediction including $\epsilon_{mod}^{\theta=0°}$ (diamond marks) were plotted. The shaded area represents the 99% confidence intervals for the updated prediction (diamond marks)

corresponding true responses. Nonetheless, the true responses $\sigma_{x_{true}}^{\theta=0°}$ and $\sigma_{x_{true}}^{\theta=10°}$ were bounded by the estimated 99% confidence intervals, as reflected in Figures 7.9 and 7.10. The projectile velocity experimental error also contributed to the stresses large variation. Even if the exact magnitude of the added model errors was not accurately predicted for all levels, it was possible to estimate at which levels were model errors added. The test problem showed that given limited data it may not possible to accurately predict the model errors at all levels, but it is possible to bound with reasonable accuracy the uncertainty in the model prediction.

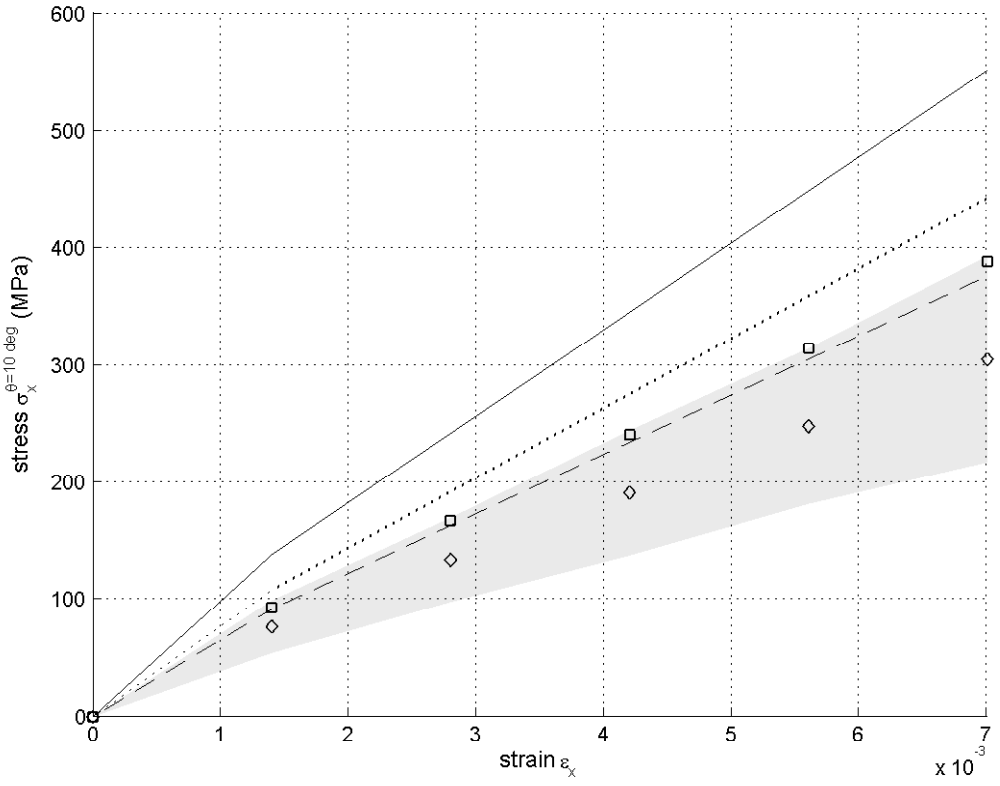

Figure 7.10: Composite lamina ($\theta = 10°$) true and predicted responses. The model prediction $\sigma_x^{\theta=10°}$ (solid line), true response $\sigma_{x_{true}}^{\theta=10°}$ (dash line), true prediction excluding $\epsilon_{mod}^{\theta=10°}$ (dotted line), updated prediction excluding $\epsilon_{mod}^{\theta=10°}$ (square marks) and updated prediction including $\epsilon_{mod}^{\theta=10°}$ (diamond marks) were plotted. The shaded area represents the 99% confidence intervals for the updated prediction (diamond marks)

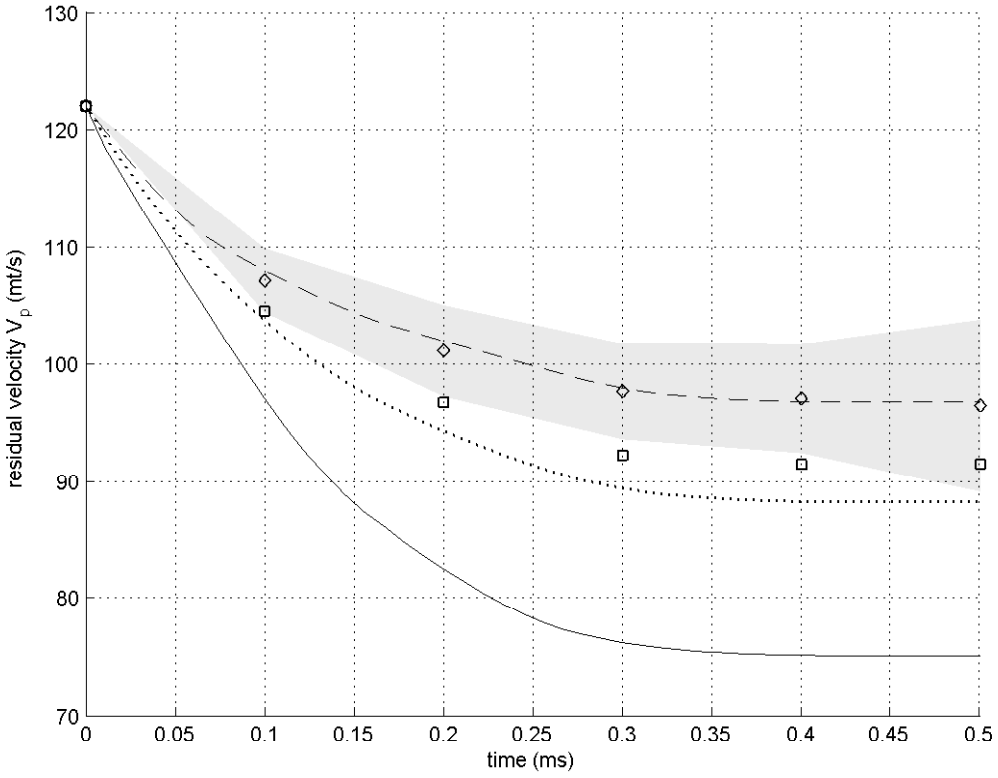

Figure 7.11: Ballistic impact test true and predicted responses. The model prediction V_p (solid line), true response $V_{p_{true}}$ (dash line), true prediction excluding ϵ_{mod}^{bal} (dotted line), updated prediction excluding ϵ_{mod}^{bal} (square marks) and updated prediction including ϵ_{mod}^{bal} (diamond marks) were plotted. The shaded area represents the 99% confidence intervals for the updated prediction (diamond marks)

Chapter 8

Summary and Conclusions

A general methodology was developed to quantify model errors at different sub scales in the ballistic impact predicted response of composite laminates using Bayes networks. First, a preliminary investigation on the effect of model analysis and parameter uncertainties in the progressive failure response of laminated composites was carried out. Different laminate designs were subjected to analysis and model parameter uncertainties and the corresponding energy absorption statistics were calculated. Laminates optimized for maximum energy absorption were sensitive to all sources of model uncertainties and resulted in large variations in the energy absorption response when all the sources of uncertainty were combined. It was shown that accurately predicting the failure sequence requires including model uncertainties along with variability in the reliability optimization.

A composite material model for high strain rates was implemented in Ls-Dyna finite element code in order to perform the ballistic impact test simulations. The Goldberg's viscoplastic model was used to simulate the response of the polymer matrix material in the

composite. The numerical implementation of the polymer model was described in detail. The model discretization scheme along with the nonlinear solver algorithms employed for solving the polymer constitutive equations were described as well. A phenomenological approach was used to represent the fiber stiffness degradation. A micromechanical model was used to obtain the composite material resultant stresses. Quantitatively speaking, the model was shown to correlate well with experimental data from tensile coupon tests.

The basic theory behind Bayesian networks was introduced. The general methodology used to quantify modeling errors was illustrated with a couple of simple algebraic examples. Model errors were expressed as polynomial type functions that could be easily implemented in the network. Response surface models were used to represent the composite model simulations at each level as explicit functions that could be implemented in the Bayesian network framework. The responses of the matrix, fiber, composite lamina and ballistic impact tests were represented in the Bayes network, along with the numerical, modeling and experimental errors. Modeling errors were added to each level in the network and it was investigated if the added model errors (assumed to be unknown) could be estimated by systematically updating the random coefficients of the model error formulation via Bayesian theory. It was shown that given limited experimental data (projectile residual velocities), it was possible to obtain confidence intervals for the model error at each level. As future work, it will be investigated if the model error estimation methodology can be used to aid in the decision making process and optimal management of resources to generate test data and develop better analytical models. The model error estimation approach could help estimate what areas of the analytical models introduce the most uncertainty into the predictions, so resources can be allocated to reduce the existent model deficiencies and improve the accuracy of the predicted response.

Bibliography

[1] P. D. Soden, M. J. Hinton, and A. S. Kaddour, "A comparison of the predictive capabilities of current failure theories for composite laminates," *Compos Sci Technol*, vol. 58, no. 7, pp. 1225–1254, 1998.

[2] P. D. Soden, A. S. Kaddour, and M. J. Hinton, "Recommendations for designers and researchers resulting from the world-wide failure exercise," *Composites Science and Technology*, vol. 64, no. 3-4, pp. 589–604, 2004.

[3] M. J. Hinton, P. D. Soden, and A. S. Kaddour, "Evaluation of failure prediction in composite laminates: background to part b of the exercise," *Compos Sci Technol*, vol. 62, pp. 1481–1488, 2002.

[4] M. J. Hinton, A. S. Kaddour, and P. D. Soden, "Evaluation of failure prediction in composite laminates: background to part c of the exercise," *Compos Sci Technol*, vol. 64, no. 3-4, pp. 321–327, 2004.

[5] M. J. Hinton, A. S. Kaddour, and P. D. Soden, "A comparison of the predictive capabilities of current failure theories for composite laminates, judged against experimental evidence," *Composites Science and Technology*, vol. 62, no. 12-13, pp. 1725–1797, 2002.

[6] W. Cantwell and J. Morton, "The impact resistance of composite materials-a review," *Composites*, vol. 22, no. 5, pp. 347–362, 1991.

[7] M. P. Flanagan, M. A. Zikry, J. W. Wall, and A. El-Shiekh, "An experimental investigation of high velocity impact and penetration failure modes in textile composites," *Journal of Composite Materials*, vol. 33, no. 12, pp. 1080–1103, 1999.

[8] W. J. Cantwell and J. Morton, "Impact perforation of carbon fibre reinforced plastic," *Compos. Sci. Technol.*, vol. 38, pp. 119–141, 1990.

[9] W. R. Lee and C. T. Sun, "A quasistatic penetration model for composite laminates," *J. Compos. Mater.*, vol. 27, pp. 251–271, 1993.

[10] G. J. Czarnecki, "Dual mode fracture of composite laminates penetration by spherical projectiles," in *18th Congress of the International Council of the Aeronautics Science*, (Beijing, China), ICAS-92-5.6.2, September 1992.

[11] F. Keisuke, A. Motokazu, K. Noriyuki, Y. Eiichi, and T. Yasuhiro, "Impact perforation behavior of cfrps using high-velocity steel sphere," *International Journal of Impact Engineering*, vol. 27, no. 5, pp. 497–508, 2002.

[12] S. Venkataraman and P. Salas, "Optimization of composite laminates for robust and predictable progressive failure response," *AIAA Journal*, vol. 45, pp. 1113–1125, May 2007.

[13] I. M. Daniel, E. E. Gdoutos, and Y. D. S. Rajapakse, *Major accomplishments in composite materials and sandwich structures: an anthology of ONR sponsored research*. London: Springer, 2009.

[14] R. L. Sierakowsky, "Strain rate effects in composites," *Composites Part B Rev*, vol. 50, no. 11, pp. 741–761, 1997.

[15] D. Z. Zhang, "Shock dispersion in composite material with polymer binder." American Institute of Physics 0-7354-0181-0, 2004.

[16] C. T. Sun and J. L. Chen, "A micromechanical model for plastic behavior of fibrous composites," *Composite Science and Technology*, vol. 40, no. 2, pp. 115–129, 1991.

[17] J. Tsai and C. T. Sun, "Constitutive model for high strain rate response of polymeric composites," *Composites Science and Technology*, vol. 62, pp. 1289–1297, 2002.

[18] C. T. Sun and J. L. Chen, "A simple flow rule for characterizing nonlinear behavior of fiber composites," *Journal of Composite Materials*, vol. 23, pp. 1009–1020, 1989.

[19] H. D. Espinosa, H.-C. Lu, P. D. Zavattieri, and S. Dwivedi, "A 3-d finite deformation anisotropic visco-plasticity model for fiber composites," *Journal of Composite Materials*, vol. 35, no. 5, pp. 369–410, 2001.

[20] C. A. Weeks and C. T. Sun, "Modeling non-linear rate-dependent behavior in fiber-reinforced composites," *Composites Science and Technology*, vol. 58, pp. 603–611, 1998.

[21] G. R. Johnson and W. H. Cook, "A constitutive model and data for metals subjected to large strains, high strain rates and high temperatures." Proceedings of the 7th International Symposium on Ballistics, 1983.

[22] R. K. Goldberg and D. C. Stouffer, "High strain rate deformation modeling of a polymer matrix composite: Part-i matrix constitutive equations." NASA/TM-1998-206969, Lewis Research Center, August 1998.

[23] R. K. Goldberg, G. D. Roberts, and A. Gilat, "Implementation of an associative flow rule including hydrostatic stress effects into the high strain rate deformation analysis of polymer matrix composites." NASA/TM-2003-212382, Glenn Research Center, June 2003.

[24] S. R. Bodner, *Unified plasticity for engineering applications*. New York: Kluwer Academic Plenum Publishers, 2002.

[25] A. S. Khan and S. Huang, *Continuum theory of plasticity*. New York: John Wiley and Sons, 1995.

[26] J. K. Chen, F. A. Allahdadi, and T. C. Carney, "High-velocity impact of graphite/epoxy composite laminates," *Composite Science and Technology*, vol. 57, pp. 1369–1379, 1997.

[27] L. B. Lucy, "A numerical approach to the testing of the fission hypothesis," *Astron. J.*, vol. 82, pp. 1013–1020, 1977.

[28] R. A. Gingold and J. J. Monaghan, "Smoothed particle hydrodynamics: Theory and application to nonspherical stars," *Mon. Not. Roy. Astr. Sot.*, vol. 181, pp. 375–389, 1977.

[29] W. Wang, G. Makarov, and R. A. Shenoi, "An analytical model for assessing strain rate sensitivity of unidirectional composite laminates," *Composite Structures*, vol. 69, pp. 45–54, 2005.

[30] A. Tabiei and Q. Chen, "Micromechanics based composite material model for crashworthiness explicit finite element simulation," *Journal of Thermoplastic Composite Materials*, vol. 14, pp. 264–289, 2001.

[31] J.-L. Tsai and K.-H. Chen, "Characterizing nonlinear rate-dependent behaviors of graphite/epoxy composites using a micromechanical approach," *Journal of Composite Materials*, vol. 41, no. 10, pp. 1253–1273, 2007.

[32] M. Paley and J. Aboudi, "Micromechanical analysis of composites by the generalized cells model," *Mechanics of Materials*, vol. 14, no. 2, pp. 127–139, 1992.

[33] J. Aboudi, *Mechanics of composite materials - a unified micromechanical approach.* Amsterdam and New York: Elsevier, 1991. Studies in Applied Mechanics, Vol. 29.

[34] X. Zheng, R. K. Goldberg, W. K. Binienda, and G. D. Roberts, "Ls-dyna implementation of polymer matrix composite model under high strain rate impact." NASA/TM-2003-212583, 2003.

[35] "Ls-dyna keyword user's manual, version 971." Livermore Software Technology Corporation, Livermore CA., 2005.

[36] L. Zhu, A. Chattopadhyay, and R. K. Goldberg, "Transient response of strain rate dependent polymer matrix composite laminates," in *46th AIAA/ASME/ASCE/AHS/ASC Structures, Structural Dynamics & Materials Conference*, (Austin, Texas), American Institute of Aeronautics and Astronautics, April 2005.

[37] L. Zhu, A. Chattopadhyay, and R. K. Goldberg, "A 3d micromechanics model for strain rate dependent inelastic polymer matrix composites," in *47th AIAA/ASME/ASCE/AHS/ASC Structures, Structural Dynamics & Materials Conference*, (Newport, Rhode Island), American Institute of Aeronautics and Astronautics, May 2006.

[38] A. Shukla, G. Ravichandran, and Y. Rajapakse, *Dynamic failure of materials and structures.* New York: Springer, 2009.

[39] A. G. Mamalis, D. E. Manolakos, G. A. Demosthenous, and M. B. Ioannidis, *Crashworthiness of composite thin-walled structural components.* CRC Press, 1998.

[40] A. K. Kaw, *Mechanics of composite materials, Second edition.* Boca Raton, FL: Taylor and Francis Group, 2006.

[41] Z. Hashin, "Failure criteria for unidirectional fiber composites," *J. Appl. Mech*, vol. 47, pp. 329–334, 1980.

[42] R. Hill, *The mathematical theory of plasticity.* London: Oxford University Press, 1950.

[43] S. W. Tsai and E. Wu, "A general theory of strength for anisotropic materials," *Journal of Composite Materials*, vol. 5, no. 1, pp. 58–80, 1971.

[44] T. A. Boggeti, C. P. R. Hoppel, V. M. Harik, J. F. Newill, and B. P. Burns, "Predicting the nonlinear response and progressive failure of composite laminates," *Composites Science and Technology*, vol. 64, pp. 329–342, 2004.

[45] A. Kuraishi and S. W. Tsai, "A progressive quadratic failure criterion for a laminate," *Composites Science and Technology*, vol. 58, pp. 1023–1032, 1998.

[46] P. A. Zinoviev, S. V. Grigoriev, O. V. Lebedeva, and L. P. Tairova, "The strength of multilayered composites under a plane-stress state," *Composites Science and Technology*, vol. 58, pp. 1209–1223, 1998.

[47] A. Puck and H. Schurmann, "Failure analysis of frp laminates by means of physically based phenomenological models," *Composites Science and Technology*, vol. 58, no. 3-4, pp. 1045–1067, 1998.

[48] R. G. Cuntze and A. Freund, "The predictive capability of failure mode concept-based strength criteria for multidirectional laminates," *Composites Science and Technology*, vol. 64, pp. 343–377, 2004.

[49] C. A. Coulomb, "Essai sur une application des règles de maximis & minimis *à* quelques problèmes de statique, relatifs *à* l'architecture," *Mémoires de Mathématique et de Physique*, vol. 7, pp. 343–382, 1776.

[50] S. J. Mayes and A. C. Hansen, "Composite laminate failure analysis using multicontinuum theory," *Composites Science and Technology*, vol. 64, pp. 379–394, 2004.

[51] S. Mayes and A. C. Hansen, "Multicontinuum failure analysis of composite structural laminates," *Mechanics of Composite Materials and Structures*, vol. 8, pp. 249–262, 2001.

[52] P. S. Theocaris, "Positive and negative failure-shears in orthotropic materials," *Journal of Reinforced Plastics and Composites*, vol. 11, pp. 32–55, January 1992.

[53] P. S. Theocaris, "Failure characterization of anisotropic materials by means of the elliptic paraboloid failure criterion," *Advances in Mechanics*, vol. 10, no. 3, pp. 83–102, 1987.

[54] L. Iannucci, "Progressive failure modelling of woven carbon composite under impact," *International Journal of Impact Engineering*, vol. 32, pp. 1013–1043, 2006.

[55] A. F. Johnson and A. K. Pickett, "Impact and crash modelling of composite structures: a challenge for damage mechanics." German Aerospace Center (DLR), Institute of Structures and Design, Stuttgart, Germany.

[56] R. Dechaene, J. Degrieck, L. Iannucci, and M. Willows, "A constitutive model for glass fibre fabric composites under impact," *Journal of Composite Materials*, vol. 36, no. 8, pp. 983–1004, 2002.

[57] W. Roux and K. Craig, "Validation of structural simulations considering stochastic process variation." SAE International, 06M-67, 2005.

[58] S. F. Wojtkiewicz, M. S. Eldred, R. V. F. Jr., A. Urbina, and J. R. Red-Horse, "Uncertainty quantification in large computational engineering models." American Institute of Aeronautics and Astronautics, AIAA-2001-1455, 2001.

[59] W. L. Oberkampf, S. M. DeLand, B. M. Rutherford, K. V. Diegert, and K. F. Alvin, "Estimation of total uncertainty in modeling and simulation." Sandia Report, SAND2000-0824, Unlimited Release, April 2000.

[60] W. R. Logan and C. K. Nitta, "Verification & validation: process and levels leading to qualitative or quantitative validation statements." Lawrence Livermore National Laboratory. U.S. Department of Energy, UCRL-TR-200131, October 2003.

[61] W. R. Logan, C. K. Nitta, and S. K. Chidester, "Risk reduction as the product of model assessed reliability, confidence, and consequence," *The Society for Modeling and Simulation International*, vol. 2, pp. 191–207, October 2005.

[62] G. I. Schuller, "Computational stochastic mechanics - recent advances," *Computers and Structures*, vol. 79, p. September, 2225-2234 2001.

[63] M. Beer and M. Liebscher, "Designing robust structures - a nonlinear simulation based approach," *Computers and Structures*, vol. 86, pp. 1102–1122, 2008.

[64] R. d´ Ippolito, S. Donders, L. Hermans, H. V. der Auweraer, and D. Vandepitte, "Reliability-based design optimization for aerospace and automotive structures." The Marie Curie Fellowships Annals, 4.

[65] J. Faragher, "Probabilistic methods for the quantification of uncertainty and error in computational fluid dynamics simulations," in *Report DSTO-TR-1633*, (Australia), Published by DSTO Platforms Sciences Laboratory, October 2004.

[66] L. A. Zadeh, "Fuzzy sets as a basis for a theory of possibility," *Fuzzy Sets Syst*, vol. 1, pp. 3–28, 1978.

[67] L. A. Zadeh, "Fuzzy sets," *Information control*, vol. 8, pp. 338–353, 1965.

[68] J.-L. Batoz, P. Chedmail, G. Cognet, and C. Fortin, *Integrated design and manufacturing in mechanical engineering '98*. Hluwer Academic Publishers, Springer, 1999.

[69] B. S. L. P. de Lima, E. X. Teixeira, and N. F. F. Ebecken, "Probabilistic and possibilistic methods for the elastoplastic analysis of soils," *Advances in Engineering Software*, vol. 32, pp. 569–585, 2001.

[70] A. Saltelli, M. Ratto, T. Andres, F. Campolongo, J. Cariboni, D. Gatelli, M. Saisana, and S. Tarantola, *Global sensitivity analysis*. John Wiley & Sons, 2008.

[71] R. G. Ghanem and P. D. Spanos, *Stochastic finite elements: A spectral approach*. Courier Dover Publications, 2003.

[72] D. S. Yates, D. S. Moore, and D. S. Starnes, *The practice of statistics, 3rd Edition*. W. H. Freeman & Company, 2008.

[73] K. Black, *Business statistics for contemporary decision making, Sixth Edition*. John Wiley & Sons, 2009.

[74] E. J. Pedhazur and L. Pedhazur, *Measurement, design, and analysis: an integrated approach*. Lawrence Erlbaum Associates, 1991.

[75] S. M. Kerry and J. M. Bland, "The intracluster correlation coefficient in cluster randomisation," *British Medical Journal*, vol. 316, pp. 1455–1460, May 1998.

[76] T. Barth, "A brief overview of uncertainty quantification and error estimation in numerical simulation." Exploration Systems Directorate, NASA Ames Research Center Presentation.

[77] R. L. Iman, J. M. Davenport, and D. K. Zeigler, *Latin hypercube sampling (program user's guide)*. OSTI:5571631.

[78] R. F. Harrington, *Field computation by moment methods*. Piscataway, NJ: IEEE Press, 1993.

[79] B. J. Debusschere, H. N. Najm, P. P. Pebay, O. M. Knio, R. G. Ghanem, and O. P. L. Maitre, "Numerical challenges in the use of polynomial chaos representations for stochastic processes," *SIAM Journal on Scientific Computing*, vol. 26, no. 2, pp. 698–719, 2005.

[80] G. J. Klir, "Is there more to uncertainty than some probability theorists might have us believe?," *Int J Gen Syst*, vol. 15, pp. 347–378, 1989.

[81] G. J. Klir, "On the alleged superiority of probability representation of uncertainty," *IEEE Trans Fuzzy Syst*, vol. 2, pp. 27–31, 1994.

[82] W. L. Oberkampf, "Uncertainty quantification using evidence theory." Presentation for Advanced Simulation & Computing Workshop Error Estimation, Uncertainty Quantification, And Reliability in Numerical Simulations, Stanford University, August 22-23 2005.

[83] J. Helton, J. Johnson, W. Oberkampf, and C. Sallaberry, "Sensitivity analysis in conjunction with evidence theory representations of epistemic uncertainty," *Reliab Eng Syst Safety*, vol. 91, pp. 1414–34, 2006.

[84] G. J. Klir and M. J. Wierman, *Uncertainty-based information*. New York: Physica-Verlag, 1999.

[85] J. C. Helton, J. D. Johnson, and W. L. Oberkampf, "An exploration of alternative approaches to the representation of uncertainty in model predictions," *Reliab Eng Syst Saf*, vol. 85, no. 1-3, pp. 39–71, 2004.

[86] A. S. Kangas and J. Kangas, "Probability, possibility and evidence: approaches to consider risk and uncertainty in forestry decision analysis," *For Policy Econ*, vol. 6, pp. 169–188, 2004.

[87] G. J. Klir, "Generalized information theory: aims, results, and open problems.," *Reliab Eng Syst Saf*, vol. 85, no. 1-3, pp. 21–38, 2004.

[88] B. Moller and M. Beer, "Engineering computation under uncertainty capabilities of non-traditional models," *Comput Struct*, vol. 86, no. 10, pp. 1024–41, 2008.

[89] J. T. Oden, I. Babuska, F. Nobile, Y. Feng, and R. Tempone, "Theory and methodology for estimation and control of errors due to modeling, approximation, and uncertainty," *Comput Methods Appl Mech Engrg*, vol. 194, pp. 195–204, 2005.

[90] J. T. Oden and S. Prudhomme, "Goal-oriented error estimation and adaptivity for the finite element method," *Comput Math Appl*, vol. 41, no. 5-6, pp. 735–756, 2001.

[91] J. T. Oden and K. Vemaganti, "Estimation of local modeling error and goal-oriented estimates and adaptive algorithms," *J Comput Phys*, vol. 164, pp. 22–47, 2000.

[92] J. M. Bernardo and A. F. M. Smith, *Bayesian theory*. New York: John Wiley, 2000.

[93] R. Rebba, S. Mahadevan, and S. Huang, "Validation and error estimation of computational models," *Reliability Engineering and System Safety*, vol. 91, pp. 1390–1397, 2006.

[94] S. A. Richards, "Completed richardson extrapolation in space and time," *Comm Numer Methods Eng*, vol. 13, pp. 558–573, 1997.

[95] X. Jiang and S. Mahadevan, "Bayesian structural equation modeling method for hierarchical model validation," *Reliability Engineering & System Safety*, vol. 94, no. 4, pp. 796–809, 2009.

[96] L. E. Nielsen and R. F. Landel, *Mechanical properties of polymers and composites: second edition, revised and expanded*. New York: Marcel Dekker, Inc., 1994.

[97] K. Lyle, E. Fasanella, M. Melis, K. Carney, and J. Gabrys, "Application of non-deterministic methods to assess modelling uncertainties for reinforced carbon-carbon debris impacts," in *Proc. 8th International LS-DYNA Users Conference*, (Detroit, MI), 2004.

[98] C. C. Chamis, "Probabilistic simulation of multi-scale composite behavior," *Theoretical and Applied Fracture Mechanics*, vol. 41, pp. 51–61, 2004.

[99] C. Chen, D. Duhamel, and C. Soize, "Probabilistic approach for model and data uncertainties and its experimental identification in structural dynamics: Case of composite sandwich panels," *Journal of sound and vibration*, vol. 294, pp. 64–81, 2006.

[100] A. K. Noor, J. H. S. Jr., and J. M. Peters, "Uncertainty analysis of composite structures," *Comput Methods Appl Mech Engrg*, vol. 185, pp. 413–432, 2000.

[101] G. V. Vinckenroy and W. P. de Wilde, "The use of monte carlo techniques in statistical finite element methods for the determination of the structural behaviour of composite materials structural components," *Composite Structures*, vol. 32, pp. 241–253, 1995.

[102] G. Cederbram, I. Elishakoff, and L. Librescu, "Reliability of laminated plates via the first-order second-moment method," *Composite Structures*, vol. 15, pp. 161–167, 1990.

[103] H. Zhao and Z. Gao, "Reliability analysis of composite laminate by enumerating significant failure modes," *Journal of Reinforced Plastics and Composites*, vol. 14, pp. 427–444, 1995.

[104] S. Mahadevan, X. Liu, and Q. Xiao, "A probabilistic progressive failure model for composite laminates," *Journal of Reinforced Plastics and Composites*, vol. 16, no. 11, pp. 1020–1038, 1997.

[105] X. Liu and S. Mahadevan, "Ultimate strength failure probability estimation of composite structures," *Journal of Reinforced Plastics and Composites*, vol. 19, no. 5, pp. 403–426, 2000.

[106] L. P. Chao, M. V. Gandhi, and B. S. Thompson, "A design-for-manufacture methodology for incorporating manufacturing uncertainties in the robust design of fibrous laminate composite structures," *Journal of Composite Materials*, vol. 27, no. 2, pp. 175–194, 1993.

[107] A. Charnes and W. W. Cooper, "Chance constrained programming," *Management Science*, vol. 6, pp. 73–79.

[108] T.-U. Kim and H.-C. Sin, "Optimal design of composite laminated plates with the discreteness in ply angles and uncertainty in material properties considered," *Computers and Structures*, vol. 79, pp. 2501–2509, 2001.

[109] I. Elishakoff and J. H. Starnes, "A deterministic method to predict the effects to unknown-but-bounded elastic moduli on the buckling of composite structures," *Comput Meth Appl Mech Eng*, vol. 111, pp. 155–167, 1994.

[110] Y.-S. Liao and C.-Y. Chiou, "Robust optimum designs of fiber-reinforced composites using constraints with sensitivity," *Journal of Composite Materials*, vol. 40, no. 22, pp. 2067–2081, 2006.

[111] A. Kuraishi, S. W. Tsai, and K. Liu, "A progressive quadratic failure criterion," *Compos Sci Technol*, vol. 62, pp. 1683–1695, 2002.

[112] P. Salas and S. Venkataraman, "Controlling failure using structural fuses for predictable progressive failure of composite laminates," *Structural and Multidisciplinary Optimization Journal*, vol. 34, no. 6, pp. 473–489, 2007.

[113] K.-S. Liu and S. W. Tsai, "A progressive quadratic failure criterion for a laminate," *Compos Sci Technol*, vol. 58, pp. 1023–1032, 1998.

[114] G. S. Padhi, R. A. Shenoi, S. S. J. Moy, and G. L. Hawkins, "Progressive failure and ultimate collapse of laminated composite plates in bending," *Compos Struct*, vol. 40, no. 3-4, pp. 277–291, 1997.

[115] D. R. Ambur, N. Jaunky, and M. W. Hilburger, "Progressive failure studies of stiffened panels subjected to shear loading," *Compos Struct*, vol. 65, no. 2, pp. 129–142, 2004.

[116] I. M. Ward, *Mechanical properties of solid polymers*. New York: John Wiley and Sons, 1983.

[117] C. J. F. Ridder, "Ieee transaction on circuits and systems," *CAS*, vol. 26, pp. 979–980, 1979.

[118] W. H. Press, B. P. Flannery, S. A. Teukolsky, and W. T. Vetterling, *Numerical recipes: the art of scientific computing, Third Edition*. Cambridge University Press, 2007. 1256 pp.

[119] R. L. Burden and J. D. Faires, *Numerical Analysis, 7th Edition*. Brooks/Cole, 2000.

[120] R. K. Goldberg, "Strain rate dependent deformation and strength modeling of a polymer matrix composite utilizing a micromechanics approach." NASA/TM-1999-209768, 1999.

[121] S. Mahadevan and R. Rebba, "Validation of reliability computational models using bayes networks," *Reliability Engineering and System Safety*, vol. 87, pp. 223–232, 2005.

[122] B. A. Berg, *Markov Chain Monte Carlo simulations and their statistical analysis*. Singapore: World Scientific, 2004.

[123] G. R. Gilks, S. Richardson, and D. J. Spiegelhalter, *Markov chain Monte Carlo in practice*. London: Chapman and Hall, 1996.

[124] G. Casella and E. I. George, "Explaining the gibbs sampler," *The American Statistician*, vol. 46, no. 3, pp. 167–174, 1992.

[125] D. Spiegelhalter, A. Thomas, N. Best, and D. Lunn, "Openbugs user manual, version 3.0.2." MRC Biostatistics Unit, Institute of Public Health, Cambridge, UK., September 2007.

[126] B. Efron, "Bootstrap methods: another look at the jackknife," *Annals of Statists*, vol. 7, no. 1, pp. 1–26, 1979.

[127] G. E. P. Box and K. B. Wilson, "On the experimental attainment of optimum conditions," *Journal of the Royal Statistical Society Series B*, vol. 13, no. 1, pp. 1–45, 1951.

[128] K. F. Alvin, W. L. Oberkampf, K. V. Diegert, and B. M. Rutherford, "Uncertainty quantification in computational structural dynamics: a new paradigm for model validation." Sandia National Laboratories Albuquerque, NM.

[129] F. M. Hemez and S. W. Doebling, "Review and assessment of model updating for non-linear, transient dynamics," *Mechanical Systems and Signal Processing*, vol. 15, pp. 45–74, January 2001.

[130] R. G. Hills and I. H. Leslie, "Statistical validation of engineering and scientific models: validation experiments to application." Sandia Report SAND2003-0706 Unlimited Release Printed, March 2003.

[131] T. I. Zohdi and D. Powell, "Multiscale construction and large-scale simulation of structural fabric undergoing ballistic impact," *Computer Methods in Applied Mechanics and Engineering*, vol. 195, pp. 94–109, January 2006.

[132] M. G. Morgan, M. Henrion, and M. Small, *Uncertainty: a guide to dealing with uncertainty in quantitative risk and policy analysis*. Cambridge University Press, 1990.

[133] G. Kerschen, J. Golinval, and F. M. Hemez, "Bayesian model screening for the identification of nonlinearn mechanical structures," *Journal of Vibration and Acoustics*, vol. 125, pp. 389–397, July 2003.

[134] R. H. Myers and D. C. Montgomery, *Response surface methodology: process and product in optimization using designed experiments, 1st edition*. New York: John Wiley and Sons, Inc., 1995.

[135] A. I. Khuri and J. A. Cornell, *Response surfaces, designs and analyses, Seconde Edition, revised and expanded*. New York: Marcel Dekker, Inc., 1996.